Toxicity of Source-Oriented Ambient Submicron Particulate Matter
Contract Number 06-331

Final Report to the State of California Air Resources Board,
Research Division

Anthony S. Wexler and Kent Pinkerton
Co-Principal Investigators
University of California
Davis, CA 95616

May 2012

Prepared for the California Air Resources Board, the California Environmental Protection Agency, and the Electric Power Research Institute

Disclaimer

The statements and conclusions in this Report are those of the contractor and not necessarily those of the California Air Resources Board. The mention of commercial products, their source, or their use in connection with material reported herein is not to be construed as actual or implied endorsement of such products.

Acknowledgment

This work was carried out by a large number of dedicated researchers including Drs. Keith Bein, Yongjing Zhao, and Laurel Plummer, and Mr. Chris Carosino at the University of California, Davis.

This Report was submitted in fulfillment of ARB contract number 06-331 titled "Toxicity of Source-Oriented Ambient Aerosol" by the University of California, Davis under the partial sponsorship of the California Air Resources Board and the Electric Power Research Institute.

This project is funded under the ARB's Dr. William F. Friedman Health Research Program. During Dr. Friedman's tenure on the Board, he played a major role in guiding ARB's health research program. His commitment to the citizens of California was evident through his personal and professional interest in the Board's health research, especially in studies related to children's health. The Board is sincerely grateful for all of Dr. Friedman's personal and professional contributions to the State of California.

Table of Contents

List of Figures

List of Tables

Abstract

Current National Ambient Air Quality Standards for particulate matter regulate the mass concentration of particles in the atmosphere. There is growing evidence that different sources of these particles have different levels of toxicity. In this work, a system was developed for collecting source oriented particles from the atmosphere suitable for toxicity testing, as described in Chapter 2 of this report. Briefly a single particle mass spectrometer identified particle sources in real time; the mass spectrometer selected a ChemVol associated with each source category to collect size-selected PM while those particles were being observed. This system was operated in Fresno, CA during the summer of 2008 and winter of 2009. The toxicity of the collected samples was assessed in a mouse model. Samples were chemically analyzed to associate them with sources prevalent in Fresno, CA. Most of the toxicity was associated with automobile and cooking sources in both seasons while in the winter toxicity was also associated with secondary compounds.

Executive Summary

Background. Particles are emitted into the atmosphere from a wide range of natural (e.g., sea spray) and known toxic (e.g., diesel exhaust) sources. The National Ambient Air Quality Standards do not distinguish between these source since they are based solely on mass in given particle size ranges. The research carried out here was the first time that particles have been sampled from the atmosphere in a way that they can be (a) associated with sources and (b) collected in sufficient quantities to test their toxicity.

Methods. A single particle mass spectrometer (RSMS-II) sampled air in Fresno, CA during Summer of 2008 and Winter of 2009. RSMS-II was operated for three weeks in each season to characterize the mixing state of the atmosphere. Ten ChemVol samplers were controlled by the RSMS-II such that (a) only one operated at a time and (b) RSMS-II only operated each one when a pre-programmed source dominated local air pollution at any given time. This system was fully automated, operated remotely from UC Davis, and monitored and collected air pollution particles 24 hours per day for about 4 weeks in each season to collect the minimum required particulate matter on each ChemVol sample and stage. Each ChemVol had two stages collecting particles smaller than 170 nm and particles in the 170 to 1,000 nm range of aerodynamic diameter.

Novel methods were then developed to extract particulate matter from the filter and polyurethane foam substrates, so that (a) as much of the particulate matter was extracted from the substrates and (b) hydroscopic and hydrophobic compounds in the particulate matter were extracted evenly.

Mice were exposed by oropharyngeal aspiration to equal doses of ultrafine (UF) and submicron fine (SMF) source-oriented PM. At 24 hours post-aspiration, mice were examined for indicators of pulmonary and systemic inflammation and cytotoxicity.

The RSMS-II spectra were analyzed to associate ChemVol samples and stages with sources in Fresno. Chemical analysis of the metals content of the samples was performed to further bolster the reliability of this source assignment.

Results. Ten ChemVol samples were collected in Summer of 2008 and 9 in Winter of 2009. Sufficient mass of the samples were collected and extracted that they could all be assessed for their relative toxicity in an in vivo mouse model. The degree of measures of cardiopulmonary inflammation, cytotoxicity and hematology were statistically different for each source-oriented PM sample compared to control values and between source-oriented samples for a given size and season. Source-oriented PM elicited inflammatory responses that were the most significant in the lung compared to the blood at 24 hours following exposure. In general, UF PM was more pro-inflammatory compared to SMF PM.

Conclusions. Direct toxicity testing of source-oriented PM can increase understanding of the associations between adverse health effects and PM exposure. Different source-oriented and size-resolved samples of sub-micron particulate matter elicited differing levels of response in an array of toxicity measures, supporting the founding hypothesis for this study that different

sources and combinations of sources of particulate matter have different levels of toxicity. The unanticipated result was that the sources were toxic in different ways. Ultimately, these advances will contribute to more specific regulations of particulate matter in order to provide greater protection of human health.

Toxicological and epidemiological studies continue to show significant health effects at current NAAQS levels motivating continued decreases in NAAQS concentrations. But these concentrations are now approaching background levels so will be increasingly difficult and costly to attain. Ultimately, the primary purpose of the Clean Air Act is to protect human health. Since logic and substantial epidemiological evidence suggests that different sources of PM have different toxicity, the next wave of PM regulation may focus more on PM source than on overall PM mass. This report describes the toxicology of different sources of PM collected from the atmosphere for the first time, identifying vehicle and cooking emissions as of primary pulmonary health concern in Fresno, California. But Fresno has a limited range of emissions sources, so this study should be repeated in other locations in California and around the country to explore the relative toxicity of a wider range of sources.

Chapter 5 discusses the toxicological results in detail and it and Chapter 6 relate these toxicological endpoints to their sources. In summary,

- Based on particle size, UF PM was a more potent inducer of inflammatory and cytotoxic response compared to SMF PM on a per mass basis.
- For pulmonary inflammation and cytotoxicity, samples containing PM from vehicular sources or metals had the high biological response for summer samples, while PM from vehicular sources, regional processes background, and nighttime inversions had the highest response for winter samples.
- In general, the same PM sample produced greater inflammatory and cytotoxic responses in lung samples than in the blood samples under the conditions used in this study.
- Analysis of systemic inflammation did not reveal major differences between the collected samples.

Chapter 1
Introduction

Numerous epidemiological studies demonstrate that elevations in PM10 and PM2.5 are correlated to increases in acute morbidity and mortality in the population. Current research in many countries is investigating what properties of emissions lead to health effects and what health effects they cause. The Lovelace Respiratory Research Institute and others have been investigating the toxicity of emissions from sources, such as those from vehicle exhaust, but without substantial atmospheric processing (e.g., Seagrave et al., 2005). Humans do not breathe direct emissions from one source. The real atmospheric situation is much more complicated. A given urban area hosts a range of emissions sources, including light and heavy duty vehicles, power plants, entrained dust, and biomass burning, that mix in the atmosphere and are subjected to photochemical processing. Thus, humans typically breathe photochemically processed emissions from mixtures of sources.

But how can we relate the toxicity of ambient PM to the sources that emitted them? That is, there is a huge literature establishing the epidemiological association between ambient PM and health effects but that work does not indicate which sources are responsible for the health effects. Likewise, there is a huge literature on the toxicity of (a) ambient PM that is not associated with emissions sources and (b) source emissions without ambient processing.

The overall objective of this project was to obtain toxicity profiles of atmospherically processed source-oriented fine and ultrafine particulate emissions. This experiment had never been performed previously because it involved a unique combination of instruments and skills that have only recently become available and fortunately are all available at UC Davis. The underlying hypothesis was that the atmospherically processed emissions from different sources (and their differing degrees of atmospheric processing) lead to a range of acute toxicity profiles and that these profiles are different for the fine and ultrafine particle size ranges.

In this work we developed new instrumentation and performed a series of experiments in Fresno California designed to link the toxicity of ambient aerosols (particles and gases) to the source or sources that emitted them, thus providing a key link between the toxicity of ambient particles and their associated gases, and the sources that emit them.

A wide range of sources emit particles and gases that may react in the atmosphere to form particles. Since epidemiological studies show strong correlations between ambient particulate matter and adverse health effects, two questions arise: What is it about the particles that elicits health effects and what health effects are elicited? In this work, we focused our attention on the first question. More specifically we investigated the relative toxicity profile of mixtures of sources that have been processed in the atmosphere – that is, they have been exposed to the photochemical milieu of the atmosphere that may chemically and physically alter the emitted particles via a range of atmospheric processes. Measurements of the toxicity of direct emissions miss (a) the photochemical processing and (b) synergy that mixtures of particles from a range of sources may have on toxicity. Similarly, measurement of the ambient toxicity does not always lend itself to understanding the range of sources that lead to the observed toxicity. In this work, we collected source-oriented ambient samples and performed tests on them to elucidate their relative pulmonary toxicity using the same mass for each exposure.

We hypothesized that different sources, source combinations, and levels of atmospheric processing elicit different levels of pulmonary and systemic toxicity. Exploration of this

hypothesis involved the collection of source oriented ambient samples and performing pulmonary toxicity tests on them.

This was the first time that source-oriented sampling has been performed. Why is that? First, meteorological conditions change continuously. Wind speeds and directions bring different emissions to a given receptor. Inversion heights change the level of dilution. Actinic flux changes the rate of photo-oxidation of organic compounds. Humidity changes the OH radical concentration and the water content of hygroscopic particles. Second, each source has its pattern of emission depending on its activity level throughout the day. Thus a myriad combination of meteorological and emissions characteristics result in the multidimensional, wide ranging, and temporally dynamic character of particles and their co-pollutant gases observed in the atmosphere. Third, capturing this involves real-time characterization of and sampling the ambient particles, and then characterizing their pulmonary toxicity. We used our extensive experience in all of these areas to design and deploy the source-oriented sampler.

Due to development of new instrumentation and methods to carry out this work, schedules slipped many times, but in the end the work was carried out as promised in the original proposal. Chapter 2 of this report is a paper published in Environmental Science and Technology describing the sampling technique and field sampling results obtained from both seasons in Fresno. Chapter 3 describes the sample extraction protocol employed. Briefly, many protocols are available for extracting PM from filters and PUFs for toxicological and analytical studies, but they all had artifacts that may skew toxicological results. We developed a much more thorough extraction method that should better represent the material collected. In Chapter 4, we attribute the source-oriented samples and their associated toxicity to the primary and secondary sources observed in Fresno. Finally, Chapter 5 discusses the toxicity of the source-oriented samples in normal mice.

References

Seagrave, JC, JD McDonald, JL Mauderly, In vitro versus in vivo exposure to combustion emissions. Experimental and Toxicologic Pathology 57:233–238, 2005.

Chapter 2
Conditional Sampling for Source-Oriented Toxicological Studies using a Single Particle Mass Spectrometer

*K.J. Bein[1], Y. Zhao[1] and A.S. Wexler[1,2,3,4]
[1]Air Quality Research Center, [2]Mechanical and Aeronautical Engineering, [3]Civil and Environmental Engineering, and [4]Land, Air and Water Resources, University of California Davis

Published as

Bein, K.J., Y. Zhao and A.S. Wexler, Conditional Sampling for Source-Oriented Toxicological Studies using a Single Particle Mass Spectrometer. Environ. Sci. Technol. 43:9445-9452, 2009.

Abstract

Current particulate matter regulations control the mass concentration of particles in the atmosphere regardless of composition, but some primary and/or secondary particulate matter components are no doubt more or less toxic than others. Testing direct emissions of pollutants from different sources neglects atmospheric transformations that may increase or decrease their toxicity. This work describes a system that conditionally samples particles from the atmosphere depending on the sources or source combinations that predominate at the sampling site at a given time. A single particle mass spectrometer (RSMS-II), operating in the 70-150 nm particle diameter range, continuously provides the chemical composition of individual particles. The mass spectra indicate which sources are currently affecting the site. Ten ChemVol samplers are each assigned one source or source combination and RSMS-II controls which one operates depending on the sources or source combinations observed. By running this system for weeks at a time, sufficient sample is collected by the ChemVols for comparative toxicological studies. This paper describes the instrument and algorithmic design, implementation and first results from operating this system in Fresno California during summer 2008 and winter 2009.

1. **Introduction**

Although air pollution regulations save the US economy billions of dollars per year, these same regulations are costly to industry and consumers (*1*). One reason for the high cost is that all sources of particulate matter (PM) are subject to controls regardless of their relative toxicity. Epidemiological studies have implicated PM in increased morbidity and mortality in many cities (*2*), which motivates the regulations. Although these types of studies have also shown correlation between certain health effects and particular sources (*3*), in many cases the literature lacks toxicological support. Efforts to understand the relative toxicity of different sources of air pollution have been performed on direct emissions from select sources, whereby the animals breathe the gases and particles, individually or together (*4*). By design, these studies do not include inevitable atmospheric processing and multi-source effects that may alter the toxicity of the inhaled mixture. The relative toxicity of different sources may arise out of their atmospheric processing, possibly in the form of secondary components or in other ways not yet understood. Unfortunately, once the emissions have entered the atmosphere where they mix, react and form secondary compounds, their source may be obscured so separating them from each other is problematic. Single particle measurements in several US cities, however, have indicated that on sufficiently short time scales parcels of air pollutants associated with different sources are potentially separable (*5-11*).

Single particle mass spectrometers practical for the atmospheric science community were introduced nearly 20 years ago (*12, 13*). These instruments analyze the chemical composition and size of particles one-by-one in real time. The Rapid Single-ultrafine-particle Mass Spectrometer family (RSMS-II and RSMS-III) analyze particles in the size range from 30 nm to 1 μm (*14*) and were deployed at the Atlanta, Houston, Baltimore and Pittsburgh EPA Supersites (*6, 8, 9, 11*) . Measurements from all four cities revealed that at most 3 different particle types, indicating three different sources, are observed at the same time. Layered on these source-oriented particles are secondary components that add to their chemical complexity, but relative amounts of such secondary material can also be discerned by single particle analysis.

The technique described here uses RSMS-II to control a bank of ChemVols (*15*). By taking advantage of the temporal patterns of PM observed in urban air sheds, each ChemVol samples when particles from a unique source or source combination affect the site, such that a sufficiently large sample is collected over the course of weeks that it can be bulk analyzed and used for toxicological studies. This work presents the experimental design and how it was implemented in summer 2008 and winter 2009 to collect milligrams of source-oriented PM in Fresno, California.

2. **Experimental Design**

In this section, the basic constructs used to define the compositional state of the atmosphere and to identify transitions between states are set forth, followed by a brief description of the ChemVol sampling train. For the former, particle composition was the sole metric employed and the output of RSMS-II was translated into a snapshot of the

mixing state of the atmosphere using a multi-tiered cluster analysis. A brief description of RSMS-II, which has been described elsewhere (*9, 14*), and details of how system components were interfaced to achieve conditional sampling – including sampling algorithms, runtime parameters and real-time data flow – are provided in Supporting Information.

Data Constructs

Data clustering is common to many fields of study and has found widespread use in single particle mass spectrometry due mainly to the size of the datasets and complexity of the data (*6, 16*). The fundamental goal of clustering is to partition datasets into **particle classes**, or subpopulations, based on the distribution of mass spectral peaks with the understanding that different classes correspond to different particle compositions. Particle composition is the most revealing signature of the source and history of particles (*5, 6, 8*). In this sense, a particle class can be thought of as being synonymous with a source and/or process. This is essential to any real-time estimate of the mixing state of the atmosphere, in terms of source input and composition, and thus provides the impetus for the work being presented here.

Rarely do continuous single particle observations reveal the same particle type, or class, for any significant duration. Some exceptions include isolated events when a single source impacts a site, typically driven by meteorological conditions such as wind or nocturnal inversions (*7, 10, 17*). This is exacerbated, however, by the fact that even single sources, or source categories, can emit multiple types of particles with different compositional signatures, as well as the potential for secondary processing. As a result, it is far more common that a mixture of particle types is observed in some alternating succession such that responding to each particle observation in an attempt to conditionally sample PM is an ineffective strategy. The approach adopted for the current work is to search for mixtures, or combinations of particle classes, that appear with some degree of consistency in relative proportions over a predefined time period.

In this effort, the concept of a **particle class combination** is introduced. Since RSMS-II is a real-time instrument, single particle observations – each corresponding to a specific particle class – are sequential. Analyzing this chronological sequence of classes over sufficiently long periods reveals that certain combinations of classes frequently appear together in repeatable proportions. Consider, for instance, the situation where a sampling site is downwind of a freeway lined by restaurants with meat broilers so that both sources are observed together in some proportion. This near coincident observation of particles from different classes – i.e. different sources in this case – together is termed a class combination. It is parcels of air associated with these class combinations that are sampled by the ChemVols.

Mathematically, class combinations are represented by vectors where each dimension in the vector corresponds to a different particle class and the magnitude of the dimension is proportional to the relative number of times that class was observed in a given time interval. As single particle mass spectra are acquired, they are assigned to a particle class.

At some point, the timestamp of the current single particle observation is used to go back in time and compile all observations within a specified time interval. For this subpopulation, the number of observations in each particle class is summed, the sum is binned into its respective dimension in the class combination vector for this time period and the resulting vector normalized, thus generating a unit class combination vector.

Going forward in time, a new class combination vector is constructed after a specified number of particles, beginning with the last observation of the current class combination, have been observed. The process is continuously reiterated to provide a rolling snapshot of the mixing state of the atmosphere. In application, two parameters – the time interval for constructing class combination vectors and the number of single particle observations between successive class combination vectors – must be tuned with respect to the underlying single particle analysis rate (or hit rate) to provide temporal overlap so that transitions between states can be realized.

Executing this type of experiment is facilitated by a pre-study, where the single particle instrument is deployed alone collecting data for several days to weeks to characterize the mixing state of the air shed. Pre-study data are then analyzed to identify the dominant particle classes and class combinations, which are subsequently used to make ChemVol assignments and construct libraries prior to the actual collection of source-oriented PM. A description of the pre-study analysis is given in Supporting Information.

ChemVol Sampling Train

ChemVol samplers were developed more than 6 years ago to collect ambient, size-resolved PM (*15*). They are impactor-based samplers with annular slots, where the width of the slot, in part, determines the range of particle diameters transmitted through the stage. Impactor stages are available for a range of size cuts and operate at 900 lpm for large volume sampling. For efficiency of notation, ChemVol stages will be referred to by particle diameter, with the understanding that the 50% cutoff diameter of the impactor stage is being referenced.

The ChemVols used in this study were obtained from Harvard University. The original characterization of the 0.1 μm stage (*15*) was retested using a more robust procedure, revealing that the value for the 50% cut-point diameter is actually 0.17 μm (P. Koutrakis, personal communication 2008).

Since the goal of the current study was to investigate the relative toxicity of fine and ultrafine source-oriented PM, coarser particles were removed using 2.5 μm and 1 μm stages. The subsequent 0.17 μm stage collected what will be termed submicron fine PM – that is, particles with diameters nominally between 0.17 and 1 μm – while an afterfilter collected particles smaller than 0.17 μm in diameter, referred to here as ultrafine PM.

The ChemVol sampling train is detailed in Supporting Information so only a brief overview is provided here. Following the air flow, the basic components include: *(a)* sampling stack, *(b)* bank of ten ChemVol stacks, where each stack includes an afterfilter

support and 0.17 and 1 μm stages, *(c)* solenoid valves attached to each afterfilter support and *(d)* blower assembly. ChemVol stacks are connected together via upstream and downstream manifolds. The solenoid valves are controlled by the algorithm detailed in Supporting Information and determine which stack is sampling at a given time.

3. **Results and Discussion**

The summer 2008 and winter 2009 experiments, both consisting of a pre-study followed by ChemVol sampling, were conducted in the rear parking lot of the UC Center in Fresno, CA. All single particle results are presented together in this section with an emphasis on system performance, proof of concept and sources of uncertainty. A robust treatment of source attribution, atmospheric composition and air quality dynamics in the Fresno air shed is outside the scope of this paper.

Metadata

Several adjustments were made to the algorithms and runtime parameters prior to winter 2009 based on knowledge gained during summer 2008. Furthermore, the sampling strategy was modified to accommodate seasonal effects on atmospheric composition and the performance of the single particle mass spectrometer. These differences will be addressed below. The different runtime parameters and metadata for the two experiments are given in Tables S1 and S2, Supporting Information, respectively. The distribution of single particle observations among the particle classes constructed based on the pre-study data are shown in Figure 2-1.

For summer 2008, the classification scheme was straightforward and particle classes were constructed based on the constituents consistently observed together in individual particles, thus representing different sources and degrees of atmospheric processing. There was a shift in the distribution of particle observations during ChemVol sampling relative to the pre-study, which was due to the effects of seasonal changes (see Figure 2-1). During winter 2009, however, the classification was designed to separate particles based on the relative amounts of primary versus secondary components and the nature of the carbon content. Also, there was very little shift in the distribution of particle observations during ChemVol sampling relative to the pre-study. The winter particle classes are described below:

- **MsC** – particles with small metal seeds and large amounts of carbonaceous material, where the presence of a primary metal seed indicates that the carbon condensed and thus is organic in nature.
- **CAN** – carbonaceous ammonium nitrate, where there are no primary metal seeds, indicating the presence of soot in the absence of nucleation, and the carbon to nitrate signal ratio falls in the 0.5-3 range.
- **EC** – elemental carbon, or soot, with very little evidence of any organic carbon
- **MCAN** – primary metal particles with various amounts of organic carbon and ammonium nitrate, where the distribution of ion signal among the constituents is, on average, about equal.
- **PMP** – primary metal particles having no traces of any secondary components.

- **Carbon** – particles composed entirely of carbonaceous material; no metal seeds or ammonium nitrate and the ratio of EC to OC is unknown.

Analyses of the particle classes observed in the pre-studies resulted in seven separate ChemVol assignments for summer 2008 and six for winter 2009, referenced as ChemVols 1-7 and 1-6. The actual class combinations associated with each ChemVol are shown in the following section and were selected based on: *(1)* the temporal distribution and frequency of observation, *(2)* the amount of sampling time required to collect the target mass for toxicological studies and *(3)* the significance of differences between class combinations. For both experiments, ChemVol 10 (termed the auxiliary ChemVol) was used when the composition of the atmosphere was unknown (see Supporting Information) and ChemVol 9 was used during RSMS downtime; i.e. it was timed to capture the contents of the mixed layer, sampling daily from ~ 09:00-17:00 local time. ChemVol 8 was not used during summer but was timed to correlate with morning rush hour traffic during winter, sampling daily from 06:00-09:00 during RSMS downtime. ChemVol 7 was only used towards the end of the winter experiment and sampled daily from 17:00-20:00.

For each ChemVol and experiment, single particle statistics and gravimetric analysis are provided in Table S3 and SMPS data in Table S4, Supporting Information. Results are summarized as follows: *(a)* not including the auxiliary and timed ChemVols, the majority of sampling was through ChemVols 1 and 2 during summer and more evenly distributed during winter, *(b)* particles and class combinations were analyzed at an average rate of one every 20 ± 2 and 90 ± 20 seconds, respectively, for summer and 3.8 ± 0.9 and 12 ± 2 seconds for winter, *(c)* mass collection rates scale approximately linearly to 1/3 milligram per hour at a concentration of 6 $\mu g/m^3$, e.g. 1/3 mg in 2 hours at 3 $\mu g/m^3$, *(d)* during summer, sampling was marginal for ChemVols 3 and 4 and poor for 5 and 7 due to the effect of seasonal changes on atmospheric composition, *(e)* with the exception of the timed ChemVols, the average number distributions ($dN/dlogD_p$) were similar in form with a leading shoulder at ~ 30-40 nm and a dominant mode at ~ 70-90 nm, *(f)* ultrafine number concentrations were a factor of ~ 2-3 times greater in winter than summer, owing to the disparities in the analysis rates of comment *b*, as well as the ultrafine mass collection rates, *(g)* for winter, ultrafine number concentrations were roughly a factor of 3 lower for ChemVols 8 and 9 due to the effects of boundary layer dynamics, and *(h)* the SMPS estimates of collected PM mass are surprisingly accurate for winter with an average measure-to-estimate ratio of 1.1 ± 0.3 over all ChemVol stages.

Fidelity

This section addresses the fidelity and accuracy of the ChemVol sampling algorithms in replicating the class combinations constructed from the pre-study data and clustering the single particle observations according to the pre-study classification. Figures 2 and 3 show side-by-side comparisons of the pre-study pooled within-cluster average class combination vectors and the ChemVol-composite class combination vectors for summer and winter, respectively. The latter were constructed post-experiment by compiling particle observations by ChemVol sampling interval, summing and binning by particle

class dimension over all sampling intervals independently for each ChemVol and then normalizing.

ChemVols 1, 2 and 6 from summer and all ChemVols from winter are in good accord with the pre-study data. Accuracy decreases for summer ChemVols 3, 4 and 7 due to a shift in the atmospheric composition and the lower class combination similarity threshold used during summer. For example, the relative shift in the distribution of EC, K and CAN particles from the pre-study to ChemVol sampling (Figure 2-1) is evident in an altered ChemVol 3 mixture (Figure 2-2). Class combinations with larger K and CAN contributions still satisfied the similarity threshold and thus diluted the EC factor. Similarly, the relative drop in EC/OC particles is apparent in the loss of this factor from the ChemVol 4 mixture. This was remedied during winter by increasing the similarity threshold, along with greater temporal stability in the particle class distribution.

Dot products are used to compare the spectrum vectors and class combination vectors observed during ChemVol sampling to those in the cluster and class combination libraries. Since all vectors are normalized, perfect agreement gives a dot product of one. The comparisons are summarized in Tables 2-1 and 2-2 for summer and winter, respectively. Only the top 7 particle classes, accounting for 94% of the single particle observations, are shown for summer. In all cases, intra-matrix trends reveal maxima along the diagonal and minima for off -diagonal averages and vice versa for standard deviations, indicating: *(a)* a high degree of intra-cluster similarity with little spread, i.e. accurate and dense clusters, and *(b)* low inter-cluster similarities with large spread, i.e. widely distributed and dissimilar particle classes and class combinations.

The apparent inter-matrix variation in the relative difference between the diagonal and off-diagonal values, as well as the absolute magnitudes, must be interpreted with caution since the dot product is not invariant under a change in data dimensionality; cluster/spectrum vectors have 256 dimensions while summer and winter class combination vectors had 12 and 6, respectively. In general, the spread in the intra-dataset distribution of dot products increases with increasing dimensionality since there is more opportunity for two data points to be different. Statistically, increasing the number of independent random variables in a system decreases the probability that any two realizations of the variables will be similar, thereby increasing the probability of dissimilarity, as well as the spread in the distribution of dissimilarity. Therefore, inter-matrix variations in Tables 1 and 2 can be misleading about the relative degree of similarity or dissimilarity between the various particle classes and class combinations from one dataset to the next.

Heterogeneity and Temporal Stability

Spatiotemporal heterogeneity in the mixing state of the Fresno air shed is now explored by considering the frequency and duration of different composition mixture observations. The metric used is the cumulative fraction of total ChemVol sampling time as a function of the number of successive class combination observations per sampling interval, with the understanding that greater numbers of successive observations generally indicate

greater temporal stability in the observed mixture. Figure 2-4 shows these data for various ChemVols from summer and winter highlighting the spread in the observed trends.

During summer, sampling largely alternated between ChemVols 1 and 2 – which represent essentially orthogonal class combinations (Figure 2-2) – and individual sampling intervals were long in duration with large numbers of successive class combination observations. For example, approximately 10% of the ChemVol 2 mass was collected in a single sampling interval lasting 2.9 hours and consisting of 678 consecutive class combination observations. Similar numbers exist for ChemVol 1. Other mixtures like ChemVols 3 and 4, however, were observed far less frequently and for shorter intervals with very few successive observations. Slightly higher stability was observed for ChemVol 6. In total, these data suggest small pockets, or filaments, of compositional heterogeneity in an otherwise relatively homogenous mixture that alternates between two states dominated by very different single particle compositions.

The situation was significantly different during winter. Although there was still an order of prevalence in the observation of different ChemVol mixtures (shown in decreasing order in Figure 2-4), the frequency and duration were more evenly spread over all ChemVols with moderate numbers of successive class combination observations. These trends indicate an atmospheric patchwork of partially mixed air masses under a nocturnal inversion that are slowly transitioning to background homogeneity but still maintain some degree of source integrity so that transient periods of unique mixture are observed as they are advected past the site.

Expansion in application to more accommodating air sheds is a key area of interest in the advancement of this technique. Fresno is perhaps one of the more challenging test sites given the general absence of large point sources and relatively stagnant meteorological conditions. Other urban areas, particularly in the eastern U.S., encompass large and varied point sources and winds are often highly directional, thereby facilitating the collection of source-oriented PM. Therefore, the degree of success achieved in Fresno is very encouraging in terms of accomplishing the same in other major urban areas.

Boundary Condition Uncertainties

Sampling uncertainties are associated with the conditions that trigger ChemVol switching at the temporal boundaries of individual sampling intervals. Given a certain ChemVol sampling interval, there are three ways to trigger a switch, either to another ChemVol or to the auxiliary ChemVol. The first occurs when too much time has elapsed between successive single particle observations and is termed a timeout. In this case, the system triggers the auxiliary ChemVol and the time elapsed, or mass sampled, between the last observation and the trigger represents a potential source of uncertainty. Timeouts result from low number concentrations so mass sampling rates are lowest during these periods, helping minimize potential contamination of the ChemVol mixture.

The latter two, however, deal with transitions in mixing state; i.e. the transition from one ChemVol mixture to another. During this process, the evolving class combination falls below the similarity threshold of the current ChemVol, remains in an intermediate state for some period, and then passes the similarity threshold of a different ChemVol. Since transitions can occur rapidly, it is possible the entire process takes place between successive class combination observations, triggering a direct ChemVol-to-ChemVol switch without first passing through the auxiliary ChemVol. In this case, the time interval between successive observations is a potential source of uncertainty for both ChemVols. For the target ChemVol, this can be avoided – as was done during winter – by requiring at least two successive observations of the associated class combination before triggering the switch, forcing all transitions through the auxiliary ChemVol. Although this minimizes uncertainty for the destination ChemVol, it does not do so for the source ChemVol. Exactly analogous to the case where the similarity violation is directly observed and the auxiliary ChemVol instantly triggered, the potential uncertainty is the time interval, or mass sampled, from the most recent class combination observation to the actual particle that caused the violation.

As alluded to above, sampling uncertainties can be interpreted from the perspective of mass sampled or sampling time; i.e. the ratio of mass sampled during periods of uncertainty to the total mass sampled by each ChemVol, or the fraction of total sampling time associated with periods of uncertainty. Although estimating mass is straightforward using SMPS data, it is not clear what fraction of that mass, if any, actually contaminates the ChemVol mixture. The situation is further complicated by the fact that mixture contaminating particles from one sampling interval can partially offset the effect of those from another sampling interval so overall uncertainty is not a superposition of the individual intervals. In this sense, and from a single particle perspective, analysis of transition uncertainties is pointless since the ChemVol-composite class combination vectors shown in Figures 2 and 3, which include all particle observations, are the most accurate depictions available for the true ChemVol contents. Discrepancies with the pre-study data, although possibly transition related, are collectively interpreted as an indicator of sampling, or clustering, accuracy.

Therefore, sampling time – interpreted as relating to single particle analysis rather than mass sampled and thus consistent with experimental design – is the more appropriate uncertainty metric. More specifically, the time period at the end of each sampling interval between the last single particle observation and the ChemVol trigger relative to the single particle analysis rate. Summing over all sampling intervals and dividing by total sampling time independently for each ChemVol, uncertainty estimates are provided below in the following format: ChemVol # (percent uncertainty).

- Summer 2008: 1(6.9); 2(6.6); 3(14.8); 4(15.2); 5(13.4); 6(8.8); 7(15.0)
- Winter 2009: 1(4.9); 2(9.7); 3(11.1); 4(5.9); 5(9.2); 6(7.9)

The average percent uncertainty across all ChemVols is 12 ± 4% and 8 ± 2% for summer and winter, respectively. These numbers are measurement uncertainties, not error estimates of the ChemVol contents

Finally, it is important to understand that this experiment is not based on the true composition of the atmosphere, but rather on single particle mass spectral observations of the atmosphere. The question remains whether this realization, including its uncertainties and inaccuracies, is sufficient to elicit relative differences in toxicology based on the data constructs used to define different atmospheric composition mixtures and the precision of current toxicological techniques. There is certainly a large gap between estimating the relative influence of different sources and atmospheric processes and robustly measuring precise atmospheric composition. The motivation here is simply to use the technology available to begin separating out different components of atmospheric mixtures as best as possible with an underlying objective of narrowing in on the validity of the source-oriented relative toxicity hypothesis, which if true could redefine the way air pollution is regulated to protect human health.

Acknowledgements

This work was supported by the California Air Resources Board, Electric Power Research Institute and U.S. Environmental Protection Agency. Although the research described in the article has been funded wholly or in part by the U.S. Environmental Protection Agency through grant RD-83241401-0 to the University of California, Davis, it has not been subject to the Agency's required peer and policy review and therefore does not necessarily reflect the views of the Agency and no official endorsement should be inferred. The statements and conclusions in this publication are those of the contractor and not necessarily those of the California Air Resources Board. The mention of commercial products, their source, or their use in connection with material reported herein is not to be construed as actual or implied endorsement of such products. The authors gratefully acknowledge the help of Van Van Vleet and cooperation of the UC Center Fresno in hosting, managing and securing the sampling site.

Supporting Information Available

Details, schematics and pictures of the instrumentation, data analyses, sampling algorithms and real-time data flow are provided in Supporting Information, as well as detailed metadata for the summer 2008 and winter 2009 experiments. This information is available here on pages 26-47 and free of charge via the Internet at http://pubs.acs.org/.

References

1. Krupnick, A. J.; Portney, P. R. Controlling urban air-pollution - a benefit-cost assessment. *Science* **1991,** 252 (5005), 522-528.

2. Pope, C. A.; Burnett, R. T.; Thurston, G. D.; Thun, M. J.; Calle, E. E.; Krewski, D.; Godleski, J. J. Cardiovascular mortality and long-term exposure to particulate air pollution - epidemiological evidence of general pathophysiological pathways of disease. *Circulation* **2004,** 109 (1), 71-77.

3. Lanki, T.; de Hartog, J. J.; Heinrich, J.; Hoek, G.; Janssen, N. A. H.; Peters, A.; Stolzel, M.; Timonen, K. L.; Vallius, M.; Vanninen, E.; Pekkanen, J. Can we identify sources of fine particles responsible for exercise-induced ischemia on days with elevated air pollution? The ultra study. *Environmental Health Perspectives* **2006,** 114 (5), 655-660.

4. Mauderly, J. L.; Samet, J. M. Is there evidence for synergy among air pollutants in causing health effects? *Environmental Health Perspectives* **2009,** 117 (1), 1-6.

5. Pekney, N. J.; Davidson, C. I.; Bein, K. J.; Wexler, A. S.; Johnston, M. V. Identification of sources of atmospheric PM at the Pittsburgh Supersite, part I: Single particle analysis and filter-based positive matrix factorization. *Atmospheric Environment* **2006,** 40, S411-S423.

6. Bein, K. J.; Zhao, Y.; Wexler, A. S.; Johnston, M. V. Speciation of size-resolved individual ultrafine particles in Pittsburgh, Pennsylvania. *Journal of Geophysical Research-Atmospheres* **2005,** 110 (D7).

7. Bein, K. J.; Zhao, Y.; Johnston, M. V.; Wexler, A. S. Interactions between boreal wildfire and urban emissions. *Journal of Geophysical Research-Atmospheres* **2008,** 113 (D7).

8. Phares, D. J.; Rhoads, K. P.; Johnston, M. V.; Wexler, A. S. Size-resolved ultrafine particle composition analysis - 2. Houston. *Journal of Geophysical Research-Atmospheres* **2003,** 108 (D7).

9. Rhoads, K. P.; Phares, D. J.; Wexler, A. S.; Johnston, M. V. Size-resolved ultrafine particle composition analysis, 1. Atlanta. *Journal of Geophysical Research-Atmospheres* **2003,** 108 (D7).

10. Bein, K. J.; Zhao, Y.; Johnston, M. V.; Wexler, A. S. Identification of sources of atmospheric PM at the Pittsburgh Supersite. Part III: Source characterization. *Atmospheric Environment* **2007,** 41 (19), 3974-3992.

11. Lake, D. A.; Tolocka, M. P.; Johnston, M. V.; Wexler, A. S. Mass spectrometry of individual particles between 50 and 750 nm in diameter at the Baltimore Supersite. *Environmental Science & Technology* **2003,** 37 (15), 3268-3274.

12. McKeown, P. J.; Johnston, M. V.; Murphy, D. M. Online single-particle analysis by laser desorption mass-spectrometry. *Analytical Chemistry* **1991,** 63 (18), 2069-2073.

13. Wexler, A. S.; Johnston, M. V., Real-time single-particle analysis. In *Aerosol measurement principles, techniques, and applications*, ed.; Baron, P. A.; Wileke, K., 'Ed.'^'Eds.' John Wiley & Sons: New York, NY, 2001; 'Vol.' Chapter 13, p^pp 365-386.

14. Phares, D. J.; Rhoads, K. P.; Wexler, A. S. Performance of a single ultrafine particle mass spectrometer. *Aerosol Science and Technology* **2002,** 36 (5), 583-592.

15. Demokritou, P.; Kavouras, I. G.; Ferguson, S. T.; Koutrakis, P. Development of a high volume cascade impactor for toxicological and chemical characterization studies. *Aerosol Science and Technology* **2002,** 36 (9), 925-933.

16. Zhao, W. X.; Hopke, P. K.; Prather, K. A. Comparison of two cluster analysis methods using single particle mass spectra. *Atmospheric Environment* **2008,** 42 (5), 881-892.

17. Bein, K. J.; Zhao, Y.; Johnston, M. V.; Evans, G. J.; Wexler, A. S. Extratropical waves transport boreal wildfire emissions and drive regional air quality dynamics. *Journal of Geophysical Research-Atmospheres* **2008,** 113 (D23).

Table 2-1. Average dot product matrices comparing the spectrum vectors (top) and class combination vectors (bottom) observed during ChemVol sampling (horizontal) to the vectors in the cluster and class combination libraries constructed from the pre-study data (vertical) for the summer 2008 experiment.

Pre-study	**ChemVol Sampling (average dot product ± 1 standard deviation)**						
Class	EC	K	CAN	EC/OC	Na/K	K/C	Ca/C
EC	**0.93 ± 0.06**	0.23 ± 0.06	0.26 ± 0.08	0.27 ± 0.08	0.27 ± 0.1	0.4 ± 0.1	0.32 ± 0.06
K	0.2 ± 0.1	**0.93 ± 0.04**	0.2 ± 0.1	0.273 ± 0.09	0.2 ± 0.1	0.3 ± 0.1	0.2 ± 0.1
CAN	0.26 ± 0.09	0.25 ± 0.09	**0.92 ± 0.05**	0.234 ± 0.09	0.3 ± 0.2	0.3 ± 0.1	0.3 ± 0.2
EC/OC	0.4 ± 0.2	0.31 ± 0.06	0.32 ± 0.08	**0.90 ± 0.04**	0.33 ± 0.08	0.6 ± 0.1	0.28 ± 0.06
Na/K	0.30 ± 0.08	0.26 ± 0.05	0.31 ± 0.06	0.25 ± 0.08	**0.96 ± 0.03**	0.4 ± 0.1	0.42 ± 0.04
K/C	0.4 ± 0.1	0.27 ± 0.07	0.3 ± 0.1	0.42 ± 0.08	0.3 ± 0.1	**0.95 ± 0.03**	0.27 ± 0.08
Ca/C	0.3 ± 0.1	0.29 ± 0.06	0.34 ± 0.06	0.24 ± 0.07	0.5 ± 0.1	0.35 ± 0.09	**0.93 ± 0.04**
ChemVol	1	2	3	4	5	6	7
1	**0.86 ± 0.06**	0.5 ± 0.2	0.3 ± 0.1	0.52 ± 0.09	0.4 ± 0.2	0.39 ± 0.07	0.4 ± 0.1
2	0.3 ± 0.1	**0.83 ± 0.05**	0.2 ± 0.1	0.56 ± 0.07	0.3 ± 0.1	0.3 ± 0.1	0.4 ± 0.1
3	0.44 ± 0.08	0.6 ± 0.1	**0.88 ± 0.06**	0.47 ± 0.09	0.72 ± 0.09	0.46 ± 0.06	0.6 ± 0.1
4	0.4 ± 0.1	0.6 ± 0.2	0.4 ± 0.1	**0.78 ± 0.08**	0.5 ± 0.2	0.3 ± 0.1	0.4 ± 0.1
5	0.42 ± 0.09	0.6 ± 0.1	0.59 ± 0.06	0.65 ± 0.09	**0.83 ± 0.06**	0.44 ± 0.08	0.6 ± 0.1
6	0.4 ± 0.1	0.4 ± 0.1	0.3 ± 0.1	0.5 ± 0.1	0.3 ± 0.1	**0.80 ± 0.08**	0.4 ± 0.1
7	0.38 ± 0.09	0.5 ± 0.2	0.3 ± 0.2	0.4 ± 0.1	0.4 ± 0.2	0.3 ± 0.1	**0.73 ± 0.08**

Table 2-2. Average dot product matrices comparing the spectrum vectors (top) and class combination vectors (bottom) observed during ChemVol sampling (horizontal) to the vectors in the cluster and class combination libraries constructed from the pre-study data (vertical) for the winter 2009 experiment.

Pre-study	**ChemVol Sampling (average ± 1 standard deviation)**					
Class	MsC	CAN	EC	MCAN	PMP	Carbon
MsC	**0.98 ± 0.01**	0.43 ± 0.05	0.61 ± 0.04	0.54 ± 0.03	0.12 ± 0.03	0.19 ± 0.05
CAN	0.43 ± 0.05	**0.98 ± 0.02**	0.5 ± 0.1	0.52 ± 0.07	0.13 ± 0.03	0.17 ± 0.05
EC	0.61 ± 0.04	0.38 ± 0.05	**0.98 ± 0.02**	0.52 ± 0.03	0.12 ± 0.04	0.17 ± 0.08
MCAN	0.54 ± 0.03	0.4 ± 0.1	0.60 ± 0.09	**0.98 ± 0.02**	0.21 ± 0.06	0.4 ± 0.2
PMP	0.12 ± 0.03	0.1 ± 0.1	0.35 ± 0.07	0.31 ± 0.07	**0.98 ± 0.02**	0.5 ± 0.2
Carbon	0.19 ± 0.05	0.43 ± 0.06	0.59 ± 0.04	0.52 ± 0.03	0.11 ± 0.02	**0.99 ± 0.01**
ChemVol	1	2	3	4	5	6
1	**0.93 ± 0.03**	0.7 ± 0.2	0.5 ± 0.1	0.7 ± 0.2	0.5 ± 0.1	0.71 ± 0.08
2	0.6 ± 0.1	**0.93 ± 0.03**	0.4 ± 0.1	0.5 ± 0.2	0.47 ± 0.07	0.5 ± 0.1
3	0.6 ± 0.2	0.6 ± 0.2	**0.93 ± 0.03**	0.5 ± 0.2	0.4 ± 0.1	0.6 ± 0.1
4	0.66 ± 0.09	0.5 ± 0.1	0.44 ± 0.09	**0.94 ± 0.03**	0.46 ± 0.06	0.4 ± 0.1
5	0.6 ± 0.1	0.7 ± 0.2	0.5 ± 0.1	0.6 ± 0.2	**0.93 ± 0.03**	0.5 ± 0.1
6	0.72 ± 0.08	0.5 ± 0.2	0.5 ± 0.1	0.5 ± 0.1	0.4 ± 0.1	**0.93 ± 0.04**

Figure Captions

2-1. The distribution of single particle observations among the particle classes constructed based on the pre-study analysis for both the pre-study and ChemVol sampling periods of the summer 2008 and winter 2009 experiments. For the summer 2008 experiment, particle classes are labeled by their single particle constituents, where EC stands for elemental carbon, OC is organic carbon, AN is ammonium nitrate, and C is shorthand notation for EC/OC when observed together with other components such as metals and AN. See the text for a description of the winter 2009 particle classes.

2-2. Side-by-side comparisons of the pre-study pooled within-cluster average class combination vectors (± 1 standard deviation) and the ChemVol-composite vectors for the summer 2008 experiment. The dot products (DP) between the two vectors are listed.

2-3. Side-by-side comparisons of the pre-study pooled within-cluster average class combination vectors (± 1 standard deviation) and the ChemVol-composite vectors for the winter 2009 experiment. The dot products (DP) between the two vectors are listed.

2-4. The cumulative fraction of total sampling time (y-axis) as a function of the number of successive class combination observations per sampling interval (x-axis) for select ChemVols from the summer 2008 (S'08) and winter 2009 (W'09) experiments. Note that each figure uses a different x-axis scaling.

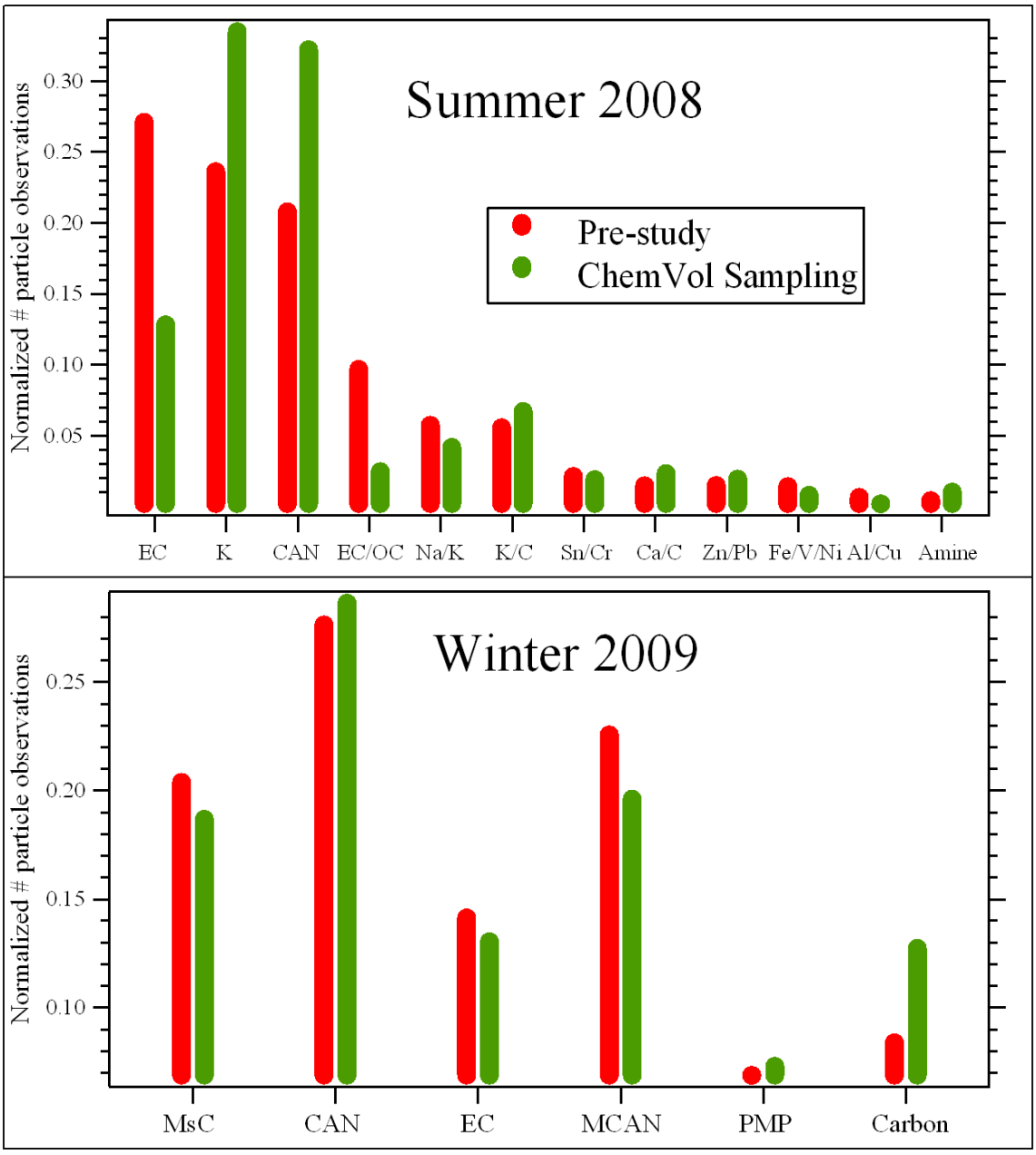

Figure 2-1. The distribution of single particle observations among the particle classes constructed based on the pre-study analysis for both the pre-study and ChemVol sampling periods of the summer 2008 and winter 2009 experiments. For the summer 2008 experiment, particle classes are labeled by their single particle constituents, where EC stands for elemental carbon, OC is organic carbon, AN is ammonium nitrate, and C is shorthand notation for EC/OC when observed together with other components such as metals and AN. See the text for a description of the winter 2009 particle classes.

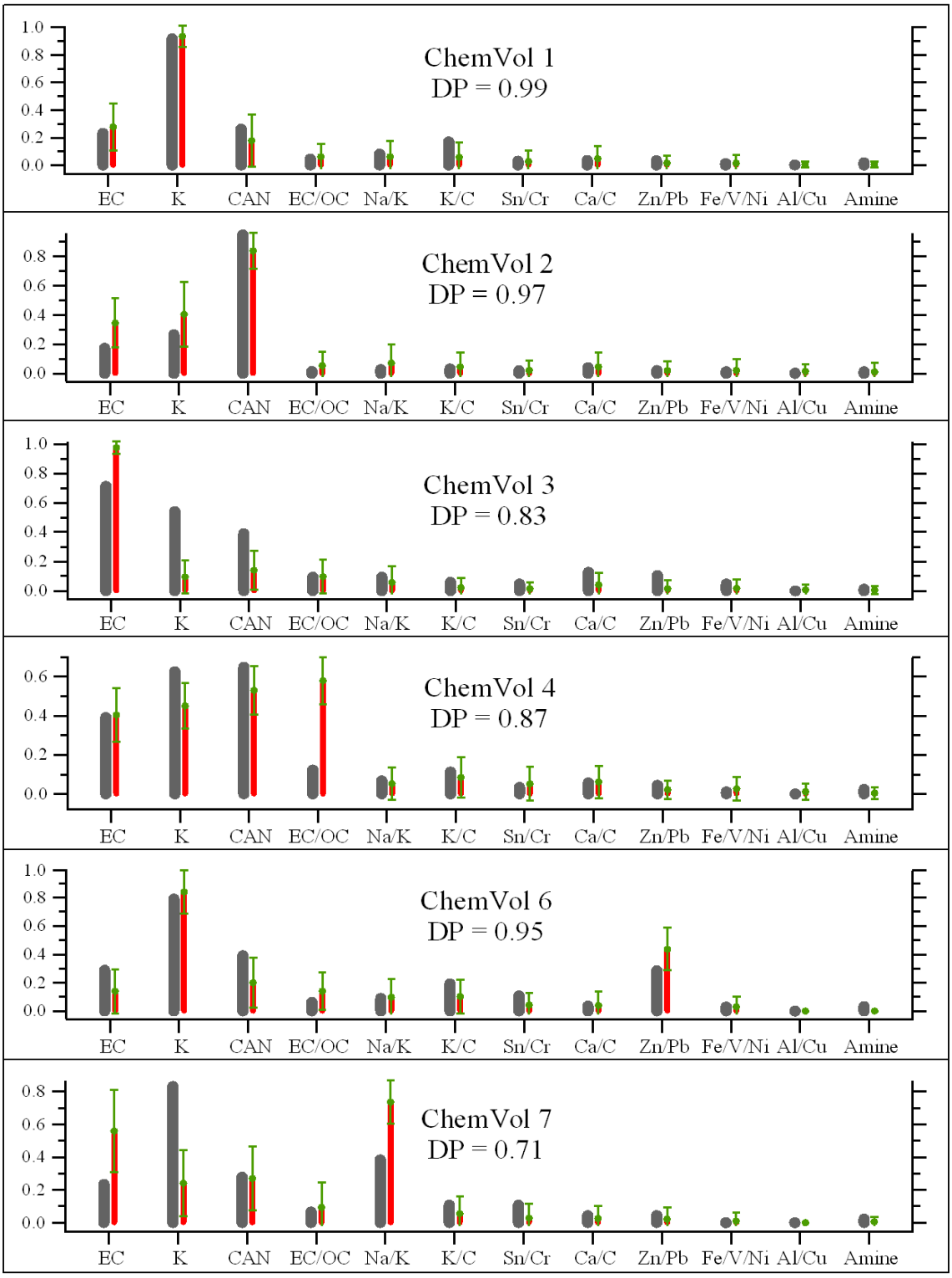

Figure 2-2. Side-by-side comparisons of the pre-study pooled within-cluster average class combination vectors (± 1 standard deviation) and the ChemVol-composite vectors for the summer 2008 experiment. The dot products (DP) between the two vectors are listed.

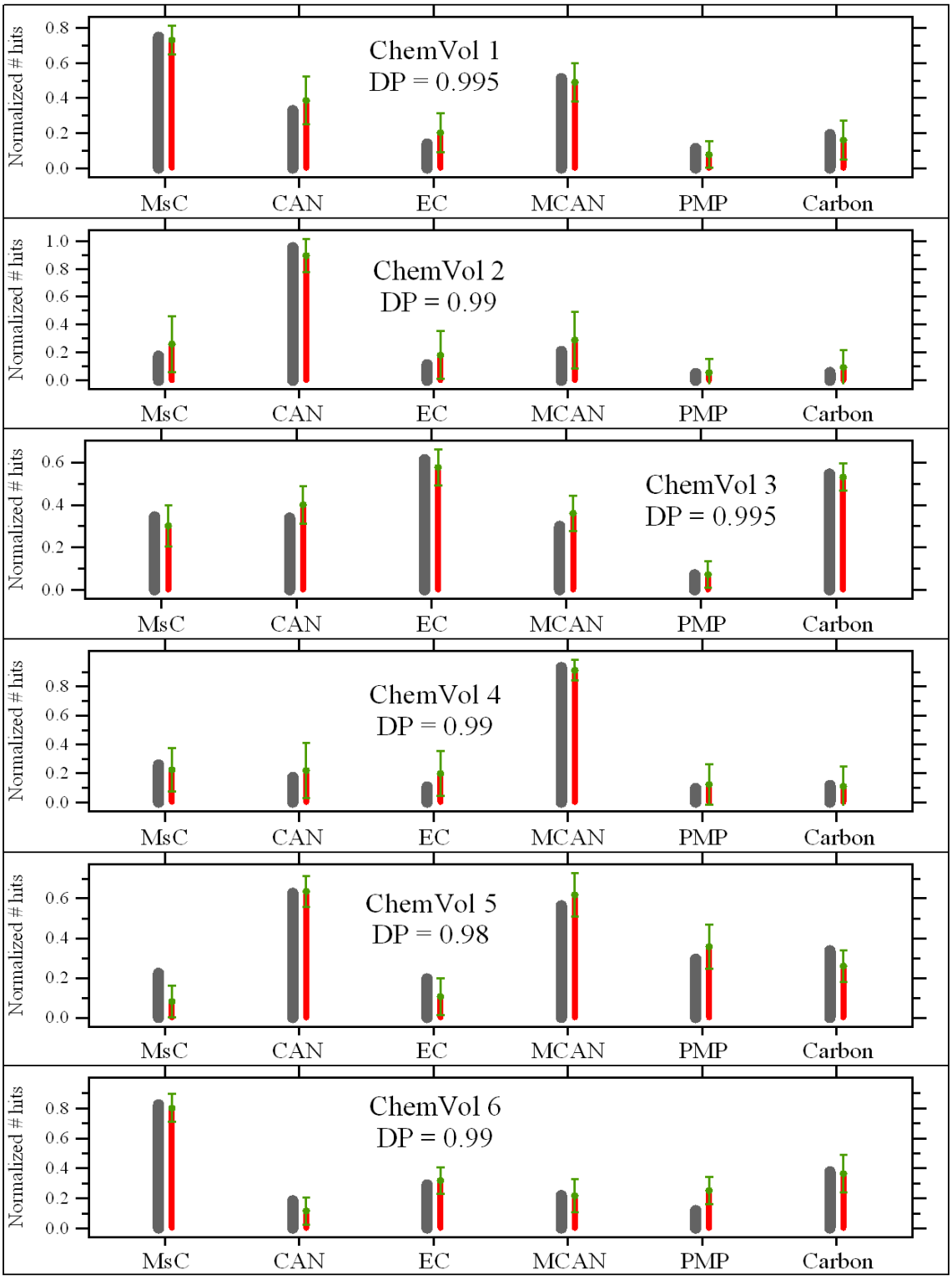

Figure 2-3. Side-by-side comparisons of the pre-study pooled within-cluster average class combination vectors (± 1 standard deviation) and the ChemVol-composite vectors for the winter 2009 experiment. The dot products (DP) between the two vectors are listed.

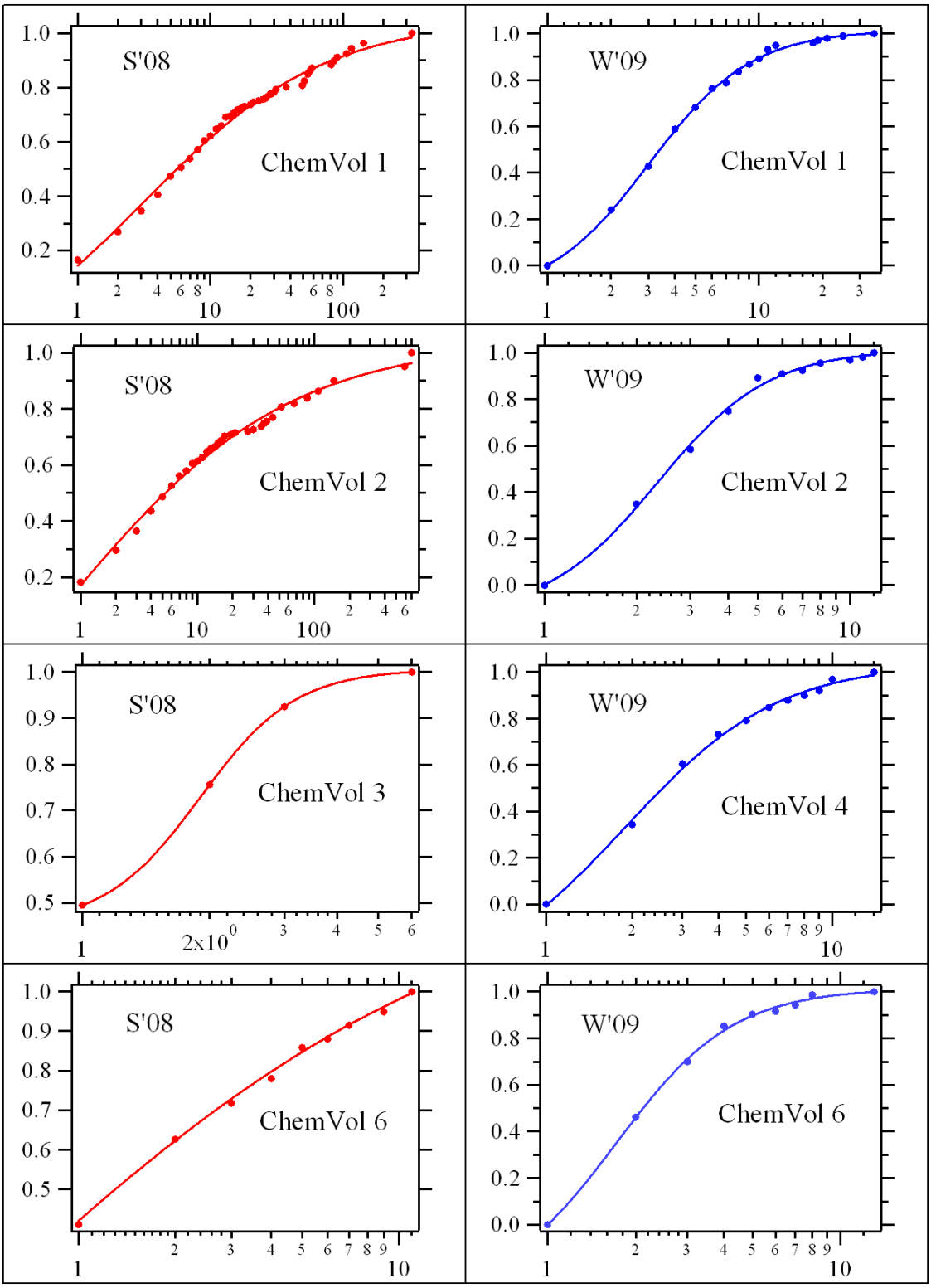

Figure 2-4. The cumulative fraction of total sampling time (y-axis) as a function of the number of successive class combination observations per sampling interval (x-axis) for select ChemVols from the summer 2008 (S'08) and winter 2009 (W'09) experiments. Note that each figure uses a different x-axis scaling.

Supporting Information

(22 pages; 4 tables; 6 figures)

Conditional Sampling for Source-Oriented Toxicological Studies using a Single Particle Mass Spectrometer

*K.J. Bein[1], Y. Zhao[1] and A.S. Wexler[1,2,3,4]

[1]Air Quality Research Center, [2]Mechanical and Aeronautical Engineering, [3]Civil and Environmental Engineering, and [4]Land, Air and Water Resources, University of California Davis

1. Rapid Single-ultrafine-particle Mass Spectrometer (RSMS)

A brief description of RSMS-II follows. Air is drawn into a Nafion drier where water is removed from the air and particles. The particle stream enters a 10 position valve that directs the stream to one of 9 critical orifices (position 10 is off). Each critical orifice limits mass flow into a chamber controlling the pressure. The particle stream exits this chamber through a second critical orifice that focuses particles near one size to a beam, where the vacuum aerodynamic diameter (D_{va}) of the focused particles depends on the upstream pressure. The beam then passes through a series of skimmers that remove the gas before the particles enter the source region of a linear time-of-flight mass spectrometer. Co-linear and counter-propagating with the particle beam is a pulsed excimer laser beam operating at 193 nm, firing at 50 Hz and tuned to provide about 5-10 mJ per pulse. The mass spectrometer has been designed so that the source region is about 4 cm in the direction of the laser and particle beams. If a particle is in the source region when the laser fires, then it is ablated and ionized. Positive ions are analyzed by the mass spectrometer. For the experiments described here, RSMS-II was set to only sample particles with D_{va} in the 70-150 nm range. A picture of the instrument housed inside the onsite mobile trailer is shown in Figure S1.

2. Pre-study Analyses

A schematic of the pre-study analysis is shown in Figure S2 and a general description follows. All single particle mass spectra are time-to-mass calibrated, integrated to obtain a binned ion current for each integer *m/z* value and normalized according to a Euclidian norm, resulting in what will be referred to as spectrum vectors. The spectrum vectors are clustered using an agglomerative hierarchical algorithm with the dot product as the similarity metric. The threshold for group membership is kept high to ensure homogeneous clusters since this step is largely aimed at data reduction. Clusters are represented by the pooled within-cluster average vector, which is continuously updated and renormalized as spectra are added or removed from the cluster. The algorithm is iterative and randomly loops through the full dataset until the number of spectra switching clusters between successive iterations drops to zero. A problem with these types of algorithms, besides their inconsistency, is that the inter-cluster distances can be quite small, smaller than the threshold used to define group membership. To correct for this, the cluster vectors from an initial pass are themselves clustered in subsequent passes through the algorithm using the same threshold until the number of cluster mergers drops to zero.

The final clusters are inspected manually and assigned a composition based on their mass spectral peaks. During this process, the pooled within-cluster average and standard deviation of the full mass spectra are used, rather than the unit-mass integrated spectra, since they contain important details for making accurate peak assignments that are obscured by integration. Analyses of standard deviations are included to identify potential instances of cluster contamination by trace components that, however small, may be important differentiating factors for source attribution.

Particle classes are constructed manually by merging clusters. This satisfies a number of goals related to the toxicological endpoints. Examples include: *(a)* merging clusters of different composition but of known similar origin to produce classes representative of a particular source or source category, *(b)* building classes based on the relative amounts of primary versus secondary components, and *(c)* isolating a specific constituent, such as carbon or metals, and creating classes based on the presence, absence and/or chemical form of that constituent. As a result, individual classes can be composed of multiple clusters and all intra-class clusters are included in the library. Libraries are simply databases containing the vector representations of the pre-study particle classes and class combinations and are integral to real-time data flow, and thus system response, during ChemVol sampling. For example, spectrum vectors are compared to cluster vectors in the cluster library to determine their particle class assignment.

Using the timestamps of the individual mass spectra, a chronological sequence of classes is assembled by which the class combination vectors are constructed. The following parameters are important thresholds to consider and define before proceeding: *(1)* the time interval for constructing class combination vectors, *(2)* the number of single particle observations between successive class combination vectors, *(3)* the minimum number of single particle observations required for each class combination vector and *(4)* the maximum time allowed between successive particle observations.

Class combination vectors are then clustered using the same algorithm and procedures discussed above to obtain class combination clusters. ChemVol assignments are created from the class combination clusters according, again, to the insight, or ultimate goal, of the investigator. Similar to particle classes, individual ChemVols can be defined by multiple class combinations but it is the class combination cluster vectors that comprise the library and all intra-ChemVol class combinations are assigned the same ChemVol number. Ideally, the ChemVol assignments would be mutually orthogonal, but the occurrence and prevalence of mass spectra in Fresno frequently hampered achievement of this goal.

As a final step, the temporal variability in the hit rate of the single particle instrument is analyzed to determine the best times of day to collect PM, with the understanding that periods of low hit rate disproportionately increase the statistical uncertainty of the ChemVol sampling accuracy. Therefore, higher hit rate periods are more desirable. A natural split here coincides with the diurnal pattern of the boundary layer; higher concentrations, and thus higher hit rates, under a nocturnal inversion and vice versa for a fully developed mixed layer. Additional benefits of this division include: *(a)* Different class combinations enhanced in particular sources, or particle classes, are more common, and show greater temporal consistency, under a nocturnal inversion due to increased atmospheric stability. Conversely, daytime turbulent mixing in Fresno tends to inhibit not only the ability to isolate distinguishably different class combinations, but also the frequency and duration for which such class combinations are observed. *(b)* The single particle instrument can be turned off during low hit rate periods to reduce wear. *(c)* While the instrument is off, ChemVols can be assigned to specific time intervals associated with sources, or source categories, known to preferentially emit at particular times of day, e.g.

morning and evening rush hour traffic, cooking, or residential heating. Conditional sampling based on the temporal variability in the relative prevalence of different sources is an entirely different, but complementary, concept and was exploited in a limited capacity during the current work; e.g., see the description of winter ChemVols 7-9 in the Results and Discussion section.

3. Real-time Data Flow

Figure S3 depicts a schematic of real-time data flow during ChemVol sampling, beginning with data acquisition and ending at the hardware interface controlling the ChemVol sampling train. A description of the various stages, in the order drawn, is given below.

The output signal from the mass spectrometer is digitized using a dual-channel 8-bit digitizer at a sampling rate of 500 MHz per channel (Acqiris DP235). Simultaneous high- and low-sensitivity digitization is achieved via dual-channel mode by offset, but overlapping, vertical settings with the objective of optimizing dynamic range. Time delay and sample size are set to scan an *m/z* range of ~ 5-250 Da.

The ablation/ionization laser is free-fired and provides the trigger for data acquisition so the output of the digitizer must be monitored continuously to differentiate valid single particle mass spectra from background noise. Data validation is accomplished using a composite height-width threshold to check for peaks in each post-trigger scan. Peak width is defined as the number of consecutive samples above a certain height. These parameters are set prior to each experiment, fine-tuned during the pre-study, and then monitored throughout ChemVol sampling. The accuracy of this step is important given the real-time nature of the experiment. Both missed and false observations can alter the class combination vectors and thus reduce sampling accuracy.

For each true particle hit, the high- and low-sensitivity data are combined, where the high-sensitivity is default but augmented by the low-sensitivity when saturated. This allows for high vertical resolution at the minimum detection limit while still capturing full peak heights. The combined data is then time-to-mass calibrated via an iterative Estimation-Maximization (EM) algorithm.

Although the calibration equation is quite simple, the calibration “constants” are actually normally distributed variables, which translate directly to the probability of the position of the vaporized particle, relative to the center of the laser beam, at the point of ionization. As a result, using a single set of values will result in mis-calibrated mass spectra, where the degree of mis-calibration increases with increasing *m/z* due to the functionality of the calibration equation. For example, the relative position of a peak using average calibration constants versus the average plus one standard deviation can be off by 1-2 Da in the 30-90 Da range, where a large majority of the chemical information resides. This can significantly impact the accuracy of clustering and, subsequently, sampling. Therefore, it is necessary to implement an algorithm – the details and

performance of which will be published elsewhere – to handle the variability. A brief description follows.

The overlying objective exploited by the EM algorithm is that during peak integration the sums are binned at integer *m/z* values to facilitate data clustering. To this effect, an initial estimate of the calibration constants is provided, peaks are assigned to the nearest integer *m/z*, and the calibration constants subsequently varied to maximize the integrated ion signal for a small *m/z* interval (± 0.25 Da) centered about the integers. Starting with peaks at the beginning of the mass spectrum, for which the potential calibration errors are smallest, the algorithm progressively scans for peaks at larger *m/z* and reiterates the EM step as they are located. Calibration constants from the previous iteration provide estimates for the current iteration and all previous *m/z* assignments are held constant during successive maximizations. In application, the average calibration constants from analysis of the pre-study data are used as the initial estimates for each mass spectrum during ChemVol sampling since they are most probable and thus minimize search time.

Following calibration, each mass spectrum is noise corrected, integrated and normalized according to a Euclidian norm to obtain a spectrum vector ($\vec{S}$). Using the dot product, the spectrum vector is compared to each of the cluster vectors ($\vec{C}$) in the cluster library and assigned the class number of its most similar partner given the similarity condition is satisfied. If the threshold condition is not met, then the spectrum vector is passed to the outlier cluster library.

The outlier cluster library is a real-time construct specifically designed to *(a)* allow particle types not observed during the pre-study to be realized and incorporated and *(b)* provide additional safeguard against any potential false or mis-calibrated data. Similar in progression to the first iteration of a hierarchical clustering algorithm, if the outlier cluster library is empty or the spectrum vector is not sufficiently similar to any of the existing outlier clusters, then a new cluster is created and added to the library. Outlier clusters are represented by pooled within-cluster average vectors, termed outlier cluster vectors ($\vec{O}_C$), which are continuously updated and renormalized as new members are added. Once group membership exceeds a specified threshold, the outlier cluster is removed and added as a new particle class to the cluster library. The dimensionality of the class combination vectors is then augmented to accommodate the new particle type.

As particle observations accumulate, the response of the system is determined by comparing the following parameters, which are continuously monitored, to specified thresholds: the number of particle observations and time elapsed since the last class combination observation; the time elapsed between successive particle observations; the number of successive outlier observations. The first two parameters determine when and how to construct new class combination vectors in a manner identical to that described in the Data Constructs section. The latter two, however, originate out of a necessity to limit potential sources of uncertainty in sampling accuracy.

It is convenient at this point to introduce the concept of an auxiliary ChemVol. That is, a ChemVol not assigned a particular class combination but rather reserved solely for those

important instances when the composition of the atmosphere is unknown, or less certain. Examples include: *(a)* too much time elapsed between successive particle observations, *(b)* too many successive outlier observations, or *(c)* too few particle observations within the specified time interval for constructing class combination vectors. In these cases, the system switches to the auxiliary ChemVol, if not already activated, to minimize the possibility of ChemVol contamination; i.e. dilution by PM of uncertain mixture.

Data handling routines for class combination vectors are exactly analogous to those described previously for spectrum vectors. Each newly constructed class combination vector is compared to all entities in the class combination library and assigned the ChemVol number of its most similar partner given they are sufficiently similar. If the similarity condition is not satisfied, then the vector is passed to the outlier class combination library. In this case, tracking outliers serves only in its capacity to identify class combinations not observed during the pre-study and thus is strictly contingent upon the availability of free ChemVols to which outlier clusters that have satisfied the observational threshold can be assigned. Regardless, all outlier observations instantly activate the auxiliary ChemVol.

An additional condition has been inserted at this stage of the process that, with the exception of the auxiliary ChemVol, delays ChemVol triggering until the number of successive observations of the associated class combination(s) has satisfied some threshold. If the threshold is greater than one, then any two successive observations associated with different ChemVols immediately triggers the auxiliary ChemVol, which remains activated until the threshold condition is met. The purpose here is to minimize potential boundary condition uncertainties when switching between ChemVols.

In terms of hardware interfacing, ChemVol numbers are converted to an unsigned 16-bit integer that determines the on/off sequencing of a 16-channel relay output board (Omega Engineering Inc., OME-DB-16R). Following a software ChemVol trigger, the bit data is transmitted via a 32-channel ADC and DIO board (Omega Engineering Inc., OME-PCI-1002L) to the relay board, which then switches a single 120 VAC power input from the normally-closed solenoid valve of the current ChemVol to that of the triggered ChemVol.

4. ChemVol Sampling Train

A schematic of the ChemVol sampling train is depicted in Figure S4 and pictures of it housed inside the onsite mobile trailer are shown in Figure S5. Design modifications were made to the sampling train prior to the winter 2009 experiment due to knowledge acquired during the summer 2008 campaign. Accordingly, the discussions that follow focus on the most recent design and changes are noted for clarity when appropriate.

Following the schematic, ambient air was drawn into an 8” diameter stack situated on top of the onsite mobile trailer and extending 7.3 m above ground level. A rain cap prevented bulk precipitation entering the stack, a fine mesh screen filtered very coarse material (bugs and leaves), and condensing water vapor was trapped at the bottom of the

stack. Using 8” diameter galvanized steel erector-set ducting (Kirk & Blum Duct, Greensboro, NC), the sampling stack was plumbed across the trailer roof and through the wall to the ChemVol manifold, which houses 10 separate ChemVol stacks. Each ChemVol stack includes an afterfilter support and 0.17 and 1 μm stages. A single 2.5 μm stage was placed upstream of the ChemVol manifold. During the summer 2008 experiments, however, each ChemVol stack consisted solely of a 0.17 μm stage and afterfilter support, and a single 1.0 μm stage was placed immediately downstream of the 2.5 μm stage. Borosilicate glass fiber filters (Pall Corporation, TX40H120WW-8X10) were used in the afterfilter supports and polyurethane foam (PUF) impactor substrates were used in all 0.17, 1 and 2.5 μm ChemVol stages (Thermo Environmental Instruments Inc., 59-007954-0010; 59-007953-0010).

Flow straighteners were inserted ~ 8” upstream of each ChemVol stack in the vertical ducting connecting manifold to ChemVol and consisted of 3 concentric cylinders 7” in length, separated in diameter by 2” and supported to each other and the outer manifold via pop-riveted Z-channel. The valve assembly attached to the bottom of each afterfilter support included high-flow quick-disconnect hose couplings (McMaster-Carr Supply Co., 6537K95, 6537K77) followed by a 3” brass nipple and then a 1” orifice direct-acting, normally-closed solenoid valve (Omega Engineering Inc., SV225). All valves were plumbed to a single manifold via 1” PVC pipe. Inserted downstream of the valve manifold and connected by brass unions was an industrial-scale inline thermal mass flow transmitter (Kurz Instruments Inc., 534FT-16A) for monitoring flow rate. At the outlet of the flow meter was a 2-to-1 reducing coupling connected to 2” steel pipe leading out the trailer floor, followed by 20’ of 2” EPDM double-reinforced suction hose (McMaster-Carr Supply Co., 5294K795) attached via locking cam-and-groove hose couplings to the inlet of the blower assembly and serving as a vacuum reservoir. Pressure transducers (Omega Engineering Inc., PX209) were placed in the center of the ChemVol manifold and immediately upstream of the flow meter to monitor pressure drop across the system.

Collectively, the blower assembly had to satisfy the following requirements: *(1)* operable using standard residential single phase 220 VAC power with 30 A breaker, *(2)* capable of pumping 900 lpm across an 11” Hg pressure drop, *(3)* equipped with flow rate control via PID set-point using feedback loop with analog output of flow meter, *(4)* remotely controllable, *(5)* deployable outdoors during all seasons, and *(6)* outfitted with multiple safety mechanisms protecting blower motor. This was accomplished through the combination of a 3-phase oil-less regenerative blower (Gast Manufacturing Inc., R4H3060A-1) and variable frequency AC drive (VFD) with PID control loops (ABB, ACH550-UH HVAC).

Briefly, the VFD powers and controls the blower by converting the single-phase 220 VAC input to 3-phase 220 VAC output, where both the frequency and magnitude of the output current are adjustable. These parameters continuously vary in response to the analog output of the flow meter through the PID control loop to maintain a flow rate set-point of 900 lpm. Remote start/stop control was achieved by feeding the 24 V digital on/off input of the VFD through the 16-channel relay output board also controlling the solenoid valves. Flow rate was monitored directly from the flow meter via serial

communication. The various safety mechanisms include: *(1)* thermocouple on blower motor/temperature relay, *(2)* pressure gauge on blower exhaust/pressure switch, *(3)* vacuum gauge on blower intake/vacuum switch, *(4)* rain-tight electronics enclosure with internal heating and cooling elements, and *(5)* pilot-operated, normally-open solenoid safety valve (Omega Engineering Inc., SV6005-NO) powered by the VFD. A custom muffler was fitted to the exhaust and the entire blower assembly was mounted on a platform with casters for portability; a picture is shown in Figure S6.

Collocated instrumentation includes: *(1)* Scanning Mobility Particle Sizer (SMPS) with nano Differential Mobility Analyzer (DMA) (TSI Inc., 3080 EC; 3025A CPC; 3085 NDMA), *(2)* SMPS with long DMA (TSI Inc., 3080 EC; 3025A CPC; 3081 LDMA), *(3)* wind speed and direction sensors (Met One Instruments Inc., 010C; 020C), and *(4)* temperature/relative humidity data logger (Omega Engineering Inc., OM-DVTH). With the exception of the nano SMPS, every facet of the experiment – including instrumentation, hardware, data acquisition, data processing and logging, clustering and networking – was controlled and executed by a custom built computer, and the entire software system, including all algorithms, was coded in LabView™ (National Instruments Inc., v8.2). Full remote control capabilities were achieved via pcAnywhere™ (Symantec Inc., v10.0) over a wireless network, with the router in an adjacent building and the receiver positioned on the trailer roof. Analog gauges and various digital displays were monitored over the same network using web cams inside the trailer.

Table 2S-1. Runtime parameters used to control system response during ChemVol sampling for the summer 2008 and winter 2009 experiments. See text for definitions.

Runtime Parameter	Summer 2008	Winter 2009
Vacuum Aerodynamic Diameter Scanned (nm)	70	150
Particle Class Library - Similarity Threshold (dot product)	0.8	0.84
Outlier Cluster Library - # Observations for New Particle Class	5	15
Maximum Time between Successive Single Particle Observations (s)	90	30
Class Combination Library - Similarity Threshold (dot product)	0.6	0.81
Class Combination Vector - Time interval (s)	300	60
Class Combination Vector - Minimum # Single Particle Observations	5	3
# Single Particle Observations between Successive Class Combination Vectors	3	3
Outlier Class Combo Library - # Observations for New ChemVol	5	15
ChemVol Switching - Minimum # Successive Observations	1	2

Table 2S-2. Metadata for the summer 2008 and winter 2009 experiments separated by pre-study versus ChemVol sampling.

Experiment		[1]Start Date	[1]End Date	[1]Total Sampling Hours	Total # Mass Spectra	Total # Particle Classes	Total # Class Combination Vectors
Summer 2008	Pre-study	8/13/2008	9/2/2008	446	21,906	12	4689
	ChemVol Sampling	9/11/2008	10/21/2008	741	35,266		8785
Winter 2009	Pre-study	1/9/2009	2/11/2009	522	100,242	6	30,810
	ChemVol Sampling	3/1/2009	4/6/2009	712	46,286		10,274

[1]Sampling was highly periodic and temporally asymmetric during these periods due to routine maintenance on RSMS-II, replacement of consumables, weather events (especially for winter 2009), and natural variations in particle loading.

Table 2S-3. Single particle summary statistics by ChemVol for the summer 2008 and winter 2009 experiments, including (from left to right) the total sampling time, the total number of single particle observations, individual sampling intervals and class combination vectors (includes ChemVol trigger), the average number of single particle observations per class combination vector (± 1 standard deviation), and the PM mass collected by the afterfilter (ultrafine) and 0.17 μm (submicron fine) stages (± uncertainty). See text for discussion.

Summer 2008 Experiment							
ChemVol	**Total Sampling Time (hrs)**	**Total # Particle Hits**	**Total # Sampling Intervals**	**Class Combination Vectors**		**[1]Scaled SMPS Estimates - Collected Mass (mg)**	
				Total #	**Average # Particles/**	**Ultrafine**	**Sub-μm Fine**
1	85.55	15283	991	4327	14 ± 8	14 ± 3	36 ± 10
2	63.69	13304	742	3844	24 ± 20	12 ± 2	41 ± 12
3	2.60	426	62	83	7 ± 2	0.42 ± 0.08	1.3 ± 0.4
4	2.26	400	61	76	8 ± 3	0.41 ± 0.07	1.1 ± 0.3
5	0.51	88	13	18	8 ± 3	0.10 ± 0.02	0.21 ± 0.06
6	5.85	1106	133	242	11 ± 6	1.1 ± 0.2	2.9 ± 0.8
7	1.45	240	38	45	7 ± 3	0.16 ± 0.03	0.4 ± 0.1
9	139.60	-	29	-	-	17 ± 3	47 ± 14
10	468.27	4419	1344	139	8 ± 7	63 ± 11	197 ± 56
Totals:	770	35266	3413	8785	-	109 ± 12	328 ± 60
Winter 2009 Experiment							
ChemVol	**Total Sampling Time (hrs)**	**Total # Particle Hits**	**Total # Sampling Intervals**	**Class Combination Vectors**		**[2]Measured Mass (mg)**	
				Total #	**Average # Particles/**	**Ultrafine**	**Sub-μm Fine**
1	6.91	7478	477	2148	12 ± 7	2.58 ± 0.06	3.21 ± 0.04
2	6.04	4087	402	1479	7 ± 2	1.30 ± 0.05	3.02 ± 0.03
3	4.41	3605	363	1239	8 ± 5	1.01 ± 0.08	2.0 ± 0.5
4	1.65	1879	137	536	11 ± 5	0.73 ± 0.04	0.8 ± 0.2
5	4.72	4423	422	1421	8 ± 3	1.33 ± 0.06	1.66 ± 0.08
6	1.98	2519	191	691	11 ± 7	0.88 ± 0.07	1.23 ± 0.04
7	8.75	-	3	-	-	1.07 ± 0.06	1.88 ± 0.06
8	92.49	-	32	-	-	11.26 ± 0.06	15.48 ± 0.05
9	257.82	-	33	-	-	27.22 ± 0.07	32.82 ± 0.08
10	356.51	22295	2081	2760	6 ± 1	37.16 ± 0.07	47.26 ± 0.09
Totals:	741	46286	4141	10274	-	85	107

[1]Gravimetric analyses of the summer filters were highly inaccurate due to a defective balance so only estimates are available. Mass estimates are based on integrated SMPS data scaled by the average ratio of measured-to-estimated mass from the winter 2009 data (ultrafine = 1.1 ± 0.2; submicron fine = 1.4 ± 0.4).

[2]Mass measurements obtained via semi-micro analytical balance (A&D Engineering Inc., HR-202i).

Table 2S-4. SMPS summary data by ChemVol for the summer 2008 and winter 2009 experiments, including (from left to right) the bimodal lognormal fit parameters for the average SMPS number distributions ($dN/dlogD_p$), the average integrated ultrafine (D_m < 0.17 μm) and submicron fine (0.17 < D_m < 685 μm = SMPS max D_m) mass concentrations, and estimates of the PM mass collected by the afterfilter and 0.17 μm stages.

[1]Summer 2008 Experiment										
ChemVol	Bimodal Lognormal Fit Parameters						Average Integrated $dM/dlogD_p$ (μg/m^3)		SMPS Estimates - Collected Mass (mg)	
	A_1	D_{pg1}	σ_{g1}	A_2	D_{pg2}	σ_{g2}	Ultrafine	Fine	Ultrafine	Fine
1	1914	36	1.51	7760	81	1.96	2.7 ± 0.9	6 ± 3	13.17	26.01
2	1287	33	1.43	7835	85	1.97	2.8 ± 0.9	7 ± 4	10.91	29.16
3	1962	34	1.45	7403	78	1.96	3 ± 1	6 ± 3	0.38	0.90
4	1800	34	1.46	8215	87	1.91	3.0 ± 0.9	7 ± 4	0.37	0.80
5	5705	38	1.47	8570	97	1.70	3.2 ± 0.8	6 ± 4	0.09	0.15
6	2220	39	1.53	8765	81	1.92	3 ± 1	6 ± 3	0.98	2.07
7	3357	49	1.64	4604	86	1.94	1.9 ± 1	4 ± 3	0.15	0.30
9	4073	31	1.41	5761	91	1.86	2 ± 1	5 ± 3	15.94	33.79
10	2128	41	1.59	6683	84	1.97	2.6 ± 0.9	6 ± 4	57.03	140.88
[1]Winter 2009 Experiment										
[2]ChemVol	Bimodal Lognormal Fit Parameters						Average Integrated $dM/dlogD_p$ (μg/m^3)		SMPS Estimates - Collected Mass (mg)	
	A_1	D_{pg1}	σ_{g1}	A_2	D_{pg2}	σ_{g2}	Ultrafine	Fine	Ultrafine	Fine
1	1080	27	1.22	22150	78	1.69	6 ± 3	7 ± 4	2.46	2.77
2	1043	31	1.36	13709	85	1.74	5 ± 2	7 ± 4	1.47	2.21
3	1079	29	1.30	16587	77	1.72	5 ± 2	6 ± 3	1.11	1.30
4	999	26	1.23	22298	77	1.68	6 ± 3	7 ± 4	0.53	0.57
5	801	24	1.23	16924	80	1.71	5 ± 2	6 ± 4	1.24	1.59
6	1220	27	1.24	22189	76	1.69	6 ± 3	7 ± 4	0.62	0.65
8	2453	32	1.40	8773	83	1.83	3 ± 2	4 ± 3	13.10	19.98
9	1493	30	1.35	6440	73	1.91	2 ± 1	3 ± 3	22.61	33.62
10	1011	29	1.29	15919	78	1.72	5 ± 3	6 ± 4	44.66	39.96

[1] SMPS calculations were performed by some combination of the following: compiling all number distributions ($dN/dlogD_p$) within the time period of each ChemVol sampling interval, interpolating distributions at the interval boundaries, converting to mass assuming spherical particles with unit density, integrating the ultrafine (D_m < 170 nm) and submicron fine fractions (170 < D_m < 685 nm), multiplying by sample volume and summing, or averaging, over all sampling intervals independently for each ChemVol.
[2]SMPS data not available for ChemVol 7 during the winter 2009 experiment.

Figure Captions

S1. Picture of RSMS-II in the onsite mobile trailer; see text for instrument description.

S2. A schematic of the pre-study data analysis; see text for discussion.

S3. Real-time data flow diagram for conditional ChemVol sampling; see text for discussion.

S4. A schematic of the sampling train and experimental setup; see text for discussion.

S5. Pictures of the sampling stack (left), ChemVol manifold (top) and valve manifold (bottom) inside the onsite mobile trailer; see text for discussion.

S6. Picture of the blower assembly (top) and variable frequency AC drive (bottom). See text for description.

Figure 2S-1. Picture of RSMS-II in the onsite mobile trailer; see text for instrument description.

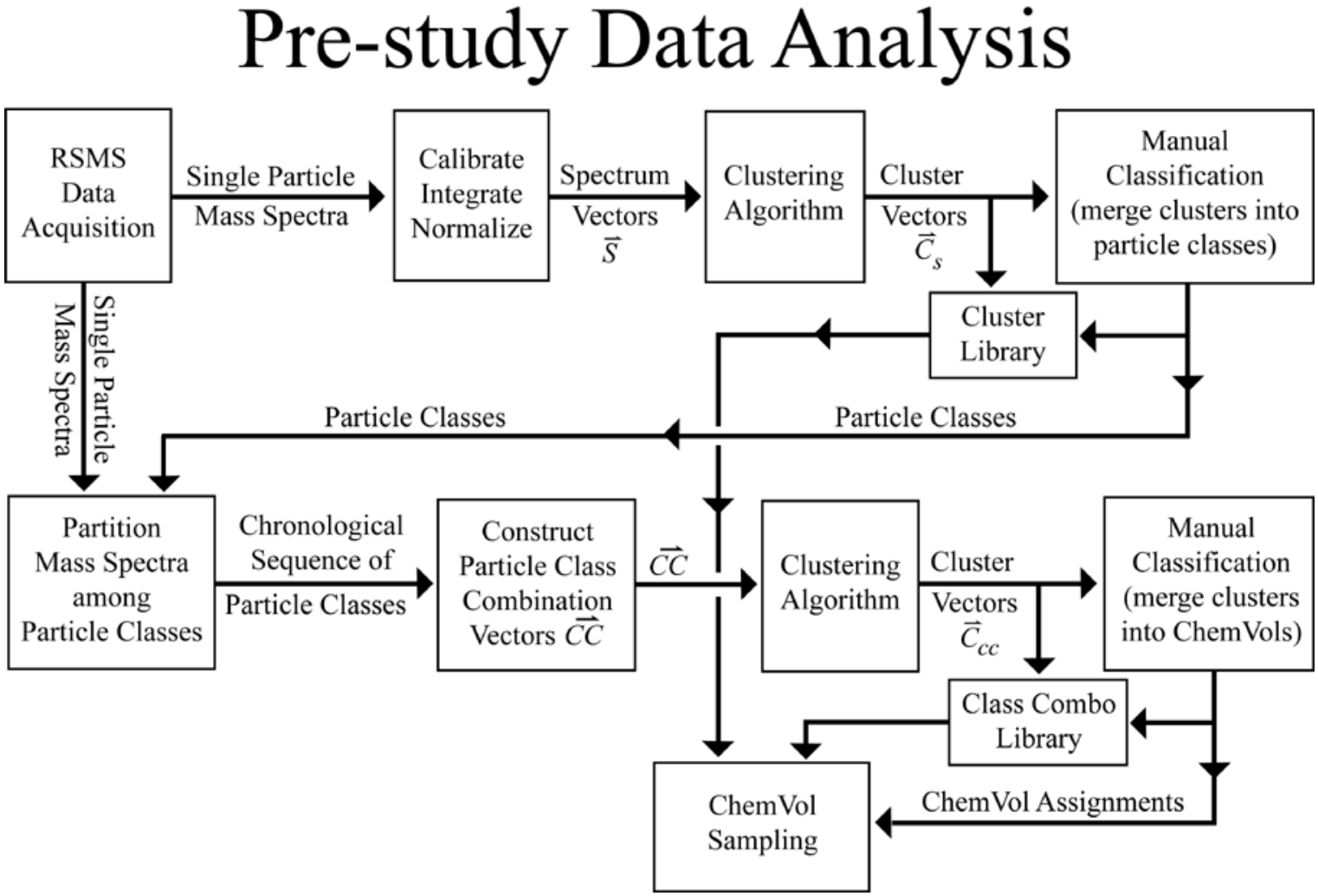

Figure 2S-2. A schematic of the pre-study data analysis; see text for discussion.

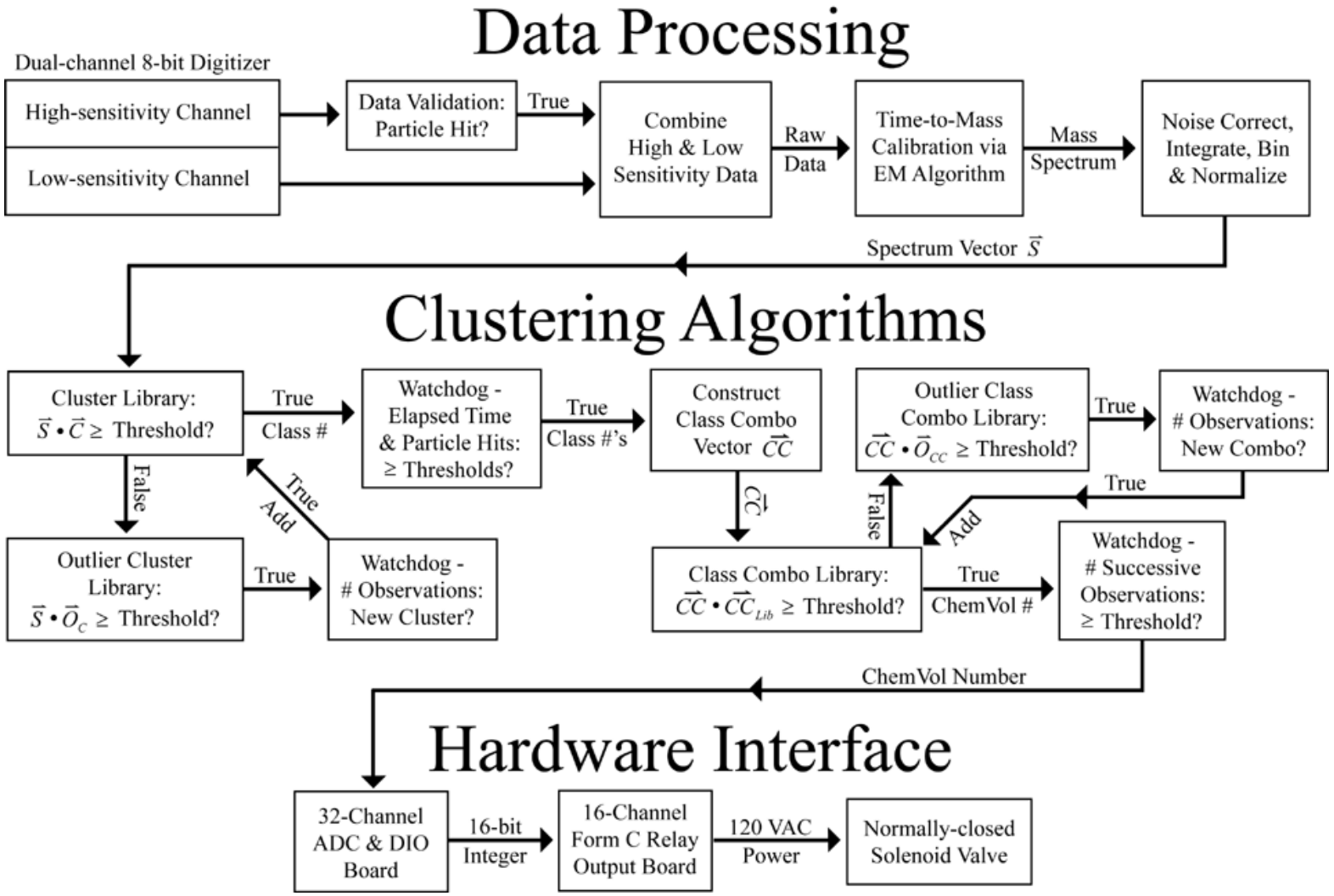

Figure 2S-3. Real-time data flow diagram for conditional ChemVol sampling; see text for discussion.

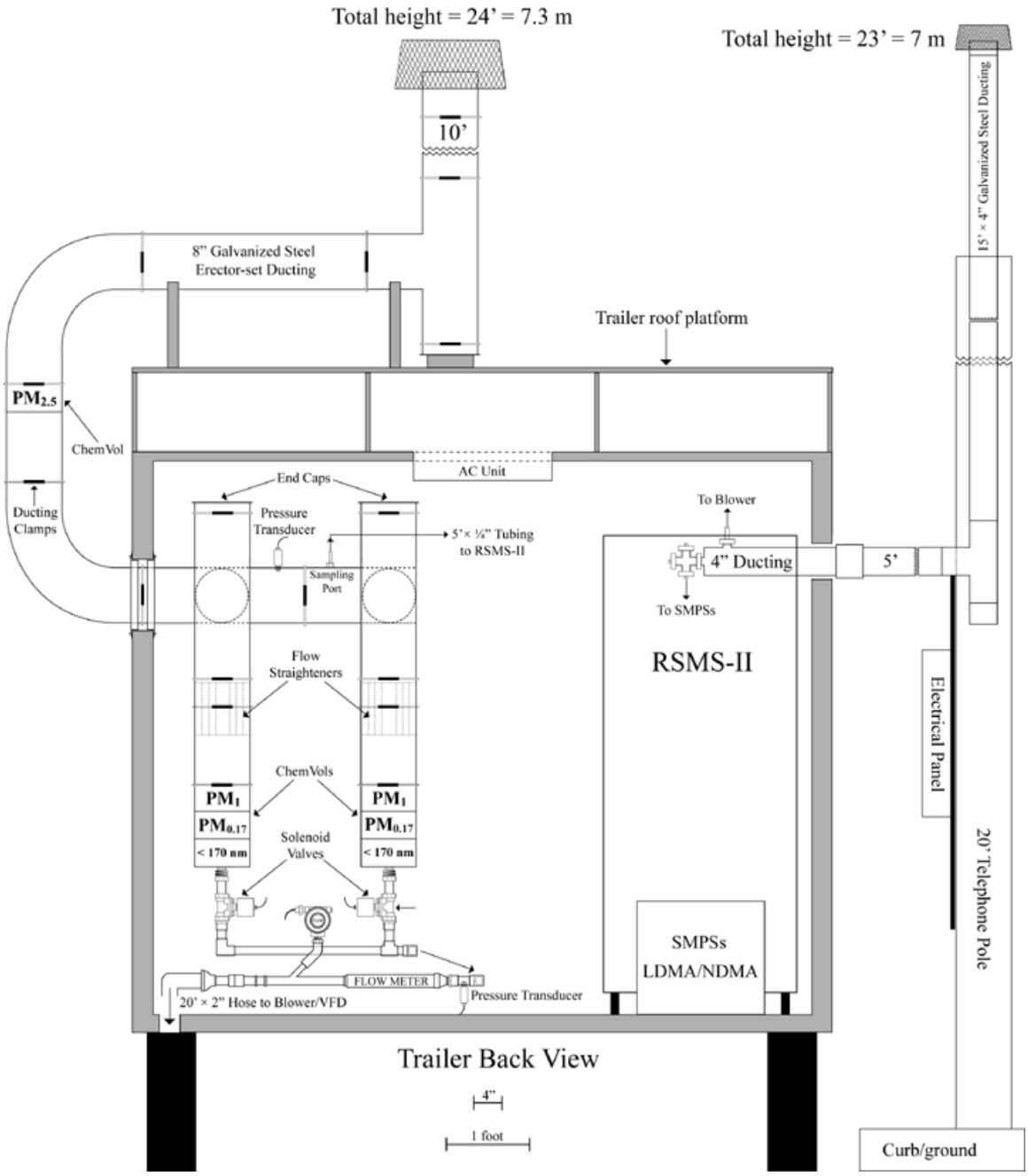

Figure 2S-4. A schematic of the sampling train and experimental setup; see text for discussion.

Figure 2S-5. Pictures of the sampling stack (left), ChemVol manifold (top) and valve manifold (bottom) inside the onsite mobile trailer; see text for discussion.

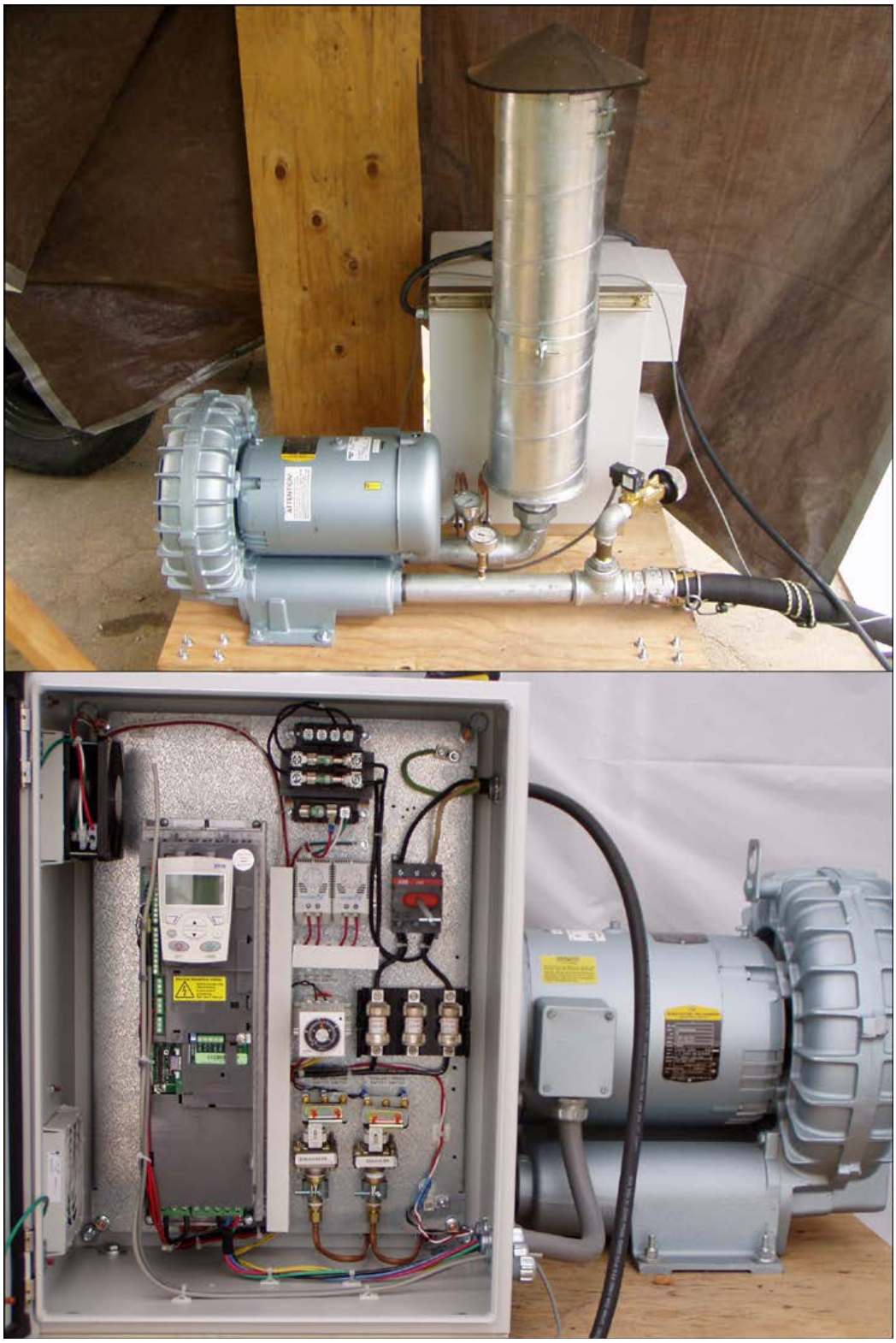

Figure 2S-6. Picture of the blower assembly (top) and variable frequency AC drive (bottom). See text for description.

Chapter 3
A High-Efficiency, Low-Bias Method for Extracting Particulate Matter from Filter and Impactor Substrates

K.J. Bein
Air Quality Research Center, University of California Davis

Introduction

Epidemiological studies associate gas and particle pollutant concentrations with a range of human health effects, but these associations rely on follow-up toxicological studies to validate these epidemiological associations and establish their cause, effect and underlying mechanism. As a result, the ARB and other stakeholder agencies such as the US EPA and NIEHS employ toxicology studies in animal models and in vitro systems to assess the toxicity and relative toxicity of atmospheric particulate matter (PM). The PM for such studies is usually extracted from filters and impaction substrates into water or other media for employment in the toxicological studies. Standard operating procedures (SOPs) for performing these extractions are available from various groups, including the US EPA, and different groups employ different SOPs, potentially resulting in outcomes that are partially or wholly dependent on the SOP employed and thus biasing inter-group comparisons. Remarkably, it appears that there has never been a systematic study to compare the various SOPs for (a) extraction efficiency in terms of total mass extracted, (b) relative extraction effectiveness as a function of particle size fraction and chemical category (e.g., minerals, metal oxides, salts/electrolytes, acids/bases, hydrophobic organics, water soluble organics and black/brown carbon), (c) extraction artifacts such as volatilization losses, chemical and/or physical alterations to the PM and incorporation of filter material into the PM sample, and (d) relative toxicity as a function of SOP employed.

Applying the underlying methodology to a large majority of filter extraction techniques, including the one used in this study and the SOP of the US EPA, involves sonication followed by lyophilization (*personal communication*, *Robert Devlin*, 2009; *Darlene Bowser*, 2009). Sonication – where ultrasonic energy is applied to a liquid to nucleate, grow and implosively collapse microscopic bubbles – is required to remove the PM from the filter media and suspend it in liquid, typically pure water. This is due to the extremely adhesive and cohesive nature of most fine and ultrafine PM, the high impaction velocity of the PM onto the filter media during sampling, as well as the fairly ubiquitous presence of hydrophobic PM components. It is the cavitation energy of the imploding microscopic bubbles that actually breaks the adhesive/cohesive forces holding the particles together and to the filter media during sonication.

In fact, the cavitation energy is sufficient to degrade the integrity of the filter to the point that microscopic pieces are broken off and further fragmented into micron-sized PM, thus contaminating the sample. This is an extraction artifact that has recently garnered much attention in the toxicology community. Although filter material (e.g. Teflon and PUF) is generally considered to be chemically inert in terms of eliciting toxicological effects, there is concern about the effects of the size and morphology of the fragmented filter particles (FFP) on the respiratory tract of the animals used for in vivo studies and the cell cultures of in vitro studies. This is especially true for traditional afterfilters, like the ones used in the current study, which have a woven glass fiber backing. There is evidence that sonication can result in the formation of micron-sized, needle-like glass fibers that have a pronounced effect on cell viability when administered to cell cultures (*personal*

communication, Fern Tablin, 2011). As a result, significant attention has been given in this study to the separation of FFP from the PM during the extraction process.

The approach chosen for the filter extraction technique being presented here takes advantage of the size difference between the sonication-produced FFP and the extracted PM to selectively filter the former from the sonication solution using a porous filter membrane of known porosity that retains the FFP but allows the particles to pass through into the filtrate. The idea stems from the fact that any mechanical abrasion based particle formation mechanism, like the production of FFP via sonication, will tend to produce a distribution of particle sizes – typically lognormal in nature – where the mean of that distribution resides high in the supermicron range. The ambient PM sampled during these experiments, however, is submicron in size and thus should be more than an order of magnitude smaller than the FFP, allowing separation. There are two caveats here, though:

1. Particles have a tendency to agglomerate on the filter during sampling and although sonication does a good job fragmenting these agglomerates and dispersing the particles into solution, it cannot completely restore the original size distribution of sampled PM and thus a small fraction of particularly "sticky" PM may be retained by the porous membrane. Although somewhat variable and in no way indicative of the particle size distributions originally sampled, Dynamic Light Scattering (DLS) measurements of sonication solutions from the filter extractions done in this study do show that post-sonication particle number distributions in solution reside almost entirely in the submicron range.
2. Although sonication predominantly forms supermicron FFP, as discussed above, the spread in the distribution is unknown and it is possible that the leading tail dips down into the micron and submicron ranges. Any FFP smaller than the membrane pore size will likely pass through into the filtrate and contaminate the sample. There is evidence for this in the fact that filter material is still recovered even when selective filtration is applied to the sonication solutions from the extraction of clean filter blanks using pore sizes less than a micron, as will be shown later. However, significantly more filter surface area is exposed during sonication of filter blanks compared to filters loaded with PM and thus the amount and size of FFP formed will likely be different.

Membrane filters are available in a variety of pore sizes and the objective is choosing the pore size that maximizes FFP removal and minimizes particle loses. The pore size chosen for the filter extractions performed in this study was 8 μm since *(a)* smaller pore sizes did not measurably decrease the mass of FFP recovered from the extraction of filter blanks and *(b)* it is still an order of magnitude larger than the particle size fractions that were collected.

Some groups have also raised concern about the production of reactive oxygen species (ROS) during the sonication process that may alter the chemical composition of the PM (*personal communication, Cort Anastasio*, 2010). They have suggested less energetic approaches such as shaker tables where the filter is submerged in a fluid and then shaken to remove the PM and suspend it in solution, which would also likely eliminate the

formation of FFP. Although certainly a valid concern that deserves further attention, this technique generally results in very low extraction efficiencies and it is not clear that the extraction is not compositionally biased in terms of what PM, or PM components, are removed vesus what is left on the fiter. For most toxicological studies, extraction efficiency will be extremely important in terms of removing sufficient PM to conduct the experiment – this is especially true for the source-oriented sampling being discussed here – and minimizing the compositional bias of the extraction. As a result, sonication remains the extraction technique of choice and ROS and FFP production are currently accepted artifacts in lieu of maximizing extraction efficiency.

Lyophilization (or freeze drying) is used to recover the dry PM after sonication by removing the water and is necessary to determine the mass of extracted PM for toxicological studies, which rely heavily on accurately knowing the administered dose. During lyophilization, the sonication solution – comprising extracted PM suspended in water – is frozen to a very low temperature, typically on the order of -80° C, and then subjected to high vacuum to sublimate the ice, leaving dry PM behind. Initially, the PM is completely encased in ice and protected from vacuum conditions but as the ice recedes and the particles are exposed, there is concern that a significant amount of material may volatilize from the PM. In fact, during the final stages of lyophilization the PM is subjected to high vacuum for extended periods while the last remaining amounts of ice are sublimated. There is no doubt that semi-volatile PM components, and even some portion of the nonvolatile organics, will be lost during this process. For example, preliminary results from our studies have shown that as much as 20-40% of the solvent extractable organics can be lost during lyophilization. Given the importance of the organic PM fraction in terms of toxicological testing, this is an artifact that was given significant attention when developing the filter extraction techniques deployed in the current study. The novel approach taken to circumvent this artifact was to use various chemical solvents to remove the organics prior to lyophilization and then add them back to the dry PM afterwards.

Numerous organic solvents with varying properties are readily available but for the purposes of the current study. The selection criteria included the following: (1) Since the organics are being removed from particles suspended in water after sonication, the solvent must be immiscible with water so that the two can be separated from each other. Therefore, only non-polar or polar aprotic solvents can be used. (2) The solvent must have a very high vapor pressure so that it can be evaporated quickly and thoroughly. (3) It must be a universally strong solvent but unreactive to maximize the number of organic compounds solvated and ensure they are chemically unaltered. Given these requirements, and in attempts to cover the polarity range of organic compounds, dichloromethane (DCM; polar aprotic) and hexane (Hx; non-polar) were chosen for the current study. DCM and Hx are also commonly used in the filter extraction step of sample preparation protocols for GC-MS analysis of particulate organic carbon for molecular speciation (*Schauer et al.*, 1996, 1999; *Sheesley et al.*, 2004; *Fine et al.*, 2001, 2004; *Ham et al.*, 2011). Other organic solvents, such as acetone, have been used in the filter extraction step of sample preparation for trace element analysis via ICP-MS (*Herner et al.*, 2006). Although acetone is miscible with water so inappropriate here, these studies suggest that

organic solvent extraction is necessary for trace element and molecular analyses of most combustion generated aerosol and/or SOA since (1) the trace metals are typically encapsulated by layers of organic compounds and (2) most organic compounds are hydrophobic and thus are not likely removed from the filter to any significant degree by water alone.

In the current study, DCM and Hx are sequentially added to the particle laden water from the sonication step in a separatory funnel and shaken vigorously. The layers are separated and the solvents evaporated to recover the solvent soluble fractions. Some fraction of the water soluble organic compounds are likely removed during this process as well since DCM is polar, but it is not clear how much and for which compounds. The solvent soluble fractions are then added back to the dry PM recovered from lyophilization of the H_2O sonication solution.

To avoid any compositional biases in what is removed from the filter, as well as increase overall extraction efficiencies, the filters from the current study were sequentially sonicated in DCM and Hx after the initial water sonication. This was done to remove any hydrophobic particles or particulate components not removed by sonication in water and still adhering to the filter media. PM is clearly still visible on the filters after sonication in water and the solvent sonications do a good job of removing a bulk of the remaining material. For example, the average percent of the total extracted PM mass recovered by the solvent sonications for all the afterfilters used in this study is 20 ± 10%. Note that solvent sonication is not possible for the polyurethane foam (PUF) substrates used in the $PM_{0.17}$ and $PM_{1.0}$ stages of the ChemVols since the solvents will partially dissolve these filters, leaving a contaminant residue in the sample. For example, during the testing stages of protocol development for the current study an average of 6.0 ± 0.06 mg of filter material was removed by solvent sonication.

Similar to the water sonication extract, the solvent sonication extracts are filtered to remove any FFP and then added back to the dry PM recovered from lyophilization. The order in which the sonications were performed in the current work was water followed by DCM and then Hx. This order was chosen since water is by far the strongest sonication medium, followed by DCM and then Hx, and the extracted particles exhibited significantly higher mobility in water compared to the solvents. For example, the study average percent of total extracted PM mass recovered from water sonication was 70 ± 10%. When DCM or Hx is used first, which was also tested during protocol development, significantly less mass is removed from the filter compared to water and the particles tended to adhere to the surfaces of the glassware rather than remaining suspended in solution, making them hard to transfer between glassware. Also, it does not matter that water sonication is performed first since the water sonication extract is washed with both solvents prior to lyophilization. A more detailed discussion of the filter extraction methodology used in this work is given in the following section.

Methodology

The ChemVols used during these experiments require two different types of filter media: Teflon coated borosilicate glass fiber afterfilters (Pall Corporation, TX40H120WW) for collecting the ultrafine fraction (D_p < 170 nm) and polyurethane foam (PUF) substrates (ThermoFisher Scientific, $PM_{1.0}$ substrates) for collecting the submicron fine fraction (170 < D_p < 1000 nm). For reasons discussed above, these two filter media require different extraction protocols. Descriptions of the protocols are given below and flow diagrams are shown in Figures (1) and (2) for the afterfilters and PUF, respectively.

Afterfilter Extraction Protocol (Figure 1)

1. Weigh filters to obtain a pre-weight for the filter extraction process; all weighing was performed using an A&D model HR-202i semi-micro analytical balance (0.01 mg readability); see following section (*Gravimetric Analyses*) for details on the gravimetric analysis procedures

2. Sonicate filters for ~ 1-2 hours in crystallization dish with ~ 600 mL milli-Q H_2O using a 5.5 gallon bath-style Branson model 8510 Bransonic® tabletop ultrasonic cleaner; circular stainless steel wire mesh screen is placed on top of filter to keep it submersed in milli-Q H_2O during sonication

3. Filter H_2O sonication extract solution (H_2O Ex) through an 8.0 μm Millipore membrane filter using a class M (10-15 μm porosity) fritted glass disc Buchner funnel

4. Transfer filtered H_2O Ex to a 2 L separatory funnel, add ~ 150 mL of dichloromethane (DCM), shake vigorously for ~ 5 minutes and allow layers to separate overnight

5. Drain DCM layer from bottom of separatory funnel into 1 L beaker, partially evaporate DCM under N_2 atmosphere, transfer to 20 mL weighing beaker, evaporate remaining DCM under N_2 atmosphere, weigh to obtain DCM soluble fraction (DCMW) and store in freezer until reconstitution

6. Repeat steps 4-5 using ~ 150 mL of hexane (Hx) to obtain Hx soluble fraction (HxW)

7. Transfer filtered and solvent-washed H_2O Ex to 1.2 L lyophilization flask (Labconco Fast-Freeze® flasks), freeze to -80° C, connect to lyophilizer operating at ~ 0.1 mbar pressure and -50° C (Labconco FreeZone® 2.5 liter benchtop freeze dry system) and sublimate ice until almost gone

8. Remove flask from lyophilizer, allow ice to partially melt, quantitatively transfer remaining H_2O Ex to 150 mL lyophilization flask, refreeze to -80° C, reconnect to lyophilizer and sublimate ice until almost gone

9. Repeat step 8 for an 80 mL lyophilization flask, quantitatively split and transfer remaining H_2O Ex to final 10 mL storage vials (one aliquot for toxicological studies and one aliquot to be archived for bulk chemical analyses), refreeze to -80° C, reconnect to lyophilizer, sublimate remaining ice, seal vials under vacuum and remove from lyophilizer

10. Weigh 10 mL vials under vacuum and subtract vial pre-weights (also weighed under vacuum; see *Gravimetric Analyses* section below) to obtain filtered and solvent-washed H_2O sonication fraction (H_2OEx); store vials under vacuum in freezer until reconstitution

11. Place original filter on drying rack in RH-controlled drying chamber, allow to dry for ~ 24 hours and reweigh filters

12. Sonicate filters for ~ 1-2 hours in crystallization dish with ~ 300 mL DCM; circular stainless steel wire mesh screen used to keep filter submersed during sonication

13. Filter DCM sonication extract solution (DCM Ex) through a class F (4-5.5 μm porosity) fritted glass disc Buchner funnel, transfer DCM Ex to 1 L beaker, partially evaporate DCM under N_2 atmosphere, transfer to 20 mL weighing beaker, evaporate remaining DCM, weigh to obtain filtered DCM sonication fraction (DCMEx) and store in freezer until reconstitution

14. Repeat steps 11-13 using Hx to obtain Hx sonication fraction (HxEx)

15. Reconstitute PM sample – remove components from freezer, break vacuum on 10 mL vials containing H_2OEx (step 10), dissolve organic fractions (DCMW, HxW, DCMEx and HxEx) back into appropriate solvents and quantitatively split and transfer to 10 mL vials (DCM and Hx are evaporated under N_2 atmosphere as the fractions are successively added), put 10 mL vials back under vacuum using lyophilizer and reweigh to obtain total extracted PM mass; crimp-seal with aluminum seal and store in a -20° C freezer until the toxicological studies

PUF Substrate Extraction Protocol (Figure 2)

1. Weigh filters to obtain a pre-weight for the filter extraction process; see following section (*Gravimetric Analyses*) for details on the gravimetric analyses procedures

2. Sonicate filters for ~ 1-2 hours in 1 L beaker with ~ 300 mL milli-Q H_2O; circular stainless steel wire mesh screen used to keep filter submersed during sonication

3. Perform steps 4-11 from the *Afterfilter Extraction Protocol* section on the initial H_2O sonication extract solution (H_2O Ex)

4. Cut filter into small pieces, add pieces to commercial grade blender with ~ 300 mL milli-Q H_2O, mechanically chop on high speed for ~ 3-5 minutes, transfer solution to 1L beaker and sonicate for ~ 1-2 hours; circular stainless steel wire mesh screen used to keep filter pieces submersed during sonication

5. Filter mechanically chopped H_2O sonication extract solution (MCH_2O Ex) through an 8.0 μm Millipore membrane filter using a class M (10-15 μm porosity) fritted glass disc Buchner funnel

6. Perform steps 4-10 from the *Afterfilter Extraction Protocol* section on the filtered MCH_2O Ex except that in step 9 the remaining MCH_2O Ex is added to the 10 mL vials containing the initial H2O Ex from step 3 above

7. Reconstitute PM sample – remove components from freezer, break vacuum on 10 mL vials containing H_2OEx + MCH_2OEx, dissolve organic fractions back into appropriate solvents and quantitatively split and transfer to 10 mL vials (DCM and Hx are evaporated under N_2 atmosphere as the fractions are successively added), put 10 mL vials back under vacuum using lyophilizer and reweigh to obtain total extracted PM mass; crimp-seal with aluminum seal and store in a -20° C freezer until the toxicological studies

Gravimetric Analyses

Gravimetric analysis – comprised of pre- and post-weighing filters, weighing beakers and storage vials – is by far the most difficult part of the entire filter extraction process but also one of the most important steps in terms of quantifying dose response and normalizing all ChemVols and size fractions to equal mass doses in the toxicological studies. There are numerous reasons for this, as will be discussed below, but the underlying fundamental challenge is subtracting two relatively large masses (filters, weighing beakers and storage vials are on the order of tens of grams) to obtain a very small mass (PM component masses at various stages of the filter extraction process are on the order of tens to hundreds of micrograms), where there is a 5 orders of magnitude difference between the two. As a result, measurement errors are large and these errors are compounded as they propagate through the various calculations of the analyses.

Random errors associated with the actual measurements are modest (on the order of tens of micrograms) and fairly easy to quantify by weighing the same object multiple times to obtain the average and standard deviation in the measurement, which can be used to define the confidence interval. Confidence intervals are then propagated through the calculations to obtain an error estimate for the calculated values. Systematic errors due to the effects of day-to-day fluctuations in environmental variables on both the balance and mass of an object, however, can be significantly larger (on the order of milligrams in some cases) and harder to track. The most important environmental variables are (*1*) temperature and relative humidity, which can affect the mass of an object (e.g. filters and PM), (*2*) the mass of the air column above the balance and the mass of any air within the

object relative to the surrounding air (e.g. buoyancy effects for weighing beakers and storage vials), (*3*) background electromagnetic radiation, which directly affects the operation of the balance and the concentration of charged particles in the air, (*4*) static charge, which alters the mass of an object by affecting its interaction with the surrounding environment and the operation of the balance, and (*5*) in the case of storage vials, the amount of time under vacuum during the lyophilization process.

The latter phenomenon, which was an unexpected finding of this work, deals with the adsorption of gas phase molecules on the surfaces of the storage vials when they are exposed to ambient lab air for extended periods, and the desorption of these molecules during the lyophilization process when the vials are subjected to vacuum. First, it is important to note that all storage vials are placed under vacuum prior to weighing. Not only does this sync best with the extraction process since the vials are already under vacuum when disconnecting from the lyophilizer, but more importantly, and for reasons outlined above, it has proven substantially more robust and precise compared to weighing vials with their contents at ambient conditions; note that the mass of air in a 10 mL vial at SATP is on the order of 17 mg.

The difference in the weight of a given vial under vacuum can vary between zero and more than a milligram depending on the difference in time the vial was put under vacuum prior to weighing. During pre-weighing, vials are attached to the lyophilizer and pumped down to operating conditions (~ 0.1 mbar), which takes less than a minute, before being sealed, removed and weighed. This process can be repeated with a high degree of precision in the measured masses. During lyophilization of an actual extracted PM sample, the vial remains under vacuum for periods on the order of several hours and the actual mass of the vial decreases due to this desorption phenomenon. Therefore, using the difference between pre- and post-weights of vials in these situations creates a systematic error in calculated PM masses.

The best way to track and quantify these errors, as well as the other systematic errors listed above, has been to incorporate standard reference vials and weighing beakers that are subjected to the exact same procedures and conditions as the sample vials and weighing beakers but never have anything added to them. Tracking differences in the measured masses of these standards throughout the entire filter extraction process provides a quantitative metric of systematic error that can be used to correct the PM mass calculations. This has been done for all of the calculations presented in this chapter. For example, the average mass lost by standard reference vials during lyophilization was 0.7 ± 0.2 mg and the variation in weighing beaker mass – note that weighing beakers are not weighed under vacuum and the error is largely due to static charge and buoyancy effects – was on the order of ± 30 μg.

Finally, pre- and post-weighing afterfilters and PUF substrates has proven extremely challenging and highly unreliable throughout this entire work. This is due to a combination of factors, namely (1) the size of the filters relative to the balance weighing pan (afterfilters are 6.75” in diameter and PUF substrates are annular rings with an outer diameter on the order of 5” while the weighing pan is only 3.1” in diameter), (2) the

effects of static charge, especially for the PUF, and (3) the effects of relative humidity on the absorption of water by both the filter substrate and deposited PM. Weighing clean filters is considerably more accurate than filters loaded with PM but is still challenging and not as reliable or precise as storage vials and weighing beakers. As a result, calculations involving differences between filter weights at various stages of the extraction process have been omitted from the results and discussions that follow.

Results and Discussion

The filter extraction techniques described above have been applied to all of the afterfilters and PUF substrates used during both the summer 2008 and winter 2009 source-oriented sampling experiments described in Chapter 2. This includes the ultrafine and submicron size fractions for ChemVols 1-7 and 9-10 for summer 2008 and ChemVols 1-10 for winter 2009, as well as duplicate afterfilter and PUF field blanks.

PM Component Distributions

The fractional distribution of total extracted mass among the PM components removed during the various steps of the filter extraction process are shown in Figures (3) and (4) for the ultrafine fractions collected during summer 2008 and winter 2009, respectively, and Figures (5) and (6) for the associated submicron fine fractions. The relevant PM components for the afterfilter extractions are: *(1)* filtered and solvent-washed H_2O sonication extracts (**H_2O Extract**), *(2)* DCM and Hx soluble fractions removed by solvent-washing the H_2O sonication solutions (**DCM Soluble** and **Hx Soluble**), and *(3)* filtered DCM and Hx sonication extracts (**DCM Extract** and **Hx Extract**). For the PUF extractions, the relevant components are: *(1)* solvent-washed H_2O sonication extracts (**H_2O Extract**), *(2)* DCM and Hx soluble fractions removed by solvent-washing the H_2O sonication solutions (**DCM Soluble (H_2O Ex)** and **Hx Soluble (H_2O Ex)**), *(3)* filtered and solvent-washed H_2O sonication extracts of mechanically chopped filters (**MC H_2O Extract**), and *(4)* DCM and Hx soluble fractions removed by solvent-washing the mechanically chopped H_2O sonication solutions (**DCM Soluble (MC Ex)** and **Hx Soluble (MC Ex)**). From these figures, it is clear that the largest fraction of total extracted ultrafine mass is recovered by water sonication (study average = 0.7 ± 0.1), followed by DCM sonication (study average = 0.2 ± 0.1) and then Hx sonication (study average = 0.03 ± 0.03). The average fractional contributions of the DCM and Hx soluble fractions to total extracted ultrafine mass were 0.1 ± 0.1 and 0.01 ± 0.01, respectively, for the W09 experiments and 0.07 ± 0.07 and 0.00 ± 0.01, respectively, for S08. For the PUF extractions, the study average fraction of total extracted submicron fine mass recovered from the initial water sonication was 0.6 ± 0.1 while water sonication of the mechanically chopped filter recovered 0.4 ± 0.1. The average S08 values for **DCM Soluble**, **Hx Soluble, DCM Soluble (H_2O Ex)** and **Hx Soluble (H_2O Ex)** are 0.14 ± 0.06, 0.01 ± 0.01, 0.04 ± 0.03 and 0.00 ± 0.01, respectively, and for W09 these values are 0.07 ± 0.04, 0.01 ± 0.01, 0.05 ± 0.03 and 0.00 ± 0.01, respectively.

Extraction Efficiencies

Extraction efficiency is defined as the fraction of the total PM mass sampled onto a filter that is removed during the filter extraction process. Although extraction efficiencies could not be directly calculated due to the various problems encountered when pre- and post-weighing filters, as described in the *Gravimetric Analyses* section, the increased efficiency of the filter extraction techniques deployed in this study compared to conventional methods can be readily inferred from the data shown in Figures 3-6. The conventional H_2O sonication and lyophilization method will only yield the **H2O Ex** fraction, as well as some portion of the **DCM Soluble** and **Hx Soluble** fractions, in these figures. The remaining fraction of total extracted mass – i.e. the **DCM Ex** and **Hx Ex** fractions from the afterfilter extractions and the **MC H_2O Ex**, **DCM Soluble (MC Ex)** and **Hx Soluble (MC Ex)** fractions from the PUF extractions – represents an increase in extraction efficiency. On average, conventional methods can only account for roughly 60-70% and 55-65% of the total extracted ultrafine and submicron PM mass, respectively, obtained using the filter extraction techniques described here. This is extremely important in the current study since the mass collected by CVs associated with the more infrequently observed sources or source combinations is close to the target mass required for the toxicological studies and these high extraction efficiencies are necessary to ensure the health effects studies can be properly conducted.

Mass Closure

For the filter extraction techniques deployed in this study, mass closure was assessed by comparing the total extracted PM mass obtained from weighing the reconstituted composite extracts in the final storage vials to that obtained by summing the masses of the individual PM components extracted during the various steps of the filter extraction process; i.e. H2OEx + DCM soluble + Hx soluble + DCMEx + HxEx. These data are shown by ChemVol and aliquot in Tables (1) and (2) for the ultrafine and submicron PM fractions collected during the summer 2008 and winter 2009 experiments, respectively. A graphical depiction has been included in Figure (7) showing the percent difference between the composite mass and component sum by ChemVol, size fraction and sampling campaign. The average percent difference over all filter extractions performed during this study was only 4%, demonstrating good mass closure given the large sources of uncertainty in this analysis.

Conclusions

A method was presented for extraction of deposited particulate matter from filter and PUF impactor substrates that has a much higher efficiency and likely less composition bias than other methods. The method was employed on nearly 40 different composition samples, half from filters, half from PUFs, collected in Fresno, California as part of a study to collect ambient particulate matter associated with different sources.

Although numerous methods are available in government, industry and academic laboratories for extracting collected particulate matter from filter and impactor substrates, these methods were insufficient for the requirements posed by Source-Oriented Toxicity research for two reasons. First, some of the ChemVols have a very small amount of mass

deposited so that higher extraction efficiencies are required so that enough material is available for the toxicity studies. The extraction efficiencies for common methods are near 70% (*personal communication, Robert Devlin*, 2009) and our goal was to develop a method closer to 90%, or even higher. Second, the low extraction efficiencies might mean that material was extracted off the substrates in such a way as to result in a composition bias. That is, material left on the substrate is likely to be more sticky or less soluble in the method's solvents than material that was successfully extracted and this material may be more or less toxic than the extracted material resulting in bias in the toxicological results.

Another requirement for the extraction protocol needed for toxicity studies is a clear indication of the mass extracted so that dose response relationships can be elucidated. Weighing substrates, extracting and then reweighing to obtain an estimate of extracted mass may introduce error since some of the solvent may still be on the substrate and subtracting two large numbers to obtain a small difference, the mass extracted, is error prone. The methods presented here involve lyophilization, so a direct measure of PM mass is obtained minimizing artifacts from the substrate.

The extraction method presented here is generally more time consuming than those available in other laboratories since careful attention was paid to quantifying and characterizing each stage of the process for publication. If only the final mass of extracted PM is desired, then the entire process can be completed in ~ 10 days for a single sample. The capacity of our lab allowed four samples to be extracted in parallel. This method may not be suitable for all studies but for studies where high extraction efficiencies are desired and where minimizing composition bias in the extracts is a goal, the method presented here is appropriate.

References

Anastasio, Cort, Department of Land, Air and Water Resources, University of California Davis, Davis, CA, personal communication, 2010.

Bowser, Darlene, Standard operating procedure for PUF and filter CAP extraction. New York University School of Medicine, NY, personal communication, 2009.

Devlin, Robert, Standard operating procedure for extraction of concentrated particulate matter from PUF and G5300 media. National Health and Environmental Effects Research Laboratory, U.S. Environmental Protection Agency, Research Triangle Park, NC, personal communication, 2009.

Fine, P.M., Cass, G.R., Simoneit, B.R.T., Chemical characterization of fine particle emissions from fireplace combustion of woods grown in the northeastern United States. *Environmental Science & Technology* 35, 2665-2675, 2001.

Fine, P.M., Cass, G.R., Simoneit, B.R.T., Chemical characterization of fine particle emissions from the wood stove combustion of prevalent United States tree species. *Environmental Engineering Science* 21(6), 705-721, 2004.

Ham, A.W. and Kleeman, M.J., Size-resolved source apportionment of carbonaceous particulate matter in urban and rural sites in central California. *Atmospheric Environment* 45(24), 3988-3995, 2011.

Herner, J.D., Green, P.G., Kleeman, M.J., Measuring the trace elemental composition of size-resolved airborne particles. *Environmental Science & Technology* 40, 1925-1933, 2006.

Schauer, J.J., Rogge, W.F., Hildemann, L.M., Mazurek, M.A., Cass, G.R., Source apportionment of airborne particulate matter using organic compounds as tracers. *Atmospheric Environment* 30, 3837-3855, 1996.

Schauer, J. J.; Kleeman, M. J.; Cass, G. R.; Simoneit, B. R. T., Measurement of emissions from air pollution sources 1. C1 through C29 organic compounds from meat charbroiling. *Environmental Science and Technology* 33(10), 1566–1577, 1999.

Sheesley, R.J., Schauer, J.J., Bean, E., Kenski, D., Trends in secondary organic aerosol at a remote site in Michigan's upper peninsula. *Environmental Science & Technology* 38, 6491-6500, 2004.

Tablin, Fern, Department of Veterinarian Medicine, University of California Davis, Davis, CA, personal communication, 2011.

Table 3-1. Total extracted PM mass via weighing the reconstituted composite extracts versus summing the individual components.

ChemVol	Aliquot	Winter 2009 Ultrafine Mass (mg)						Winter 2009 Submicron Fine Mass (mg)					
		Composite Mass		Component Sum		% Diff		Composite Mass		Component Sum		% Diff	
		Value	Error	Value	Error	Value	Error	Value	Error	Value	Error	Value	Error
1	1	4.08	0.08	4.19	0.16	2.54	4.20	2.72	0.15	2.73	0.16	0.46	7.97
	2	4.68	0.07	4.54	0.11	3.11	2.88	2.64	0.12	2.61	0.10	0.99	5.96
2	1	2.22	0.05	2.69	0.28	17.25	8.97	2.55	0.11	2.54	0.21	0.31	9.39
	2	2.36	0.03	2.78	0.24	15.04	7.46	2.45	0.09	2.39	0.21	2.13	9.56
3	1	1.53	0.02	1.68	0.14	9.08	7.47	2.94	0.09	2.92	0.08	0.71	4.01
	2	1.53	0.06	1.68	0.08	9.44	5.39	2.80	0.10	2.92	0.16	4.01	6.28
4	1	1.19	0.06	1.15	0.12	3.40	11.93	1.51	0.09	1.51	0.20	0.53	14.19
	2	1.26	0.11	1.28	0.15	1.68	14.41	1.50	0.18	1.44	0.11	4.13	14.92
5	1	1.96	0.06	N/A	N/A	N/A	1.27	1.59	0.08	1.60	0.14	0.29	9.96
	2	2.96	0.15	3.06	0.16	3.46	6.97	1.57	0.13	1.56	0.15	0.99	13.22
6	1	1.26	0.08	1.21	0.18	3.60	16.93	1.27	0.08	1.20	0.12	5.81	12.45
	2	1.32	0.08	1.17	0.11	11.73	12.27	1.22	0.10	1.24	0.13	1.61	13.31
7	1	2.94	0.21	2.38	0.27	19.04	16.57	1.31	0.09	1.30	0.17	0.99	14.92
	2	2.92	0.05	3.13	0.21	6.84	6.60	0.96	0.15	0.97	0.20	1.34	26.00
8	1	4.37	0.07	4.52	0.21	3.17	4.83	3.95	0.13	3.98	0.29	0.76	7.88
	2	4.68	0.07	4.76	0.13	1.66	3.04	3.99	0.17	4.02	0.28	0.85	8.00
9	1	6.08	0.06	5.51	0.15	9.49	3.20	4.41	0.13	4.47	0.15	1.36	4.29
	2	5.92	0.32	6.01	0.32	1.56	7.52	4.49	0.13	4.47	0.20	0.47	5.34
	3	5.99	0.17	5.76	0.16	3.86	3.75	4.39	0.08	4.73	0.19	7.11	4.81
10	1	N/A	N/A	N/A	N/A	N/A	N/A	3.19	0.07	3.24	0.16	1.51	5.44
	2	N/A	N/A	N/A	N/A	N/A	N/A	3.01	0.04	3.04	0.11	0.95	3.78
Field Blank	1	0.65	0.10	0.55	0.10	15.28	28.19	0.57	0.12	0.54	0.15	6.27	37.18
	2	0.66	0.13	0.57	0.14	12.65	35.17	0.63	0.13	0.60	0.14	4.78	33.19

Table 3-2. Total extracted PM mass via weighing the reconstituted composite extracts versus summing the individual components.

ChemVol	Aliquot	Summer 2008 Ultrafine Mass (mg)						Summer 2008 Submicron Fine Mass (mg)					
		Composite Mass		Component Sum		% Diff		Composite Mass		Component Sum		% Diff	
		Value	Error	Value	Error	Value	Error	Value	Error	Value	Error	Value	Error
1	1	5.62	0.06	5.57	0.20	0.7	3.7	6.43	0.09	6.41	0.12	0.2	2.3
	2	5.93	0.33	5.82	0.34	2.0	8.2	6.80	0.09	6.80	0.12	0.0	2.2
	3	5.55	0.25	5.47	0.18	1.5	5.5	0.00	0.00	0.00	0.00	0.0	0.0
2	1	5.04	0.04	4.86	0.16	3.4	3.4	5.67	0.07	5.58	0.12	1.7	2.6
	2	6.26	0.13	6.02	0.15	3.7	3.4	5.76	0.11	5.68	0.16	1.3	3.5
	3	5.50	0.20	5.31	0.14	3.3	4.3	5.65	0.06	5.80	0.13	2.6	2.5
3	1	2.50	0.17	2.25	0.17	10.2	11.3	1.41	0.10	1.37	0.10	2.5	10.4
	2	2.40	0.12	2.24	0.12	6.8	7.9	1.31	0.09	1.33	0.10	1.9	9.8
4	1	1.64	0.10	1.81	0.10	9.6	7.5	1.32	0.09	1.29	0.12	1.7	11.7
	2	1.67	0.06	1.56	0.07	6.2	6.4	1.32	0.11	1.28	0.11	3.0	12.3
5	1	1.30	0.11	1.33	0.19	2.4	16.5	0.94	0.19	0.82	0.13	12.8	28.6
	2	1.21	0.12	1.26	0.19	3.8	17.0	1.06	0.18	0.94	0.13	11.1	24.6
6	1	2.71	0.03	2.71	0.13	0.1	4.9	1.92	0.05	1.93	0.12	0.8	6.5
	2	1.42	0.19	1.40	0.23	1.7	21.5	1.84	0.07	1.84	0.12	0.2	7.3
7	1	2.14	0.13	1.95	0.09	8.9	8.5	1.76	0.08	1.84	0.18	4.5	10.4
	2	2.14	0.19	1.96	0.20	8.8	15.0	1.76	0.05	1.83	0.15	3.8	8.4
9	1	7.62	0.06	7.70	0.15	1.1	2.1	4.83	0.04	4.75	0.14	1.7	3.1
	2	7.38	0.24	7.54	0.26	2.2	4.6	4.97	0.06	4.81	0.14	3.3	3.2
	3	31.89	0.05	29.49	0.15	7.5	0.5	8.41	0.03	8.21	0.13	2.3	1.6
10	1	2.35	0.08	2.34	0.07	0.2	4.3	5.33	0.12	5.22	0.11	2.1	3.2
	2	2.44	0.08	2.44	0.09	0.1	4.8	5.02	0.11	4.94	0.11	1.5	3.1
Field Blank	1	0.66	0.10	0.64	0.11	3.8	24.6	0.50	0.11	0.57	0.12	12.8	25.9
	2	0.58	0.10	0.59	0.12	1.5	26.3	0.50	0.13	0.56	0.12	11.2	29.9

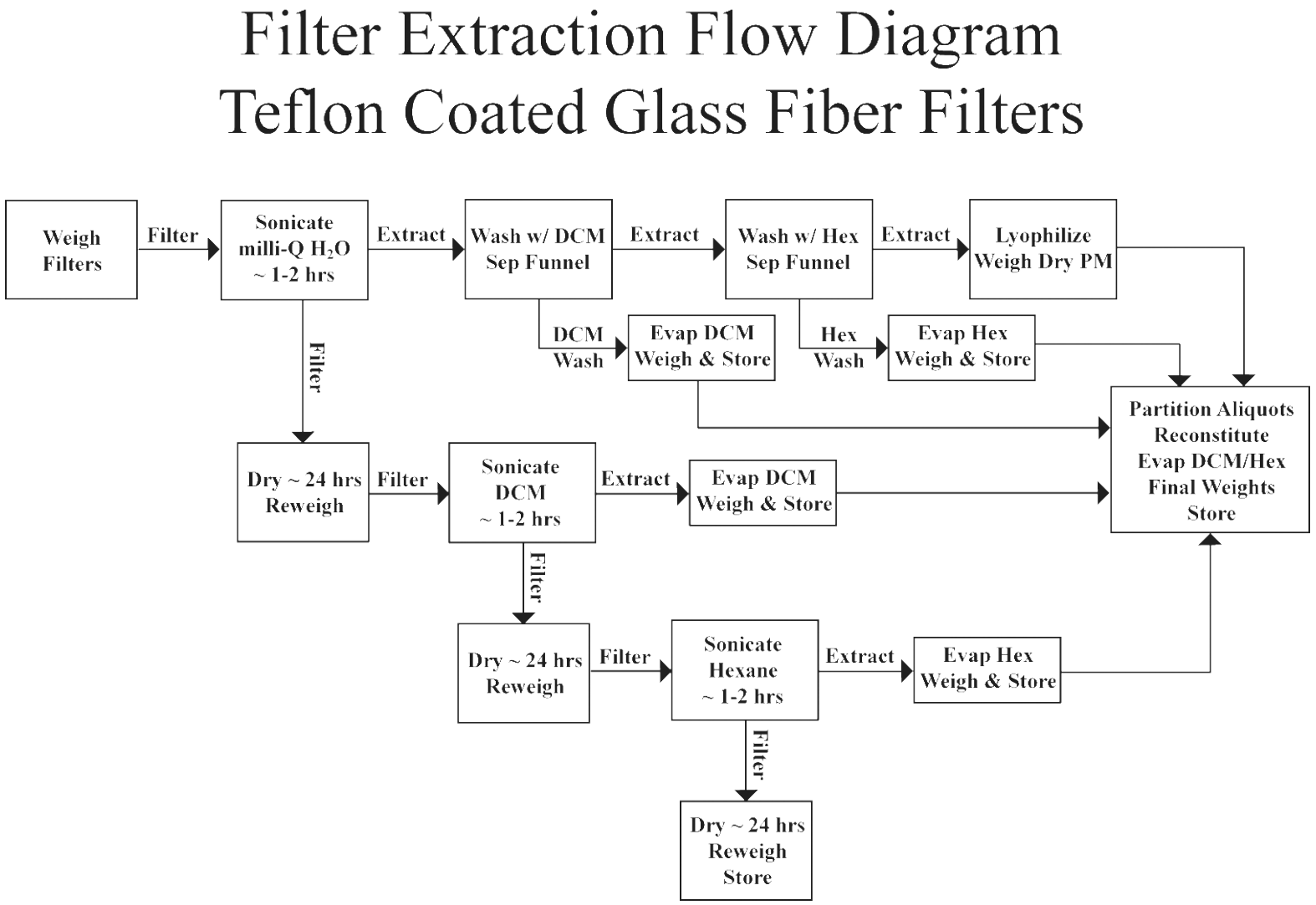

Fig 3-1. Flow diagram of the filter extraction and particle reconstitution process for Teflon coated borosilicate glass fiber afterfilters.

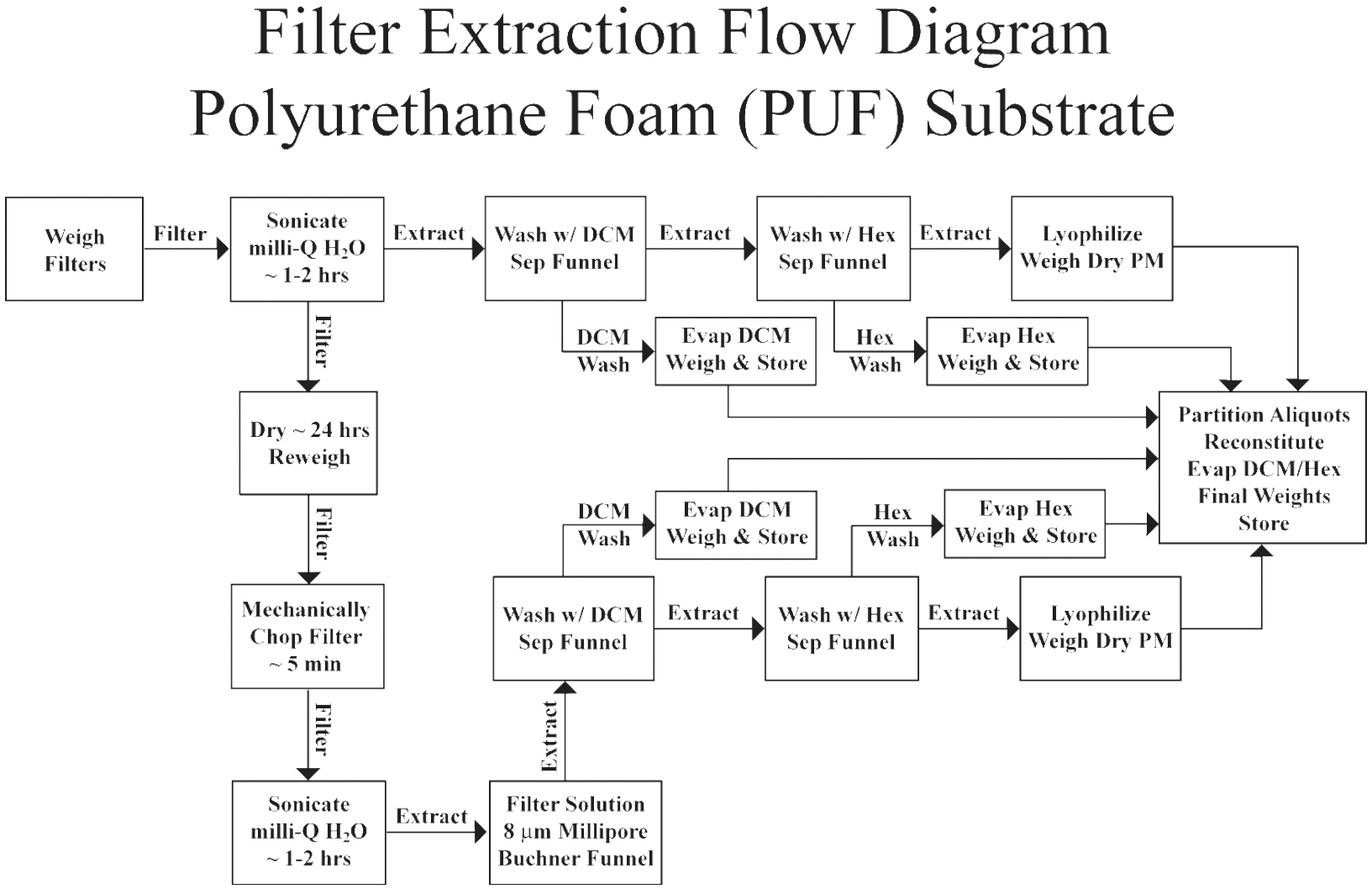

Figure 3-2. Flow diagram of the filter extraction and particle reconstitution process for polyurethane foam (PUF) substrates.

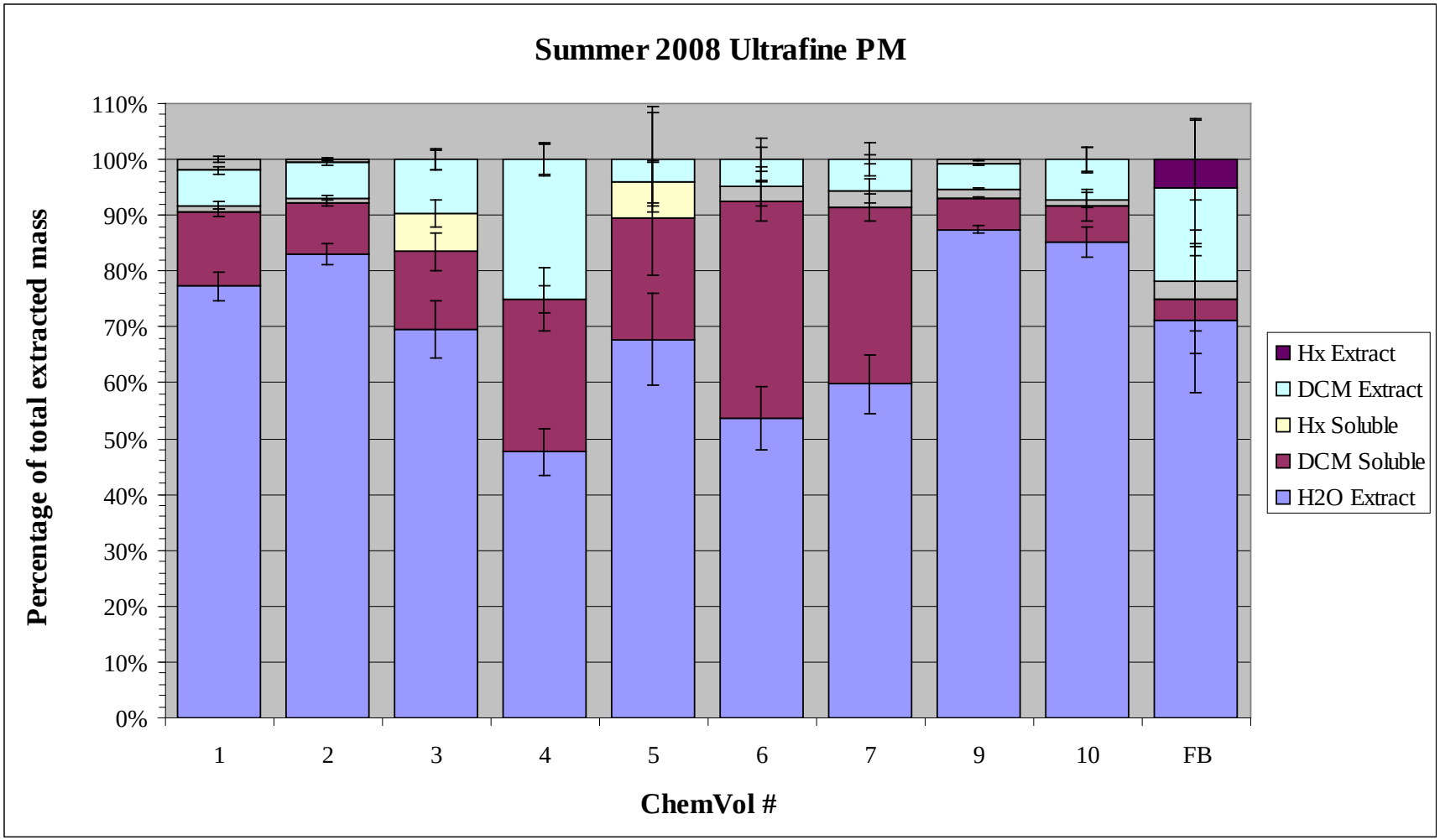

Figure 3-3. The fractional distribution of total extracted mass among the PM components removed during the various steps of the filter extraction process for the ultrafine PM fractions collected during the summer 2008 experiment by ChemVol; FB = field blank. See text for a description of the various PM components.

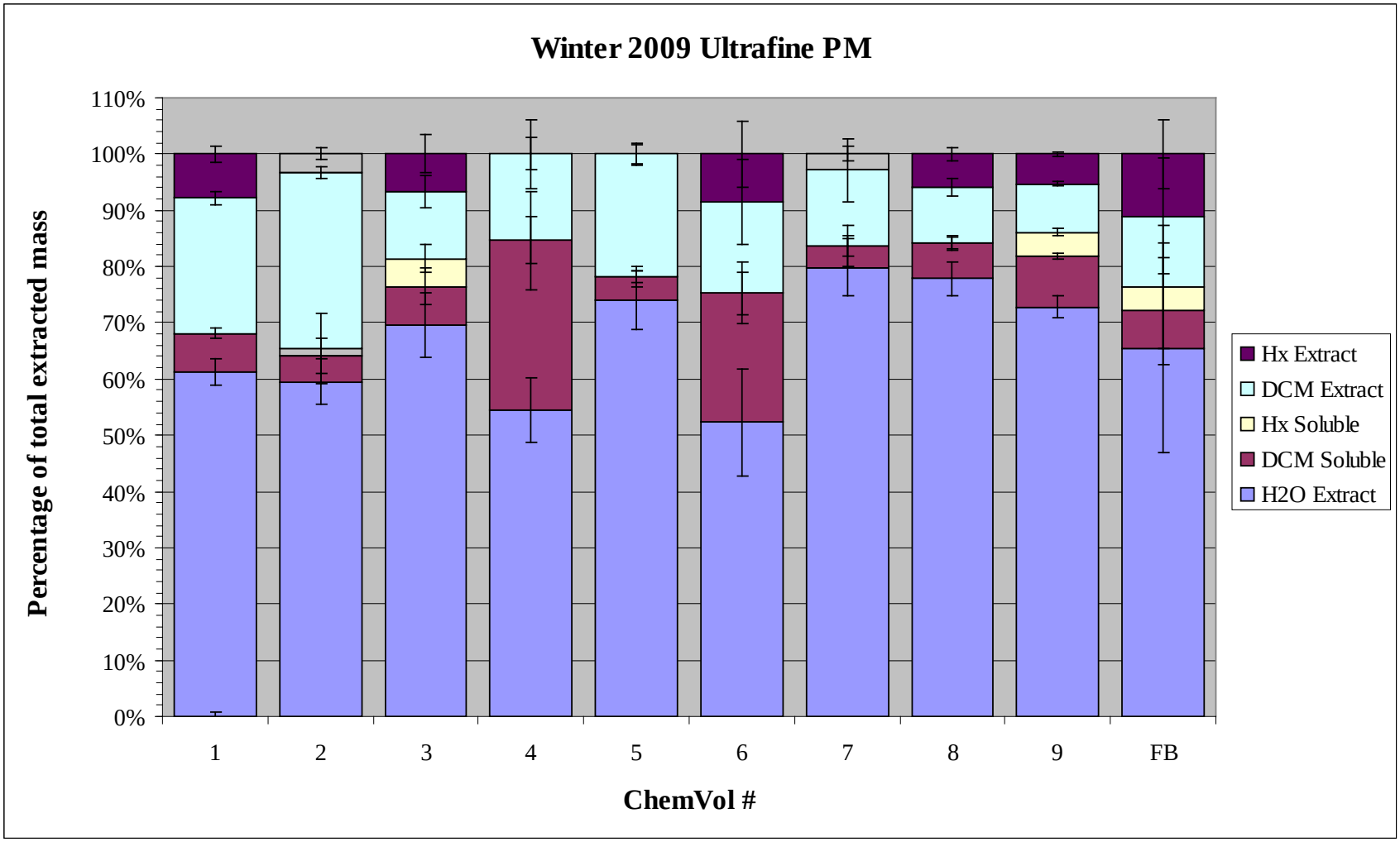

Figure 3-4. The fractional distribution of total extracted mass among the PM components removed during the various steps of the filter extraction process for the ultrafine PM fractions collected during the winter 2009 experiment by ChemVol; FB = field blank. See text for a description of the various PM components.

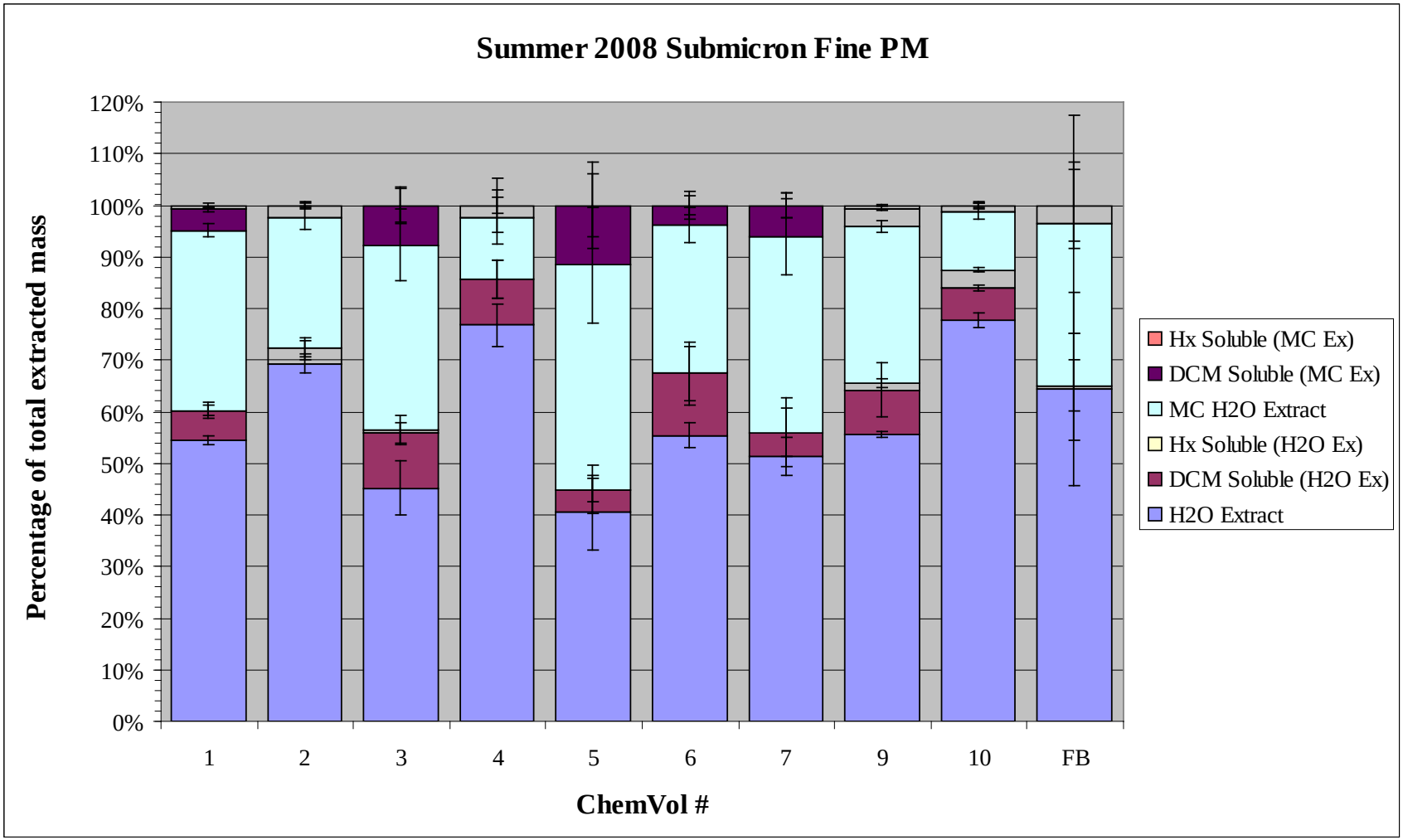

Figure 3-5. The fractional distribution of total extracted mass among the PM components removed during the various steps of the filter extraction process for the ultrafine PM fractions collected during the summer 2008 experiment by ChemVol; FB = field blank. See text for a description of the various PM components.

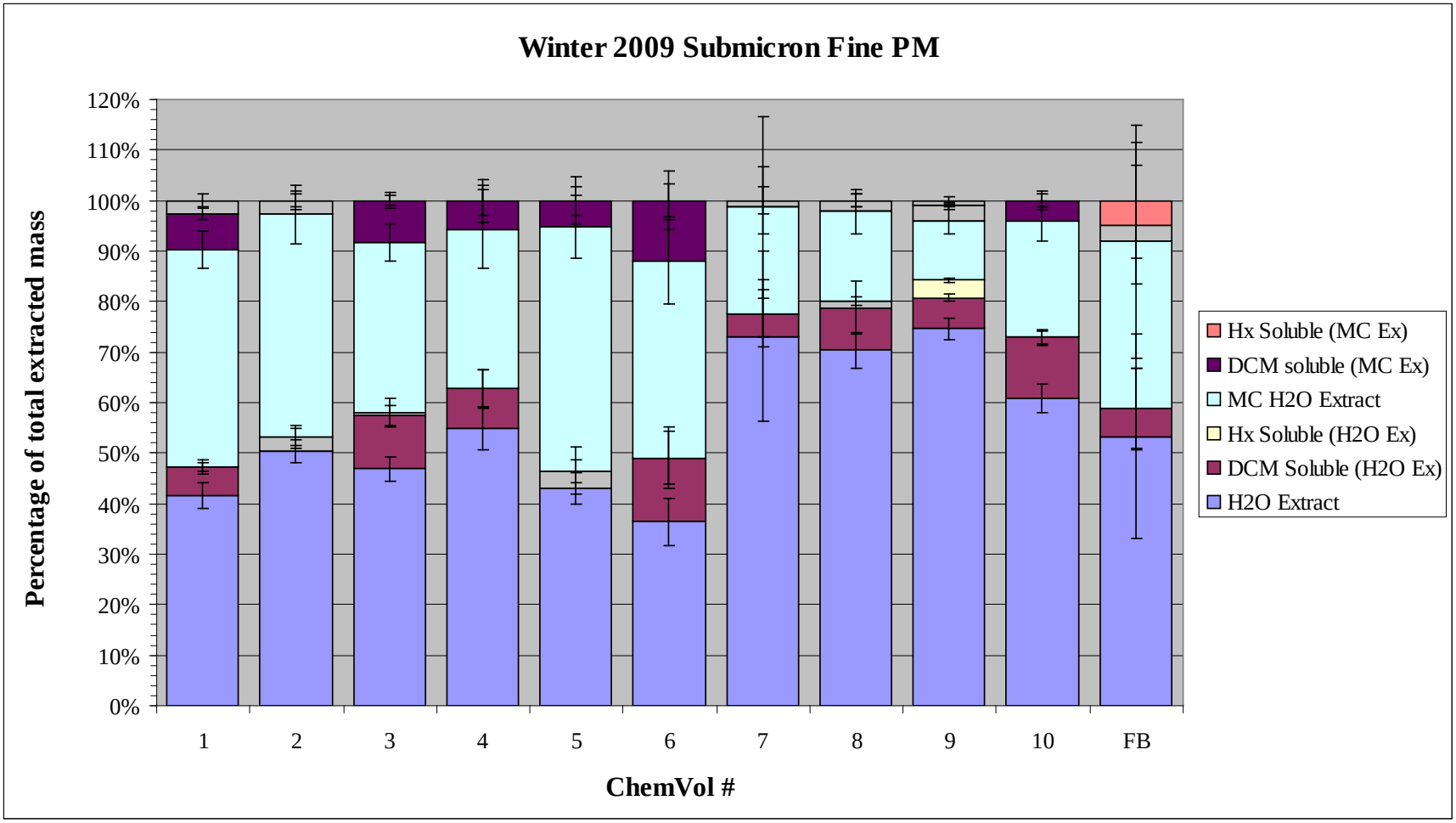

Figure 3-6. The fractional distribution of total extracted mass among the PM components removed during the various steps of the filter extraction process for the ultrafine PM fractions collected during the winter 2009 experiment by ChemVol; FB = field blank. See text for a description of the various PM components.

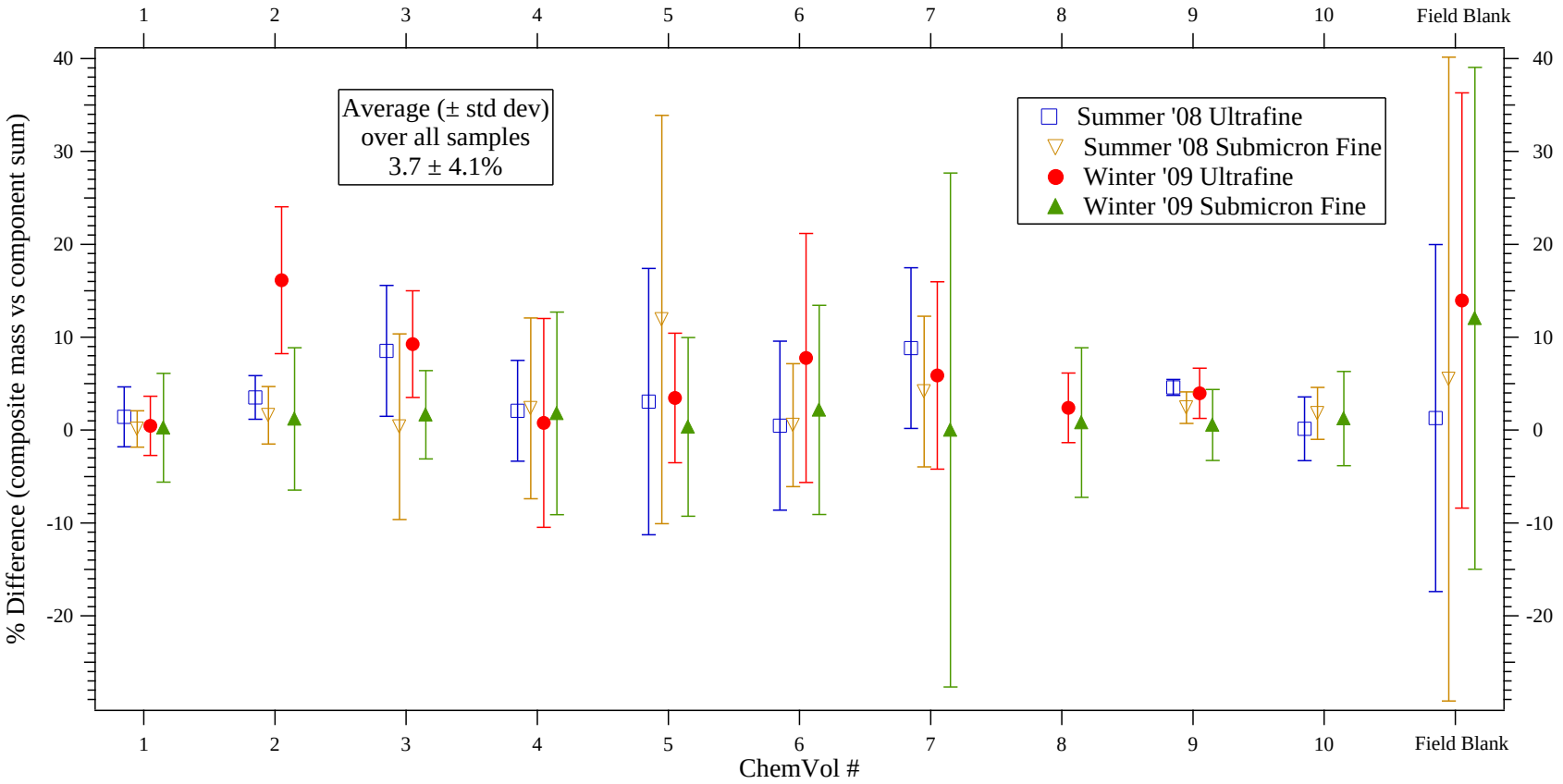

Figure 3-7. Percent difference between the total extracted mass obtained by weighing the final reconstituted composite extracts versus summing the component masses obtained during the various steps of the filter extraction process; see text for a description of the filter extraction process and associated PM components.

Chapter 4
Source Attribution for Source Oriented Sampling and Toxicity

K.J. Bein
Air Quality Research Center, University of California Davis

To be submitted for publication

Abstract

Source oriented samples were collected in Fresno California during the Summer of 2008 and the Winter of 2009. Samples were collected with 10 ChemVols that collected a submicron fine sample and an ultrafine sample. ChemVols collected samples depending on the sources sensed at a given time by a single particle mass spectrometer that analyzed the chemical composition of particle in real time. These same single particle mass spectra were analyzed in this work along with wind direction data and the prevalence of sources around the collection site on Shaw Avenue in Fresno to identify the sources of PM collected by each ChemVol. These source identifications are used in subsequent chapters to relate toxicity to emissions sources.

Introduction

Samples collected by source-oriented sampling, described in Chapter 2, are found in Chapter 5 to elicit markedly different toxicological responses. Some of the sources/sizes were relatively benign and others indicated toxic response significantly above vehicle control and/or above CV10; CV10 is a mix of the PM in Fresno during each of the two seasons and somewhat represents the PM that would have been collected at night without source-oriented sampling. This section associates each of the source-oriented samples with emission sources, emission source combinations, and secondary PM found in Fresno during both summer and winter seasons.

The single particle instrument was operated daily from the early evening, after 15:00 for summer 2008 (S08) and after 17:00 for winter 2009 (W09), until the morning, before 11:00 for S08 and 06:00 for W09, and was off for the remainder of the time. The main reasons for this operating schedule are due to the effects of daytime turbulent mixing on the concentration and mixing state of the air shed and thus on the ability of the single particle instrument to *(a)* obtain sufficient particle hit rates and *(b)* isolate distinct sources from the atmospheric mixture for sufficient periods of time to conduct these experiments. As a result, the single particle instrument was off during these periods and a single ChemVol (CV 9 for both S08 and W09) was operated instead to capture the contents of the daytime mixed layer for comparative purposes. Furthermore, this means that the source-oriented ChemVols (CVs 1-7 for S08 and 1-6 for W09) mostly represent local, nighttime sources emitting during the hours of ~ 17:00-09:00 and largely under a nocturnal inversion where turbulent mixing is less pronounced. The average particle number distributions for this period, as determined from collocated SMPS data by averaging over the entire study period, are depicted as contour images in Figure (4.1) for the S08 and W09 experiments. The significant differences between the daytime structure in the dynamics of particle size distribution between S08 and W09 suggests significantly different daytime processes are occurring and should offer an interesting basis for a comparative toxicological study.

CV 10, also termed the auxiliary ChemVol, was operated during periods when the source mixture could not be definitively discerned or did not match one of the predetermined source combinations assigned to the source-oriented ChemVols from the results of the pre-studies. Although CV 10 was by far the most frequently operated ChemVol due to the nature of these experiments, it should not be mistaken as representing the combination of all other ChemVols. Rather, it more accurately represents the background, nighttime mixture minus the source combinations assigned to the source-oriented ChemVols plus any sources or source combinations not identified and isolated during the pre-studies. Since the sampling system was only able to isolate sources and source combinations during a small minority of the nocturnal sampling period, CV10 samples contain much of the same material collected in the source-assigned ChemVols. Therefore, when comparing and contrasting results from the toxicological studies, it should be considered its own separate and unique source mixture different from the other source-oriented ChemVols but nearly represents what would have been collected by operating a ChemVol during the same hours each night (~17:00-9:00).

During the W09 experiment, CVs 7 and 8, similar to CV 9, were timed, rather than source-oriented, ChemVols; i.e., they were configured to sample daily during predetermined time intervals. The time intervals were designed to capture specific sources or source combinations known to preferentially emit at particular times of day. For example, CV 8 was operated daily during the hours of 06:00-09:00 in attempts to isolate vehicular emissions originating from the morning rush hour commute. These emissions can be seen in Figure (4.1a) as the large increase in ultrafine particle number concentrations occurring in the period 06:00-09:00. Similarly, CV 7 sampled daily from 17:00-20:00 to capture the mixture of vehicular emissions from the evening rush hour and residential and commercial cooking emissions. However, CV7 was only used during the last 5 days of the W09 experiment and was incorporated into the sampling routine based on sudden and large increases in ultrafine particle number concentrations observed in the SMPS data during that period. For a majority of the W09 experiment (30 out of a total of 35 sampling days), CV7 was not used; the single particle instrument operated normally during the 17:00-20:00 period, sampling into the source-oriented ChemVols (CVs 1-6) via the previously described sampling algorithms. Note that CV8 was not deployed during the S08 experiment.

In the source attribution efforts that follow, a synthesis of *(1)* single particle composition, *(2)* temporal trends in the activation and sampling times of the CVs, *(3)* correlations between CV sampling periods and wind direction and *(4)* knowledge of the local and regional sources, as well as secondary compounds formed by atmospheric processing, are used to reconcile and characterize the sources and source combinations assigned to each of the CVs. In terms of the latter, Figure (4.2) includes several Google Earth images of the sampling site and surrounding area at different spatial scales to show (a) sources within the immediate vicinity of the site, (b) the surrounding residential and commercial sectors, (c) a full view of the greater Fresno area and (d) regional inputs to the air shed.

It is clear from these images and prior knowledge of the sources of primary PM emissions in Fresno that the largest source contributions to the Fresno air shed will be from (*Ham and Kleeman*, 2011; *Kleeman et al.*, 2009; *Rinehart et al.*, 2006; *Chu et al.*, 2004; *Battye et al*., 2003; *Poore et al.*, 2002; *Watson and Chow*, 2002; *Schauer and Cass*, 2000; *Watson et al.*, 2000):

- **vehicular emissions** – including cold starts, idling and low to high speed operation of internal combustion and diesel engines on highways, local roads, residential streets and parking lots
- **residential and commercial emissions** – including cooking, space heating, construction and landscaping activities (e.g., two-stroke motors used in lawn mowers, leaf blowers, hedgers, trimmers, etc.)
- **agricultural emissions** – including cattle ranching (e.g., CH_4 and NH_3), agricultural machinery (e.g., off-road vehicles, trucks, tractors, harvesters and hullers), waste and debris burning and the product transportation infrastructure (mainly diesel trucks and tractor trailers)
- **long range transport** – most notably wildfires but also emissions from neighboring cites and potential trans-Pacific transport, and

- **atmospheric processing**, resulting in myriad gas and particulate phase organic (e.g. SOA) and inorganic (e.g. NH_4NO_3) species.

As a result, and on a mass basis, particle composition will be largely dominated by organic carbon (including a suite of aliphatic and aromatic hydrocarbons such as PAHs, oxygenated species, nitrogen containing compounds such as amines, and organosulfates), elemental carbon (i.e. soot, black carbon and/or brown carbon) and inorganic salts (e.g., nitrates and sulfates); see references cited above. However, since the single particle mass spectrometer measures the composition of particles one-by-one and most particles contain metals indicative of their source, most notably K (potassium) from biomass combustion, on a number basis metals will constitute a large fraction of the particle population.

Correlating CV sampling periods with predominant wind directions is possible due to the high temporal resolution of the single particle data. The timestamp of each single particle mass spectrum can be used to associate it with the wind speed and direction measured at the same time. The wind measurements were obtained from wind speed and direction sensors (Met One Instruments Inc., 010C; 020C) placed on top of the trailer at the same height as the sampling stacks for both the CV sampling train and single particle instrument. Correlating each spectrum with a wind direction helps to associate particles with their sources. A wind speed and direction is assigned to each single particle mass spectrum and the spectra are sorted and organized according to CV sampling times. For a given CV, the wind data associated with the spectra are counted across all sampling intervals and binned in wind direction degree intervals to obtain a frequency distribution showing the frequency with which the wind was blowing from a certain direction while that particular CV was sampling. These data are then normalized by the frequency distribution of all wind observations to elicit those directions preferentially sampled by each ChemVol relative to the typical wind direction profile. Results are shown in Figures (4.3) and (4.4) for each of the source-oriented CVs from the S08 and W09 experiments, respectively. All of the ChemVols sampled from specific wind sectors, some narrower than others. Knowledge of the geospatial arrangement of the surrounding sources relative to the sampling site (shown in Figure (4.2)) can be used with CVs that show high sampling directionality to help characterize and substantiate the sources or source combinations attributed to those CVs.

Lastly, temporal trends in the activation and sampling times of the CVs are shown in Figures (4.5) and (4.6) for each of the source-oriented CVs from the S08 and W09 experiments, respectively. These data are plotted as the fraction of total sampling time for a given CV as a function of hour of the day. If CV sampling is highly correlated with a certain time of day and particular sources are known to dominant during those times, then, similar to the wind direction correlations, this helps further elucidate and substantiate the sources or source combinations attributed to specific CVs.

Single Particle Composition

Below are detailed descriptions of the various single particle compositions observed during the S08 and W09 experiments that were used in the sampling algorithms to direct the operation of the source-oriented CVs. These discussions are organized around the dominant particle classes obtained from analysis of the pre-study data and used to construct the class

combinations assigned to the various CVs. A complete description of how these data were obtained and how they were used in the source-oriented sampling algorithms is given in Chapter 2.

It is important to note that the particle classes observed in the summer and winter seasons are likely from the same sources and source combinations. So for efficiency of notation and comparative clarity when discussing the various particle classes constituting the S08 and W09 ChemVol source combinations detailed below, Table 4.1 shows a mapping between the particle class notations used in Chapter 2 and new ones used from this point forward that more clearly denote the similarity between summer and winter emission sources.

Table 4.1. Reconciliation of summer and winter source categories and classes

Source Category (Chapter 4 notation)	**ChemVol Class (Chapter 2 notation)**
s-K w-K	K(d) PMP
s-CAN w-CAN	AN/EC/OC CAN
s-EC w-EC	EC EC
s-K/EC/OC w-K/EC/OC	K/EC/OC MsC
s-EC/OC w-EC/OC	EC/OC Carbon
w-K/CAN	MCAN

SMPS measurements during sampling usually show a monomodal particle size distribution centered below the ~170 nm cutpoint of the ChemVols; see Chapter 2. Although the single particle instrument was configured to analyze particle sizes near the middle of these distributions for the entirety of these experiments, the monomodal distribution suggests that the single particle compositions likely represent the relevant PM components and their internal mixing state but not necessarily the mass distribution of the observed components within individual particles. Since the size distribution of the total particle population is simply a superposition of the size distributions of individual particle types, sampling particles from the middle of the distribution should be fairly representative of all particle types comprising the entire mode.

Another complication in developing the following source assignments is that although particle classes generally represent a unique single particle composition attributable to a particular source or source category, individual sources and source categories can emit multiple types of particles and different sources or source categories may also emit the same particle type.

Summer 2008

s-K (Potassium) – According to the single particle data, this class of particles, representing 33.5% of the total number of particles detected during the CV sampling portion of the S08 experiment, is characterized by individual particles composed almost entirely of potassium salts and/or oxides with only trace signal from other constituents, most notably sodium and carbon. Given their size and composition, these particles most likely originate from local sources of biomass combustion, including residential and commercial heating and cooking, wildfires, and agricultural and waste related burning. The general absence of organic carbon – which is also emitted during biomass combustion – in these particles is an important result and could be attributed to one of several factors: (1) depending on atmospheric conditions and background concentrations, the effects of dilution could drive the semivolatile organics into the gas phase (2) if the ratio of the concentration of gas phase organics to the particle surface area available for condensation is low then the condensing organic vapors would be spread thinly over a large particle population, resulting in individual particles with only trace to undetectable amounts of organic carbon, and (3) depending on combustion conditions and biomass composition, the concentration and compositional distribution of emitted gas phase organics will vary largely, suggesting the possibility that these particles represent a specific type of biomass combustion that emits relatively low concentrations of semi- to nonvolatile organics and large numbers of ultrafine particles. For instance, this is indicative of what is observed during purely flaming, as opposed to smoldering or mixed flaming/smoldering, biomass combustion. Flaming, relative to smoldering or mixed phase, combustion is well known to produce larger particle number, lower particle mass, smaller particle size and particles rich in soot and K but depleted in organics (*Andreae and Merlet*, 2001; *Reid et al.*, 2005; and references therein). High temperature pyrolysis associated with flaming combustion, as well as the gas phase oxidation reactions, tends to convert condensable organics into lower-molecular weight species that remain in the gas phase even after dilution and cooling. Also, since the sources are local, as evidenced by the complete absence of any secondary components, the transport times will be insufficient to allow for significant oxidation to drive the organic vapors into the particulate phase.

s-CAN (Carbonaceous Ammonium Nitrate) – Representing 32.2% of the detected particles, the single particle composition of this class is characterized by a large ammonium nitrate (AN) signal with variable amounts of organic and elemental carbon (OC and EC), where the nature of the organic carbon ranges from hydrocarbons (HC) to highly oxidized species and includes nitrogen-containing compounds such as amines as well. The high signal ratio of ammonium nitrate to carbon in these particles, along with the frequency with which oxidized carbon fragment ions are observed, strongly suggests these particles have undergone a significant degree of atmospheric processing and are likely regional in origin. The underlying EC and HC signals and lack of metal oxide seed particles indicate that the primary particulate source is vehicular emissions, which is also a large source of vapor phase organics. These combined emissions would have mixed with agricultural emissions during transport and the mixture subjected to a significant degree of atmospheric processing resulting in SOA formation and the accumulation of ammonium nitrate.

s-EC (Elemental Carbon) – Comprising 12.8% of the detected particles, this class represents soot, or elemental carbon, particles with single particle mass spectra composed almost entirely of carbon cluster ions. A complete absence of oxidized species and the general absence of a significant degree of hydrocarbon ions suggest a high carbon to hydrogen ratio and thus fairly carbonized soot particles, although not entirely graphitic in nature. These are primary combustion particles most likely attributable to vehicular emissions – predominantly diesel engines but also internal combustion engines – and/or two-stroke motors associated with landscaping activities, such as lawn mowers, leaf blowers, hedgers, and trimmers. However, landscaping is typically a daytime activity and thus the potential for the source oriented ChemVols to capture these emissions will be limited and likely more concentrated in CV 9.

s-K/EC/OC (Potassium/Elemental Carbon/Organic Carbon)– More typical of what is observed during conventional biomass combustion – e.g., open vegetation fires, woodstoves and fireplaces sustaining mixed phase combustion – and in contrast to the **K** class discussed above, these particles are internal mixtures of potassium (K), elemental carbon (EC) and organic carbon (OC), accounting for 6.7% of the observed particles. The OC signal is composed of both hydrocarbon and oxygenated organic fragment ions but the general absence of any other secondary components suggests that the OC is largely primary and thus these particles are relatively unprocessed biomass combustion particles originating from local sources.

Na/K (Sodium/Potassium)– Consisting of individual particles composed almost entirely of varying mixtures of both sodium and potassium salts and/or oxides, and with infrequently detected trace amounts of carbon, this class of particles accounts for 4.2% of the single particle measurements and is nearly compositionally identical to the **K** class discussed above. The distinguishing factor is the consistent presence of sodium with signal intensities comparable to, and at times greater than, that of potassium. Interestingly, this class of particles has been ubiquitously observed in all urban air sheds where our single particle instrument has been deployed: Pittsburgh, Baltimore, Atlanta and Houston. Although sodium has certainly been observed in conventional biomass combustion particles, it is detected very infrequently and always in combination with and at low signal intensities relative to potassium. Higher observational frequencies have been reported for the combustion of biomass under coastal influences, likely from the effects of sea salt deposition on biomass composition, but this does not explain the trends observed here and in other cities. Regardless, given the size and composition of these particles they clearly originate locally from high temperature processes. This will be commented on further in the discussion of the ChemVol source combinations in a following section.

s-EC/OC (Elemental Carbon/Organic Carbon) **–** This particle class accounts for 2.5% of the detected particles and is characterized by individual particles composed of a mixture of elemental carbon (EC) and organic carbon (OC). In the absence of nucleation, the lack of metal seed particles suggests primary soot particles coated with varying degrees of condensed organic species. The OC signal is comprised almost entirely of hydrocarbon fragment ions, although some oxidized OC fragment ions were observed as well but

always in the presence of hydrocarbon fragment ions and with significantly less frequency; only 1.6% of EC/OC particles contained signal associated with oxidized organic species. The high observational frequency of hydrocarbon fragment ions can be attributed to a number of organic species but given the presence of soot is likely indicative, to a large extent, of condensed PAHs and partially oxidize and carbonized PAHs at the surface of the soot particles. Again, these are primary combustion particles most likely attributable to vehicular emissions, including diesel and internal combustion engines. These types of particles can result from biomass combustion as well but always associated with K-containing particles and usually at significantly lower number concentrations.

Ca/EC/OC (Calcium/Elemental Carbon/Organic Carbon) – This particle class represents 2.3% of the detected particles and is characterized by a single particle composition consisting of various mixtures of calcium oxides, elemental carbon and organic carbon. The EC/OC content of these particles is almost identical to that described above for the **s-EC/OC** class. The presence of calcium in combination with EC/OC in ultrafine particles is typically considered a marker for diesel exhaust, at least within the single particle community, and has been observed in previous field campaigns and other laboratory studies (*Toner et al.*, 2006; *Shields et al.*, 2007). Calcium is commonly added to lubricating oil as a dispersant/detergent and can be incorporated into the combustion chamber of an engine during 'lubrication slip'. Although this is certainly possible for internal combustion engines as well, these types of particles are more commonly associated with diesel trucks and tractor trailers.

Zn/Pb (Zinc/Lead) – Representing 1.9% of the detected particles, these are relatively pure metal oxide particles composed primarily of lead and/or zinc, although other metals such as Na and K are commonly present but in significantly lesser amounts and with only moderate observational frequency. Although lead, and to a lesser extent zinc, is fairly ubiquitous in ultrafine urban particles – likely originating from a multitude of different sources such as coal combustion and engines still burning leaded gasoline, such as small single and twin engine aircraft – the source of these particles in Fresno is not immediately clear. However, it is clear that these particles originate from local sources, given the absence of secondary components, and were formed from a high temperature process, most likely combustion. These particles will be considered further in the discussion of the ChemVol source combinations in a following section.

Winter 2009

w-CAN (Carbonaceous Ammonium Nitrate) – This particle type, representing 28.6% of the total number of particles detected during the CV sampling portion of the W09 experiment, is the wintertime analog to the **s-CAN** particle class identified during the S08 experiment. In fact, the descriptions and discussion given above for that class directly apply to this particle class as well.

w-K/CAN (Potassium/Carbonaceous Ammonium Nitrate) – These are carbonaceous ammonium nitrate particles with small metal seeds – where the metal seeds are almost

exclusively potassium salts and/or oxides – and account for 19.6% of the detected particles. This particle type was not observed during the S08 experiment and the presence of potassium indicates biomass combustion as the primary source. However, and in contrast to the S08 experiment, these particles have significant amounts of organic carbon and secondary components indicating highly processed biomass combustion emissions from sources sustaining mixed phase combustion (i.e. flaming plus smoldering combustion), such as woodstoves and fireplaces. Similar to the CAN class, these particles likely represent a large component of the background regional mixture but originated from the collective effects of regional-scale residential heating rather than vehicular emissions. These particles likely underwent similar transformations in the atmosphere when mixing with other emissions during transport and being subjected to photochemical processing resulting in SOA formation and the accumulation of ammonium nitrate. Another potential contributing factor to higher particulate OC content during the wintertime, relative to summer, is the tendency of colder temperatures to decrease saturation vapor pressure, thus resulting in increased condensation of the volatile and semi-volatile species.

w-K/EC/OC (Potassium/Elemental Carbon/Organic Carbon) – Comprised of carbonaceous particles with small metal seeds, again almost exclusively K salts and/or oxides, this particle class represents 18.7% of the detected particles and is the wintertime analog to the **s-K/EC/OC** class observed during the S08 experiment. The descriptions and discussion given above for those particles also directly apply to particles in this class. Similar to the w-**K/CAN** class, the high organic carbon content of these particles, in conjunction with the presence of K seeds, indicates biomass combustion from sources sustaining mixed phase combustion, most notably woodstoves and fireplaces. However, there is a general absence of any secondary components suggesting these particles largely originate from the collective effects of local residential heating.

w-EC (Elemental Carbon)– This is obviously the wintertime analog to the **s-EC** class identified during the S08 experiment and accounts for 13.0 % of the observed particles; the discussion above directly applies here.

w-EC/OC (Elemental Carbon/Organic Carbon)– Representing the wintertime analog to the **s-EC/OC** particle class, these particles comprise 12.7% of the measured particle population. Again, the relevant descriptions and discussion are given above.

w-K (Potassium) – Constituting 7.3% of the observed particles, this is the wintertime analog to a superposition of the primary metal particle classes identified during the S08 experiment, most notably the **s-K** and **Na/K** classes. Although other metals besides potassium and sodium were observed, similar to the S08 experiment, they were detected far too infrequently to merit separate classification and were combined with the K and Na/K particles to form an umbrella **PMP (primary metal particle)** class; see chapter 2. As a result, the descriptions and discussions given above for the **s-K** and **Na/K** classes apply here.

ChemVol Source Combination Reconciliation

Each of the particle classes discussed above were present and sampled by ChemVols in Fresno during the Summer of 2008 (S08) and Winter of 2009 (W09). Switching sampling between ChemVols as different air masses arrive at the site occurs in real time by the algorithm described previously (Chapter 2, *Bein et al.*, 2008). Since the algorithm has to sample a number of particles before it can decide to sample from a different ChemVol, each ChemVol inevitably samples primarily from its assigned source or source combination but also from other ones. In addition, some sources emit multiple particle types mixed in the same air mass so cannot be separated by the method employed here. The fidelity of the sampling is quantified in more detail previously (Chapter 2, *Bein et al.*, 2008). The dominant particle type(s) and source(s) or source combination associated with each ChemVol, detailed in what follows, is summarized in Table (4.2).

Table 4.2. Summary of the dominant particle type(s) and source(s) or source combination associated with each ChemVol for the S08 and W09 experiments.

Experiment:	**Summer 2008**		**Winter 2009**	
ChemVol	**Dominant Particle Type(s)**	**Dominant Source(s)**	**Dominant Particle Type(s)**	**Dominant Source(s)**
1	K	Local dinnertime cooking emissions	K/EC/OC	Local residential heating
2	CAN	Highly processed regional background PM	CAN	Highly processed regional background PM
3	EC	Local vehicular emissions; diesel enhancement	EC; EC/OC	Local vehicular emissions; gasoline + diesel
4	CAN; K; EC/OC	Source mixture	K/CAN	Highly processed biomass combustion PM
5	EC; EC/OC	Local vehicular emissions; gasoline + diesel	CAN; K/CAN	Regional source mixture; vehicular, biomass and ag
6	Metals	Unknown	K/EC/OC	Local dinnertime cooking emissions
7	K; Na/K	Local dinnertime cooking emissions	Timed ChemVol ~ 17:00-20:00	Evening commute and dinnertime cooking
8	N/A	ChemVol not used during this experiment	Timed ChemVol ~ 06:00-09:00	Morning commute
9	Timed ChemVol ~ 11:00-15:00	Daytime mixed layer	Timed ChemVol ~ 09:00-17:00	Daytime mixed layer
10	Uncertainty ChemVol	Nightime nocturnal inversion	Uncertainty ChemVol	Nightime nocturnal inversion

Summer 2008

ChemVol 1

On a particle class basis, the percent source composition of CV 1 is 50.2% **s**-K, 14.3% **s**-CAN, 12.6% **s**-EC, 9.3% **s**-K/EC/OC and 4.4% Na/K. This is the best resolution of the **s**-K particles that could be obtained during these experiments. Obviously, it is not possible to completely isolate a specific particle type from the background mixture, and thus the **s**-CAN particles, but the presence of the other particle types does not necessarily indicate the influence of multiple other sources. As stated previously, sources and source categories can emit multiple types of particles and it is likely that a large fraction of the **s**-EC, **s**-K/EC/OC and Na/K particles comprising this ChemVol originated from the same source category as the **s**-K particles.

As discussed in the particle class descriptions in the previous section, these particles originated from local sources close to the site and most likely from some type of biomass combustion. In the general absence of residential heating requirements during the summer months and the lack of significant amounts of agricultural related burning in the growing season, the source of these particles is somewhat elusive within the traditional framework of well known single particle source signatures. Although intensely flaming wildfires are known to produce these types of particles and wildfire activity in California was moderately high during the 2008 wildfire season, this cannot account for the frequency, consistency, persistence and number concentrations of the observed particles. Furthermore, these particles exhibit no signs of atmospheric processing associated with medium- to long-range transport and their number concentrations follow the expected trends for sources emitting under a nocturnal inversion. This can be directly inferred from the temporal trend depicted in Figure (4.5a), which indicates that the source(s) of these particles begin emitting around 18:00 and continue to emit as the nocturnal inversion develops – signified by the increase in sampling time for this ChemVol over the next few hours (19:00-22:00) which directly correlates to an increase in number concentration and particle detection – and then appear to stop emitting around 22:00, as evidenced by the plateau in CV sampling time. These particles begin to disappear around 02:00-03:00, corresponding to the observed decrease in CV sampling time, most likely due to a shift in wind direction and the emergence of a different dominant particle type.

According to the wind direction frequency distribution shown in Figure (4.3a), CV1 samples most frequently when the wind originates from the NE quadrant and, from the Google Earth images in Figure (4.2), it is clear that this quadrant is almost entirely residential in nature. As a result, and from the confluence of these data, we posit here that this CV represents the combination of residential and commercial dinnertime cooking emissions. Various types of cooking, such as pan frying, barbequing and char and flame broiling, can certainly be classified as biomass combustion and potassium is an active component in almost all living tissues so this connection is not hard to conceptualize. However, a full mechanistic description of possible particle inception and formation dynamics within the context of biomass composition and the relevant physicochemical processes associated with various cooking activities will not be attempted here.

ChemVol 2

The particle class percent composition of CV2 is 60.9% **s**-CAN, 17.0% **s**-K and 11.1% **s**-EC. Given the complexity of source-oriented sampling in the Fresno air shed, an excellent separation of the **s**-CAN particle class was obtained by this CV and dominates the source profile. From previous discussions, these are highly processed background particles originating from regional sources and containing significant amounts of secondary components, including both organic and inorganic species. As seen in Figure (4.3b), the majority of CV2 sampling begins as CV1 sampling declines (around 02:00-03:00) and continues to increase through the early morning hours. Perhaps the most revealing trend here is the fact that CV2 sampling time continues to increase to a maximum as the nocturnal inversion dissipates and the mixed layer begins developing, peaking around 08:00-10:00, and then begins declining as the mixed layer continues growing and turbulent mixing increases in the early afternoon (~ 11:00-12:00). The implication is that highly processed regional background PM trapped aloft in the residual layer from the previous day is entrained and mixed down by the developing mixed layer, rapidly increasing surface level concentrations of these particles, and then dilution takes over as the mixed layer matures and turbulent mixing intensifies, rapidly decreasing number concentrations and thus detection of these particles and CV2 sampling time.

The transition in sampling prevalence from CV1 to CV2 observed in the temporal trends is accompanied by a significant shift in wind direction from the NE quadrant to predominantly southerly to south-southwesterly, as depicted in Figure (4.3b). This direction correlates to a large shopping center complex within the immediate vicinity of the site and the greater Fresno area at larger scales, as seen in Figure (4.2). However, in this case, the significance of the shift in wind direction is not in identifying new sources but rather in explaining why the prevalence of **s**-K particles associated with CV1 starts declining and the emergence of the **s**-CAN particles, and thus CV2 sampling, begins.

In total, the contrast between CV1 and CV2 in all metrics – including particle composition, source, atmospheric processing, temporal variation and wind direction – is so prominent and convincing that the comparative toxicological analysis between these two CVs offers an excellent opportunity to test one of the most fundamental hypotheses of this work; i.e. the differential toxicity of local, unprocessed particles originating from a specific source compared to regional, highly processed particles originating from a different source and subjected to different atmospheric transformations.

ChemVol 3

Comprised of 32.1% **s**-EC, 24.4% **s**-K, 17.6% **s**-CAN and 5.7% Ca/EC/OC particles, CV3 offers the cleanest separation of **s**-EC particles that could be obtained in this experiment and a good opportunity to examine the toxicity of fresh vehicular emissions. As discussed previously, **s**-EC particles are a common single particle signature of vehicular emissions and the elevated levels of Ca/EC/OC particles also sampled by this CV corroborate this, and further suggest an enhancement in diesel tractor-trailer emissions. It should be noted that the presence of **s**-K particles in the summertime Fresno air shed was so prevalent that it was impossible to fully eliminate their presence in any of the source-oriented CVs, and such is the case here.

The temporal trend in CV3 sampling time depicted in Figure (4.5c) further substantiates the association of this CV with fresh vehicular emissions by showing dramatic increases in sampling time for both the evening (~ 18:00-20:00) and morning (~ 08:00-09:00) rush hour commutes. Also, CV3 sampling is highly correlated to wind direction, as shown in Figure (4.3c), and samples most frequently when the wind originates from the west to northwest. It is clear from Figure (4.2) that this is the direction of the north-south running Yosemite Freeway (CA SR 41), a major expressway in the area with an entrance/exit ramp intersection at Shaw Avenue where high accelerations and corresponding high emissions may occur.

ChemVol 4

CV4 appears to be largely a source mixture, containing 30.4% **s**-CAN, 29.3% **s**-K, 18.3% **s**-EC, 5.8% **s**-EC/OC and 5.2% **s**-K/EC/OC particles. It was originally included from the pre-study analysis in attempts to isolate the **s**-EC/OC particle class but during ChemVol sampling shifted more towards the **s**-CAN class, which can likely be traced back to the clustering thresholds of the sampling algorithms. The **s**-CAN and **s**-EC/OC classes differ most dramatically, in terms of their mass spectra, in the signal intensity of the NO^+ peak, which is the single particle signature for ammonium nitrate. However, in terms of data clustering, this only represents a single dimension in a highly dimensional dataset whereas the myriad fragment and cluster ions produced from the ablation of particulate EC/OC commonly occupy a much higher number of dimensions. As a result, data clustering algorithms will be more biased towards similarity in EC/OC related ions between spectra then the NO^+ peak and it is possible that EC/OC particles were misclassified as **s**-CAN particles during ChemVol sampling. Additional analyses of the single particle data are required to validate this. Figure (4.5d) does suggest a strong vehicular influence with CV4 sampling frequency showing very similar trends to CV3 and peaking close to conventional evening and morning rush hour traffic periods. However, CV4 sampling is significantly less correlated with wind direction, pointing to sources in both the east and west; not included in Figure (4.3).

ChemVol 5

Similar to CV3, CV5 symbolizes a relatively clean separation of fresh vehicular emissions, with a particle class percent contribution of 23.8% **s**-EC, 21.4% **s**-EC/OC, 21.4% **s**-CAN, 16.7% **s**-K and 11.9% **s**-K/EC/OC. However, the increased detection of **s**-EC/OC particles and the absence of the Ca/EC/OC particle class suggest a significant enhancement of internal combustion engine emissions relative to CV3. Furthermore, CV5 sampling is highly spatiotemporally resolved, as shown in Figures (4.3e) and (4.5d), clearly capturing the evening rush hour but with limited sampling during the morning commute and always sampling when the wind is blowing from the direction of the Shaw Avenue and Yosemite Freeway interchange, again similar to CV3.

ChemVol 6

For reasons similar to those mentioned previously, CV6 is the best resolution that could be obtained for some of the more infrequently observed metallic particles, most notably Zn/Pb particles. Several particle classes were intentionally lumped together in the pre-study representation of this CV, subsequently used during sampling, in attempts to obtain a composite of these rare particle types. These particles are always highly temporally correlated with the more prevalent particle types and so the latter had to be included in the pre-study representations to capture the former, resulting in a particle class percent contribution of 34.5% **s**-K, 17% **s**-CAN, 12.5% **s**-EC, 12.4% Zn/Pb, 8.4% **s**-K/EC/OC, 4.6% Sn/Cr and 3.9% Na/K. From Figures (4.3e) and (4.5f), CV6 sampling was largely confined to the early night hours (~ 21:00-01:00) and almost exclusively when the wind was blowing from the northeast, trends that most closely resemble those of CV1. The exact source of these particles is not immediately clear, but they appear to originate from local combustion sources within the residential sector and are somehow correlated to the detection of **s**-K particles.

ChemVol 7

CV7 is very similar to CV1 in its prevalence of K-containing particles and was included in attempts to isolate an enhancement of the Na/K particle class. The end result was relatively successful and CV7 consists of 39.4% **s**-K, 18.2% Na/K, 13.1% **s**-CAN, 11.1% **s**-EC, 5.1% Sn and 5.1% **s**-K/EC/OC particles. Although not as temporally resolved, due largely to relatively infrequent sampling, CV7 most closely mimics the temporal trends of CV1 but is highly associated with sources in the opposite direction to the west-southwest. Besides the major expressway discussed previously, the images in Figure (4.2) show a major shopping center complex housing a suite of different restaurants in this area, followed by another large residential neighborhood. For reasons similar to those discussed previously within the context of CV1, and due to their high correlation with **s**-K particles, we posit here that the Na/K particles also originate generally from biomass combustion associated with different cooking activities. Again, this is not hard to conceptualize given the physicochemical similarities between Na and K, the ubiquitous use of NaCl salt in cooking and the fact that it will be subjected to the same high temperature pyrolysis, char forming and flaming conditions associated with many types of cooking.

Winter 2009

ChemVol 1

The percent composition of the wintertime version of CV1 on a particle class basis is 36.8% **w**-K/EC/OC, 25.2% **w**-K/CAN, 16.2% **w**-CAN, 9.4% **w**-EC/OC, 6.8% **w**-EC and 5.5% **w**-K, making this CV clearly and overwhelmingly attributable to local sources of biomass combustion. As mentioned previously, the large organic content of the particles is indicative of sources sustaining mixed phase combustion, such as woodstoves and fireplaces, and thus a large majority of the particles sampled by CV1 are likely a result of wintertime residential heating. This is corroborated by the temporal trend shown in Figure (4.6a) where sampling typically begins around 19:00, increases rapidly over the

next couple of hours, plateaus throughout the night from 21:00 - 01:00 and then decreases in the early morning hours. Furthermore, CV1 is highly correlated to wind direction, as shown in Figure (4.4a), and points to the collective effect of residential neighborhoods in the NW quadrant as the most likely source.

ChemVol 2

Showing striking similarity to CV2 from the S08 experiment, the winter version of this source combination consists of 61.2% **w**-CAN, 13.3% **w**-K/CAN, 11.2% **w**-K/EC/OC, 7.3% **w**-EC, 3.7% **w**-EC/OC and 3.2% **w**-K particles. Again, a clear separation of the CAN class is observed, representing highly processed regional particles, as well as a temporal sampling trend that is anti-correlated to that of CV1 (Figure 4.6b) accompanied by a shift in prevalence from northwesterly driven CV1 sampling to southerly driven CV2 sampling (Figure 4.4b). As a result, CV2 presents an excellent opportunity to make a seasonal comparison between the toxicological effects of a given single particle type.

ChemVol 3

The large EC/OC content of CV3 – 27.7% **w**-EC and 24.7% **w**-EC/OC particles – is strongly indicative of a prevalence of fresh vehicular emissions. This is supported further by a high sampling directionality corresponding to the Yosemite Freeway, as shown in Figure 4.4c). However, the temporal trend in Figure (4.6c) largely excludes the evening rush hour traffic – CV 8 was configured to capture the morning commute so source-oriented sampling was terminated prior to that period – and CV3 samples somewhat consistently throughout the night. This certainly does not preclude it from representing fresh vehicular emissions but it is important to note that biomass combustion can also emit these types of particles, although typically at significantly lower number concentrations compared to K-containing particles; the percent contributions for CV 3 were 15.6% **w**-K/EC/OC, 13.5% **w**-K/CAN and 3.2% **w**-K.

ChemVol 4

Included in attempts to isolate the w-K/CAN particle class, which represents moderately to highly processed biomass combustion particles, CV4 comprises 55.3% **w**-K/CAN, 15.4% **w**-K/EC/OCC, 10.3% **w**-CAN, 7.0% **w**-EC/OC, 6.4% **w**-EC and 5.7% **w**-K particles. The temporal trend and wind direction correlation for CV4, shown in Figures (4.6d) and (4.4d), respectively, trace those of CV1 fairly well and thus are not particularly revealing in this case. Therefore, the distinguishing factors are based solely on differences in single particle composition.

ChemVol 5

CV5, with a particle class percent composition of 27.9% **w**-CAN, 25.1% **w**-K/CAN, 15.1% **w**-EC/OC, 13.2% **w**-K, 10.0% **w**-K/EC/OC and 8.8% **w**-EC, most closely resembles a mixture of CV2 and CV4. This is also evident in Figures (4.4e) and (4.6e) where the sampling trend and directionality of CV5 appears as a linear superposition of

those for CVs 2 and 4. As a result, CV5 is considered representative of highly processed particles originating from a mixture of regional emissions, including both vehicular and biomass combustion sources, as well as any wintertime agricultural emissions that may also be present.

ChemVol 6

CV6 does a fairly good job of isolating the w-K/EC/OC particle class, which represents 41% of the detected particles associated with this CV. The remaining 59% is spread relatively evenly over the remaining particle classes. Although CV1 demonstrated a similar prevalence of w-K/EC/OC particles, the temporal trend and wind direction correlation of CV6 are distinct in that sampling generally begins and ends earlier (~ 18:00 and 23:00, respectively), more abruptly and is more correlated with westerly rather than northwesterly winds. As a result, we posit that CV6 is more heavily influenced by biomass combustion emissions associated with cooking than residential heating. However, it is important to note that, due to similarities in particle composition, once these emissions start mixing in the atmosphere it becomes increasingly difficult to distinguish these two sources using the single particle instrument alone.

References

Andreae, M. O. & Merlet, P., Emission of trace gases and aerosols from biomass burning. *Global Biogeochemical Cycles* 15, 955-966, 2001.

Battye, W. et al. Evaluation and improvement of ammonia emissions inventories. *Atmospheric Environment* 27(27), 3873-3883, 2003.

Bein, K.J., Y. Zhao and A.S. Wexler, Conditional Sampling for Source-Oriented Toxicological Studies using a Single Particle Mass Spectrometer. *Environ. Sci. Technol.* 43:9445-9452, 2009

Chu, S.H. et al. PM data analysis – a comparison of two urban areas: Fresno and Atlanta. *Atmospheric Environment* 38(20), 3155-3164, 2004.

Ham, A.W. and Kleeman, M.J., Size-resolved source apportionment of carbonaceous particulate matter in urban and rural sites in central California. *Atmospheric Environment* 45(24), 3988-3995, 2011.

Kleeman, M.J., Riddle, S.G., Robert, M.A., Jakober, C.A., Fine, P.M., Hays, M.D., Schauer, J.J. and Hannigan, M.P., Source apportionment of fine ($PM_{1.8}$) and ultrafine ($PM_{0.1}$) airborne particulate matter during a sever winter pollution episode. *Environmental Science & Technology* 43, 272-279, 2009.

Poore, M.W. Levoglucosan in $PM_{2.5}$ at the Fresno Supersite. *Journal of the Air & Waste Management Association* 52(1), 3-4, 2002.

Reid, J. S., Koppmann, R., Eck, T. F. & Eleuterio, D. P., A review of biomass burning emissions part II: intensive physical properties of biomass burning particles. *Atmospheric Chemistry and Physics* 5:799-825, 2005.

Rinehart, L.R. et al. Spatial distribution of $PM_{2.5}$ associated organic compounds in central California. *Atmospheric Environment* 40(2), 290-303, 2006.

Schauer, J.J. and G.R. Cass. Source apportionment of wintertime gas-phase and particle-phase air pollutants using organic compounds as tracers. *Environmental Science & Technology* 34(9), 1821-1832, 2000.

Shields, L.G., Suess, D.T., Prather, K.A., Determination of single particle mass spectral signatures from heavy duty diesel vehicle emissions for PM2.5 source apportionment. *Atmospheric Environment* 41:3841–3852, 2007.

Toner, S.M., Sodeman, D.A., Prather, K.A., Single particle characterization of ultrafine and accumulation mode particles from heavy duty diesel vehicles using aerosol time-of-flight mass spectrometry. *Environ. Sci. Technol.* 40: 3912–3921, 2006.

Watson, J.G. et al. Air quality measurements from the Fresno Supersite. *Journal of the Air & Waste Management Association* 50(8), 1321-1334, 2000.

Watson, J.G. and J.C. Chow. A wintertime PM2.5 episode at the Fresno, CA, Supersite. *Atmospheric Environment* 36(3), 465-475, 2002.

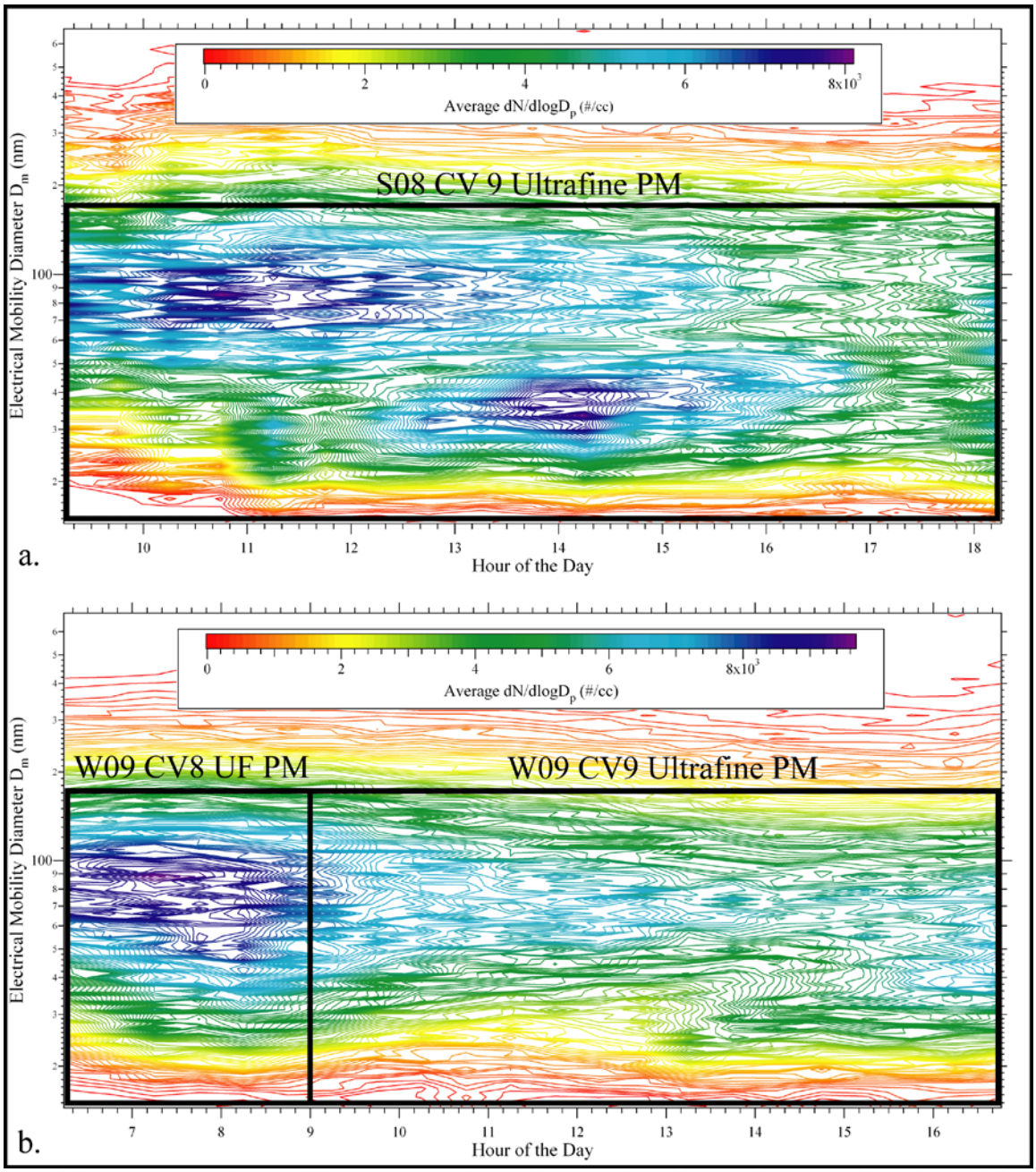

Figure 4.1. Contour plots showing the study average daytime particle number distribution for the (**a)** summer 2008 and (**b**) winter 2009 experiments. The time periods corresponding to the various timed ChemVols are outlined and labeled in the figures; see text for details.

Figure 4.2. Google Earth images of the sampling site (marked with a red dot) relative to the surrounding sources at several different spatial scales; see text for discussion.

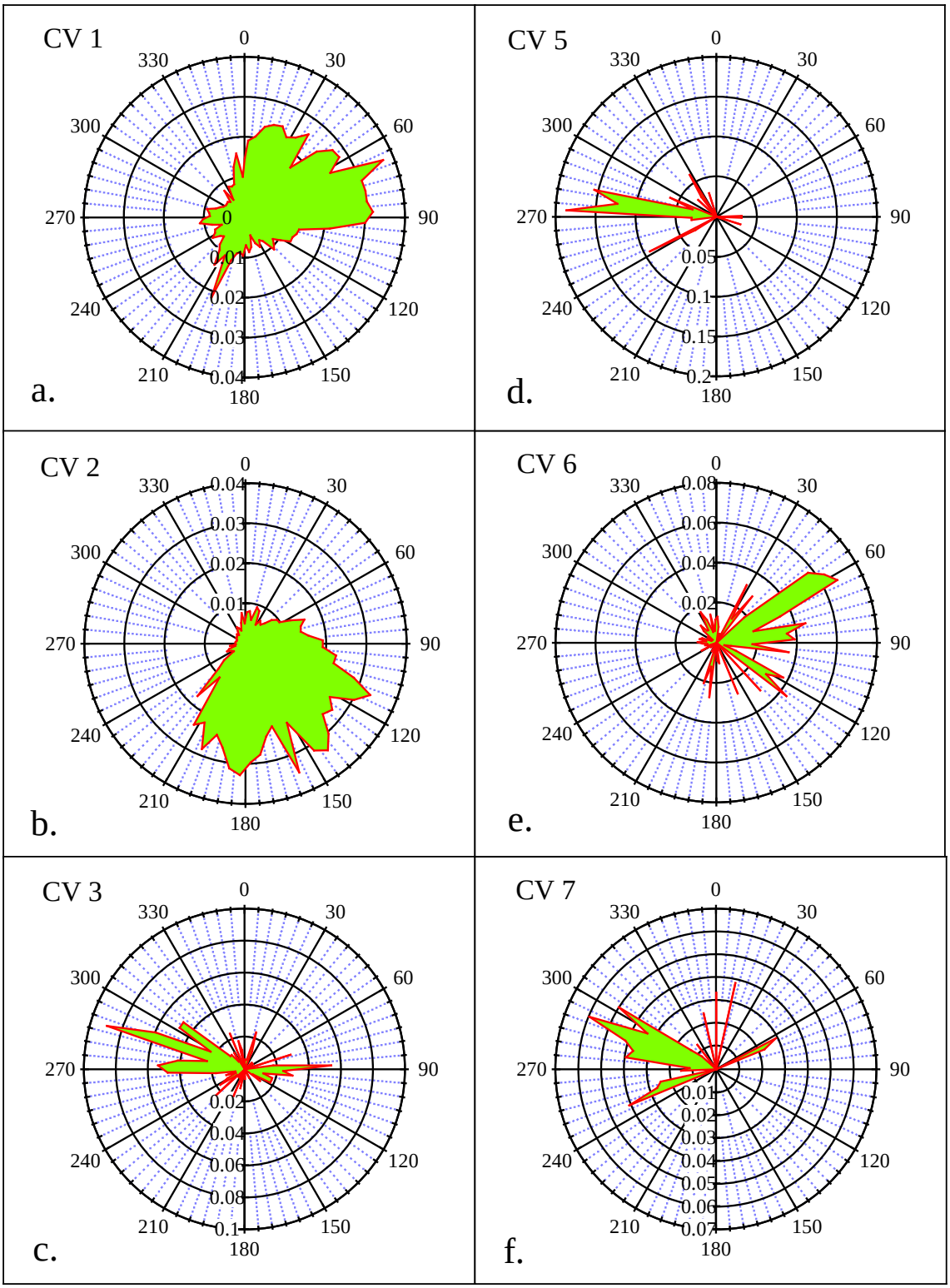

Figure 4.3. Wind direction frequency distributions for the source-oriented ChemVols during the summer 2008 experiment; see text for a discussion of these plots.

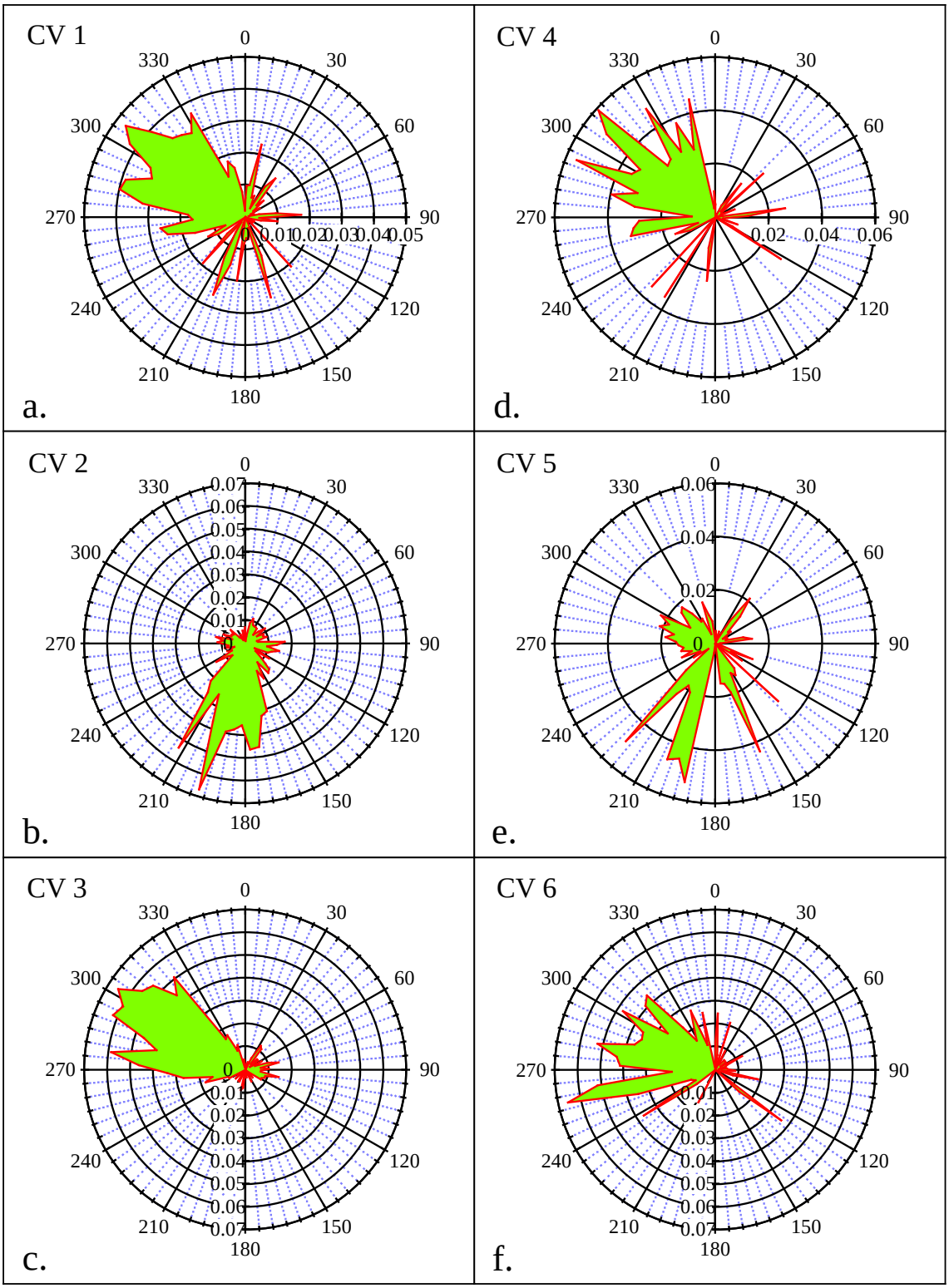

Figure 4.4. Wind direction frequency distributions for the source-oriented ChemVols during the winter 2009 experiment; see text for a discussion of these plots.

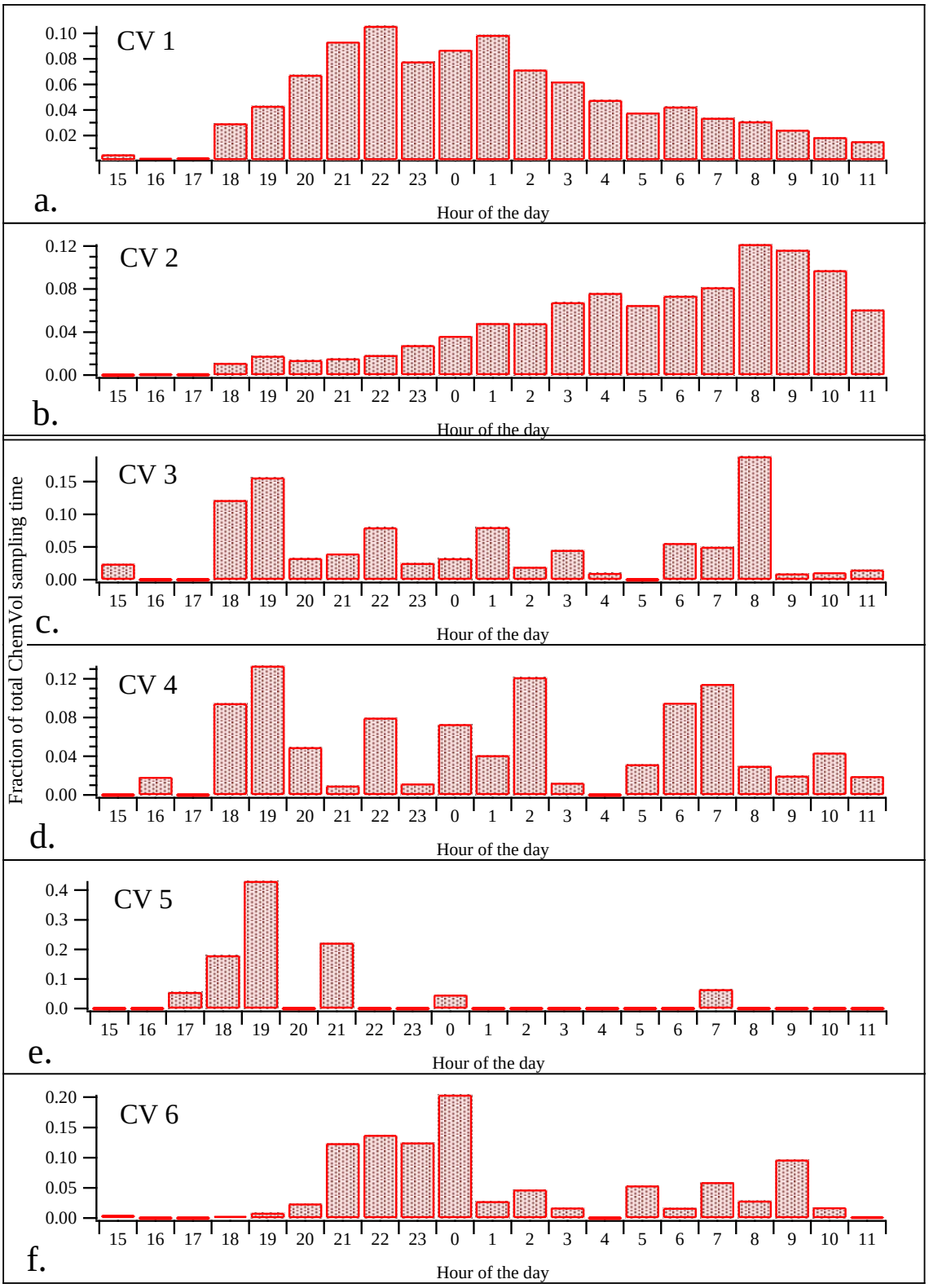

Figure 4.5. The fraction of total CV sampling time as function of hour of the day for the source-oriented ChemVols from the summer 2008 experiment; see text for discussion.

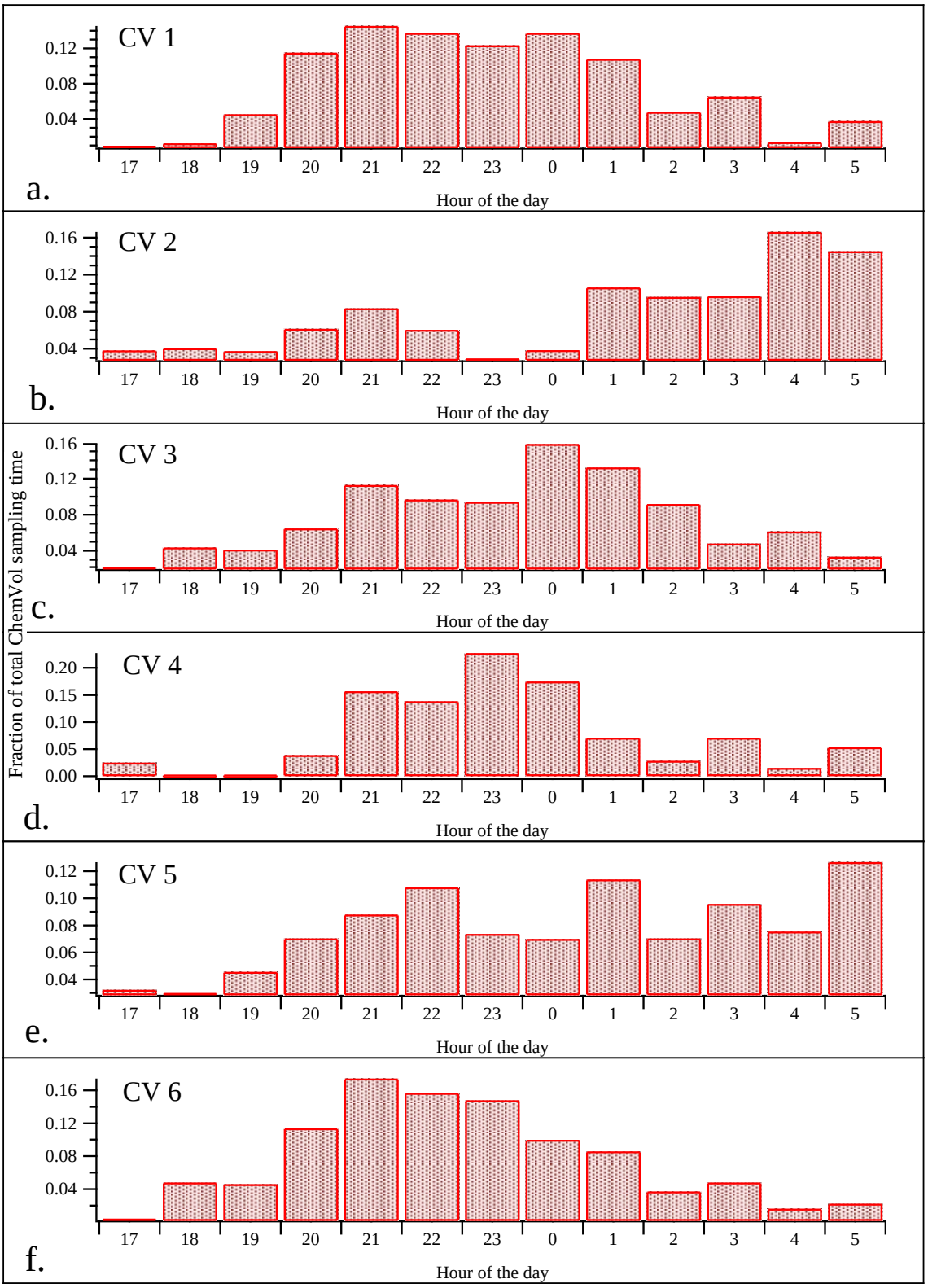

Figure 4.6. The fraction of total CV sampling time as function of hour of the day for the source-oriented ChemVols from the winter 2009 experiment; see text for discussion.

Chapter 5
Source-Oriented Particulate Matter: PM-Induced Respiratory and Systemic Responses in Mice Following Exposure

Abbreviations:

ANOVA	analysis of variance
BAL	bronchoalveolar lavage
CV	ChemVol/ChemVol® High Volume Cascade Impactor
DCM	dichloromethane
DEP	diesel exhaust particulates
DLS	dynamic light scattering
DTT	dithiothreitol
EC	elemental carbon
F/UF	fine/ultrafine
HBSS	Hank's Balanced Salt Solution
LAL	Limulus Amebocyte Lysate
LDH	lactate dehydrogenase
NAAQS	National Ambient Air Quality Standards
OC	organic carbon
$PM/PM_{2.5}/PM_{10}$	particulate matter/ particulate matter with aerodynamic diameter < 2.5 μm / particulate matter with aerodynamic diameter < 10 μm
PUF	polyurethane foam
SEM	standard error of the mean
SJ Valley	San Joaquín Valley, California
SMF	sub-micron fine, diameter between 0.17 and 1 μm
SOS	source-oriented sample(s), also designated as CV
UF	ultrafine, diameter < 0.17 μm or 170 nm
WBC	white blood cells

Abstract

BACKGROUND: Extensive literature suggests compelling evidence for a strong relationship between exposure to ambient particulate matter (PM) and cardiopulmonary health impacts. Regional, seasonal and temporal fluctuations in PM concentration and chemical composition can be attributed to a wide variety of distinct point and mobile sources. However, it is unclear how these variations may impact on respiratory and systemic responses. The current National Ambient Air Quality Standard (NAAQS) for PM is based on an average mass concentration, but not on chemical composition. PM mass does not specify sources that contribute to distinct PM characteristics or possible health effects. Sampling of PM from the atmosphere using a source-oriented approach that accounts for atmospheric transformations of pollutants could provide for enhanced understanding of particle source-specific health effects.
OBJECTIVES: To measure pulmonary and systemic markers of inflammation and cytotoxicity elicited by size-specific source-oriented PM collected in Fresno, CA. during the summer and winter seasons.
METHODS: Mice were exposed by oro-pharyngeal aspiration to equivalent doses of ultrafine (UF) and submicron fine (SMF) source-oriented PM. Indicators of pulmonary and systemic inflammation and cytotoxicity were measured 24 hours post-aspiration.
RESULTS: Measures of pulmonary inflammation/cytotoxicity, and hematology differed between source-oriented samples compared to corresponding controls as well as between particle size fractions. Source-oriented PM elicited inflammatory responses appeared to be more significant in the lung compared to the blood. In general, UF PM was more pro-inflammatory compared to SMF PM. Although a number of source-oriented samples produced some degree of biological response in the lungs compared to control, the most biologically responsive samples for the winter season were CV10 (a mix of sources present at night) UF, CV2 (highly processed regional background) SMF and CV3 (EC and OC) SMF, while for the summer season CV2 and CV5 (vehicles) UF and CV 6 (metals) SMF were most biologically reactive. In contrast, hematologic measures were more variable and did not correlate to changes in pulmonary endpoints
CONCLUSIONS AND SIGNIFICANCE: The ability to directly measure the relative toxicity of source-oriented PM increases our understanding of the association between PM sources and adverse health effects. The ultimate goal will be to provide more specific understanding of the composition and sources of PM and their effects to provide greater protection to human health.

Introduction

There is strong evidence for a relationship between exposure to ambient particulate matter (PM) and adverse cardiopulmonary health effects. However, the exact characteristics of PM driving these associations remain to be elucidated. Current mass-based National Ambient Air Quality Standards (NAAQS) are derived from epidemiological evidence (Dockery et al. 1993, Dockery 2001, Laden et al. 2000, Peters et al. 2001, Pope et al. 1995, Pope and Dockery 2006, Ostro et al. 2006, Ostro et al. 2007). For example, the CALFINE study demonstrated a correlation between a 10 $\mu g/m^3$ change in two day average San Joaquin (SJ) Valley fine/ultrafine PM concentrations and a 0.6% increase in mortality due to respiratory and cardiovascular disease (Ostro et al. 2006).

Associations between PM mass and health effects have been difficult to reproduce in a number of experimental studies and have prompted the consideration that chemical composition may be a likely candidate to explain these differences. Emerging experimental findings support epidemiological conclusions that contributions to excess risk may vary among specific $PM_{2.5}$ constituents with combustion associated pollutants being particularly important in California (Ostro et al. 2007). Growing evidence that PM chemical composition plays a significant role in observed health effects has come from concentrated ambient particle (CAPs) inhalation studies, where in addition to mass, chemical components show associations which are often stronger in terms of health effects (Saldiva et al. 2002, Kodavanti et al. 2005, Rohr et al. 2010, Morishita et al. 2009, Ghio, Kim and Devlin 2000, Harder et al. 2001, Cassee et al. 2005). Understanding which PM components represent the most significant health hazard presents several challenges to manufacturers, regulatory decision makers, toxicologists, and risk assessors who must identify PM components with the most risk and then estimate the potential for improved protection of human health that may result from significant changes in the emission profile (McDonald et al. 2004). Therefore, studies investigating source-specific contributions are needed to target emissions associated with the greatest risk.

Primary PM and precursor gases emitted into the atmosphere by mobile and stationary sources undergo atmospheric transformation and aging processes that contribute to a regionally and temporally complex mixture. Thus, elucidating the source-specific chemicals or chemical combinations contributing to adverse health effects is a challenge. Epidemiological studies that that take into consideration PM source apportionment have suggested some correlation between PM chemical composition and health outcomes (Ito et al., 2006); however, issues remain regarding the source appointment accuracy of such studies and weather-influences in the models.

We have coupled a unique source-oriented sampling approach with a number of bioassays to investigate the relative toxicity of source-oriented ambient PM. Briefly, source-oriented PM is sampled in real time using single particle mass spectrometry to detect temporally dominant sources or source combinations (Bein, Zhao and Wexler 2009). This novel approach may be applied to evaluate the relative toxicity of source-

specific particulate chemical compositions representative of a given source impacting a given site.

During summer 2008 and winter 2009, we collected source-oriented samples (SOS) in Fresno, an urban city in the San Joaquin Valley of California with one of the most complex and particle-rich air sheds in the United States. The relative toxicity of each source-oriented PM sample (SOS), also designated as ChemVol (CV) samples, was tested in laboratory mice. CVs were collected in two size-fractions; ultrafine (UF), particles with a mean mass aerodynamic diameter (MMAD) < 0.17 micrometers (μm), and sub-micron fine (SMF), MMAD between 0.17 μm and 1 μm. BalbC mice were exposed to CV samples via oro-pharyngeal aspiration. Control animals received vehicle only. Inflammatory and cytotoxic effects were compared between CV groups and control groups, UF and SMF CVs and CVs within the same particle size in the lungs and the blood as a means to examine the direct CV effect on the respiratory tract and the systemic circulation.

The methods applied in this study were designed to address the hypothesis that source (chemical speciation) and particle size play critical roles in the relative toxicity of PM as noted by standard assays indicative of cell injury and inflammation. The intent of these studies was to enhance our understanding of adverse health effects and PM sources.

Materials and Methods

Particle Collection

Sampling was conducted in Fresno, CA during summer and winter seasons of 2008-2009. All sampling devices were housed in a mobile trailer that was transported to the sampling location. A single particle mass spectrometer (RSMS-II) operating in the 70-150 nm particle size range was used to yield the chemical composition of individual particles (Bein et al. 2009). A pre-study conducted prior to ChemVol sampling during each season was done to identify the dominant site-specific sources and source combinations to be assigned to specific ChemVol High Volume Cascade Impactors (Demokritou et al. 2003, Demokritou et al. 2002). Each ChemVol sampler was assigned one source or source combination, while the output of RSMS-II controlled bin selection sampling. Sufficient mass for toxicity testing was collected over a period of several weeks. Distinct source-oriented PM was collected based on the (1) temporal distribution and frequency of the observation, (2) amount of sampling time required to collect the target mass for toxicological studies, and (3) significance of differences between class combinations. For each ChemVol, two size fractions – sub-micron fine (SMF) and ultrafine (UF) – were collected on polyurethane foam (PUF) filters (Thermo Fisher Scientific) and Teflon-coated borosilicate glass fiber filters (Pall TX-40), respectively. Filters were cleaned using sonication in Milli-Q H_2O and methanol and completely dried in a desiccator overnight before being stored in clean petri dishes wrapped in aluminum foil.

Particle collection was performed according to methods previously described (Bein et al. 2009). Two different methods for source-oriented sampling were used in the different seasons and were based on pre-study sampling to train the algorithm. In summary, the

classification scheme for summer 2008 was straightforward and particle classes were constructed based on the constituents consistently observed together in individual particles, thus representing different sources and degrees of atmospheric processing. A different classification was utilized during winter 2009 and was designed to separate particles based on the relative amounts of primary versus secondary components and the nature of the carbon content. See Chapter 4 for a detailed description of what each ChemVol collected in its SOS.

Particle Extraction

Particles were extracted using Milli-Q® H_2O and a series of solvents of varying polarity to ensure complete extraction of all PM components. See Chapter 3 for details on the extraction protocols employed. The final storage vials were weighed under vacuum (~ 0.01-0.1 mBar) to obtain total extracted mass for each sample.

Physicochemical Assessment of CV particle suspensions

The average particle size in aqueous suspension, oxidative potential and presence of endotoxin were determined for each CV sample. The average particle size in suspension was determined using dynamic light scattering (DLS) (Microtrac Particle Sizer, Microtrac Inc., Malvern, PA). Particle size readings for each PM suspension were analyzed on the day of administration to the mice via oroparyngeal aspiration. Particle suspensions were vortexed for a minimum of one minute prior to the DLS reading and underwent one hour of sonication prior to aspiration. PM samples were assayed for oxidative potential using a cell-free dithiothreitol (DTT) assay with modifications for use in a high-throughput assay (Cho et al. 2005, Li, Wyatt and Kamens 2009, Verma et al. 2009). Serial dilutions of flame-generated iron-soot dissolved in Hanks Balanced Salt Solution (HBSS) were used as a positive control (data not shown). The DTT assay was performed in duplicate or triplicate wells and repeated two times. In brief, a standard curve of 1, 4 napthoquinone and PM suspensions (1 mg/ml concentration) were incubated with 50 mM DTT at 37˚C for one hour in a 96 well plate. Following incubation, 1 mM DTNB was added to each well and read at 412 nm on a spectrophotometer after a 30 minute reaction time. The DTT assay measured the capacity of the samples to transfer electrons from DTT to oxygen in a reaction analogous to the cellular redox reaction involving NADPH and oxygen. The electron transfer was monitored by the DTT consumption of a 1, 4 napthoquinone (1,4 NQ) standard to determine the pmol 1,4 NQ equivalent for the concentration of the redox-active species in the PM sample. Endotoxin presence in PM samples was tested using a highly sensitive kinetic Limulus Amebocyte Lysate (LAL) assay according to manufacturer's instruction (KQCL-1000, Cat # 50-650U, Lonza, MD). β-glucan blocker was used to optimize the detectable responses in the PM suspension according to manufacturer instruction (β-Glucan blocker, Cat #N190, Lonza, MD). Assay limit of detection was 0.005 EU/ml. The assay was performed in a 96 well plate format using sterile reagents and equipment in a 120ºC oven for 24 hours (Alexis et al. 2006).

Animals

Male BalbC mice (9-10 weeks old) were purchased from Charles River Laboratories, Inc. (Raleigh, NC) and shipped to the University of California, Davis. Animals were housed

in AALAC approved facilities in plastic cages with TEK-Chip pelleted paper bedding (Harlan Teklad, Madison, WI). Mice were acclimated for two weeks with access to food and water ad libitum and housed on a 12-hr light/12-hr dark cycle throughout the study. Animals were handled in accordance with standards established by the U.S. Animal Welfare Acts as set forth in the National Institutes of Health Guidelines (Institute of Laboratory Animal Resources 1996) and the UC Davis IACUC guidelines from an approved Animal Care and Use Protocol for this study.

Experimental Design: Bioassay

A total of twenty four size-fractioned CVs from the summer and winter seasons were used for toxicity testing. Due to the number of CV samples, a series of sequential experiments was performed. Groups of six mice were randomly assigned to either vehicle control or source-oriented PM sample groups. Mice were anesthetized via inhalation of isoflurane with oxygen (3:1 ratio). Oro-pharyngeal aspiration was used to deliver the CV sample to the lungs (Rao et al. 2003, Gilmour et al. 2007). Mice were suspended vertically from the central incisors, and the tongue was restrained to facilitate placement of the SOS suspension at the back of the throat and ensure aspiration of PM suspension through the trachea. Control mice were exposed to 50 μl of sterile HBSS. PM exposed mice were exposed to 50 μg of PM in 50 μl of sterile HBSS (Samuelsen, Nygaard and Lovik 2009, Nygaard et al. 2009). Mice were closely monitored until they regained normal activity and necropsied 24 hours following particle aspiration by intraperitoneal injection of pentobarbital (65 mg/kg) for the collection of lung and blood samples.

Bronchoalveolar Lavage (BAL) Collection and Analysis

The trachea was cannulated and tied securely with a suture for bronchoalveolar lavage (BAL). The whole lung was lavaged with two 1 ml aliquots of HBSS. Recovered BAL was centrifuged at 2000 RPM for ten minutes at 4°C and aliquots of BAL supernatant were frozen for biochemical analysis. The cell pellet was resuspended in 0.5 ml HBSS cell counts and cell viability determination by measuring 0.4% trypan blue exclusion with a hemocytometer (Sigma, St. Louis, MO). A minimum of 100 μl of the cell suspension was used for cytospins using a Shandon Cytospin (Thermo Shandon, Inc., Pittsburg, PA). Cytospin slides were dried in air at room temperature prior to methanol fixation and DiffQuick® staining (International Reagent Corp, Kobe, Japan). BAL cell profiles were determined using light microscopy (500 cells/sample).

The supernatant from the BAL was analyzed for protein (Quick Start Bradford 1x Dye, Biorad, Hercules, CA) and LDH activity (LDH Cytotoxicity Detection Kit, Roche Applied Science, Indianapolis, IN; LDH Standard, Cayman Chemical, Ann Arbor, MI) according to the manufacturer's recommended protocols. A Bradford assay was used to determine protein concentration. This assay was performed using a standard curve of serial dilutions of a freshly made bovine serum albumin (BSA) standard dissolved in HBSS. Protein concentrations are indicated by the increased absorbance arising from increased binding of protein to Coomassie Brilliant Blue dye which upon binding shifts from green/red to blue. LDH activity, elevated in the presence of increased dead or plasma membrane damaged cells, is determined in this enzymatic test where the

reduction of NAD^+ is reduced to $NADH/H^+$ by the LDH catalyzed conversion of lactate to pyruvate. A diaphorase catalyst transfers H/H+ from $NADH/H^+$ to the yellow tetrazolium salt INT which is further reduced to red formazan. The amount of color formed in the assay is directly proportional to the number of lysed cells as indicated by the LDH standard curve.

Blood Collection and Analysis

Whole blood was collected via cardiac puncture from the inferior vena cava into pre-coated needles and drawn in 0.05% EDTA coated syringes. Complete blood counts (CBCs) were performed to determine the number of circulating leukocytes, cell differentials and hematologic parameters using an automated blood counter (ActDiff, Coulter, Miami, FL). Remaining whole blood was transferred into microtainer tubes (BD Vacutainer® EDTA tubes, BD, Franklin Lakes, NJ) and centrifuged for five minutes at 6000 rpm. Plasma was frozen for future analysis.

Statistics

JMP statistical software was used for data analysis (JMP, SAS Institute Inc., Cary NC). Descriptive statistics calculated for all cellular and biochemical data and data were log transformed to meet requirements for statistical analysis as needed. These analyses focused in BAL parameters to include cell viability, total cell numbers, cell differentials, protein and LDH values, Similar analyses were performed on all hematological parameters, including cell blood counts (CBCs), platelets, hemoglobin and hematocrit values. Data in the figures are expressed as mean values ± standard error. Each group consisted of a minimum of six animals (n = 6). An equal number of sham controls (n=6) were run for each set of experiments. Data were analyzed as previously described by Cho and colleagues (Cho et al. 2009). All data were evaluated for summer and winter seasons separately. The overall effect of particle size and SOS number (identical to CV bin number) was first analyzed using two-way analysis of variance (ANOVA). An independent variable, representing particle size and SOS number, was then used to perform a one-way ANOVA with Tukey's post test for pair-wise comparisons between control and treatment groups. Linear regression was performed between CV samples and individual biological responses. Differences were considered statistically significant when $p < 0.05$.

Results

Source/PM Characterization

The SMF and UF source-oriented (CV) samples collected for each season were each characterized and presented in Chapter 2 (Bein et al., 2009). In general, excellent fidelity was found between the desired source characteristics and those collected (see Bein et al. 2009). All initial CV PM suspensions prepared for oro-pharyngeal aspiration were characterized for size using dynamic light scattering (DLS) (figure 5.1). The oxidative potential for all initial CV samples was also measured using the DDT assay (figure 5.2). Remaining samples were not analyzed based on samples being of similar size and oxidative potential. PM size, as measured by DLS, ranged from 170 nm to 546 nm. In general, SMF PM suspensions were found to be larger in size than observed for

the UF PM suspensions. It should be noted that the extraction and sonicated suspensions of particles reflect the presence of particle agglomeration from the original collected CV samples, a condition experienced with all particle samples extracted from filters and particle collection substrates.

Source-Oriented (CV) PM Toxicity

Pulmonary Inflammation

Pulmonary inflammation elicited by summer and winter CV samples (SOS) is shown in figures 5.3 and 5.4 respectively. A significant interaction between CV# and particle size during summer was noted for all BAL endpoints, with the exception of the percentage of non-viable cells. For winter CVs, there was a significant interaction between CV and particle size for most BAL endpoints. Regardless of CV#, each summer UF PM CV sample consistently demonstrated the presence of more inflammatory cells, (i.e., total BAL cells and neutrophils), compared to the same SMF PM CV sample. For winter, a similar cellular pattern was observed with the exception of neutrophils. In general, all CV samples induced significant elevation in the number of total cells, neutrophils and eosinophils recovered by BAL. However, only those CVs that significantly elevated BAL parameters compared to the values of the vehicle control are denoted by an asterisk in the figures. Significant differences between PM size (UF versus SMF) for a given CV is denoted by the symbol, #, in the figures as well. Only, summer CV10 (nighttime undifferentiated background) and winter CV5 (vehicular) demonstrated increased biological activity of UF compared to SMF. Within each season, there were statistically significant differences in the degree of inflammatory and cytotoxic responses between CVs. There was good correlation in the total number of cells and neutrophils recruited for each CV for both summer and winter. Differences between winter UF samples were more robust than differences between winter SMF samples. Subtle differences for summer UF source-oriented samples were not significant. Eosinophils were significantly increased for UF summer CV2 (highly processed regional background) and winter CV1 (residential heating) and CV5 (regional background and vehicles) and were unchanged with exposure to all SMF particles. Summer and winter mixed atmosphere samples (CV9), collected daily from 9:00 A.M. to 5:00 P.M. for summer samples and 11:00 A.M. to 3:00 P.M. for the winter samples, could be compared across the summer and winter seasons, since this CV designation was defined in the same fashion in both seasons. Two-way ANOVA analysis demonstrated that both summer and winter CV9 UF samples induced more inflammation (total cells) and cell damage (BAL protein) compared to CV9 SMF within a given season. However, CV9 UF summer but not CV9 winter PM induced a significant increase in BAL neutrophil and eosinophil influx compared CV9 SMF. It should be noted that identical CV extraction procedures were used on filter blank controls to demonstrate no significant filter effects on the number of cells recovered from the lungs as shown in figure 5.5.

Pulmonary Cytotoxicity and Cell Damage

A number of summer and winter CVs elicited changes in lymphocyte numbers, as well as changes in BAL protein and LDH values as shown in figures 5.6 and 5.7. Regardless of CV#, UF was more potent than SMF PM for summer and winter and for LDH for winter only. The majority of CVs did not significantly impact cell viability (data not shown), as

evaluated via light microscopy, with the exception of summer CV9 UF. Select summer and winter CV UF samples induced statistically significant increases in BAL protein and LDH compared to control. BAL protein was significantly impacted by size where the CV UF fraction was more potent compared to CV SMF for summer CV2 and CV10 and winter CV10. LDH levels were significantly higher in summer CV2 SMF exposed mice compared to CV2 UF exposed mice.

Systemic Inflammation and Hematology

Systemic cellular responses in mice exposed to summer and winter CVs are shown in figures 5.8 and 5.9 respectively. No significant interaction between CV samples, based on particle size for hematologic measurements for summer or winter was observed. In contrast, only summer platelets were significantly higher in UF compared to SMF, although a single CV source (CV1 SMF) demonstrated a statistically significant reduction compared to control (figure 5.10). No significant elevations in circulating total white blood cells (WBC) were observed in mice following summer or winter PM exposure compared to control. Few CVs elicited significant decreases in circulating populations of WBC, including monocytes, neutrophils, eosinophils and basophils, suggesting little CV-induced effects under experimental conditions used in the study. There were no significant changes in circulating lymphocyte populations (data not shown). Summer CV6 (metals) UF induced a significant reduction in circulating monocytes compared to control. Summer CV1 (dinnertime cooking) UF and SMF induced significant reductions in circulating neutrophils. Summer CV3 (vehicular) induced significant decreases in circulating eosinophils (SMF only) and basophils (UF only). PM-induced hematological changes were observed following exposure to select summer and winter CVs (Figures 5.10 and 5.11). Increases in circulating platelets were marginally insignificant in mice exposed to summer CV10 UF compared to control. Winter CV10 UF significantly elevated the number of circulating platelets compared to control. All other CV exposed mice had platelet values that were unchanged compared to control. Hematological parameters; circulating red blood cells (RBC) and hemoglobin concentrations were significantly reduced following exposure to summer CV1 UF (RBC and hemoglobin), summer CV1 SMF (hemoglobin only) and winter CV8 (morning commute) SMF (RBC and hemoglobin). Other trends reflecting a reduction for other CVs did not attain statistical significance.

Correlations

In summer, cytotoxicity and pulmonary and circulating monocytes were positively correlated with size, suggesting increased cytotoxic potential for larger compared to smaller particles. In winter, DLS size was negatively correlated with total cells, neutrophils and lymphocytes suggesting that a greater response was elicited by the smallest particles. For both summer and winter, measured oxidative potential was significantly higher for SMF compared to UF for a given season. Within the lungs, oxidative potential was positively correlated with BAL protein for winter and negatively correlated with LDH levels for summer and winter. For selected hematological parameters, oxidative potential of summer but not winter PM was negatively correlated with circulating WBC, neutrophils, lymphocytes, eosinophils, basophils and platelets. These findings suggest that, based on season, DLS measured particle size and particle

oxidative potential measured by the DTT assay do not consistently predict hematological responses of CV samples in vivo.

Discussion

A primary goal of this work has been to use a single particle mass spectrometer and an algorithmic design to collect source-oriented particles for toxicity testing. With sufficient collection efficiency, particles could be extracted from each CV and delivered to the lungs of mice on an equal mass basis. Biological testing of source-oriented PM samples (CVs) collected during summer and winter in urban Fresno, CA. demonstrated a varied toxicity pattern. Using the source-oriented PM sampling methodology described in Chapter 2, PM components that consistently occurred together in the atmosphere, representing both primary sources and secondary materials described in Chapter 4, were collected for toxicity testing. Toxicological assessment of both pulmonary and systemic (i.e., hematologic) effects were evaluated in the context of the ability of PM samples to induce a biological and/or cellular response that was significantly different from three different perspectives: (1) compared to vehicle control, (2) compared to particle size within the same CV sample and (3) compared to all CV samples for a given particle size i.e., ultrafine (UF) and submicron fine (SMF). Our findings suggest source-oriented PM-induced responses are partially dependent on particle size and the source-oriented composition of each CV sample.

PM-induced cardiopulmonary responses are routinely measured using inflammatory and cytotoxic mediators in BAL, lung tissues and blood (Lotti, Olivato and Bergamo 2009, Scapellato and Lotti 2007). Inflammation and oxidative stress represent a biological response to PM that is a hall mark of several diseases such as obstructive lung and cardiovascular disease and can be used as an indicator of particle impacts in both human and animals. The precise characteristics of PM in this study that were hypothesized to contribute to a measured biological response include particle size and chemical (source-oriented) composition.

Particle Size

In general, UF PM was a more potent inducer of inflammatory and cytotoxic responses compared to SMF PM regardless of season or CV sample. Increased biological toxicity of UF PM is thought to be influenced by their small size and potential for translocation from the lung into circulation and possibly to secondary target organs (Ferin, Oberdorster and Penney 1992, Kreyling et al. 2002, Kreyling et al. 2009, Oberdorster et al. 1991). In this study, DLS showed that average PM size in solution was substantially larger than as sampled. The responses observed could be due to differences in chemical composition, aggregate morphology or if the delivered UF PM aggregates become dissociated upon deposition within the respiratory tract. The large surface to mass ratio of UF PM may allow these particles to act as a carrier of co-pollutants such as transition metals into the lung (Zhong et al. 2010).

UF and SMF PM appeared to induce greater pulmonary inflammatory and cytotoxic responses than in the blood under the conditions of particle administration and post-exposure timing used in this study. Pulmonary inflammation was significantly elevated

for the majority of CVs compared to control. Assessment of differences between CVs for a given particle size demonstrated that the primarily neutrophilic inflammatory response was significantly different between winter UF CV samples and to a lesser degree between SMF CV samples. Differences between summer CVs, regardless of size fraction, were less dramatic. Measures of cell damage (BAL protein) and cytotoxicity (LDH) demonstrated significant differences between SOS for a given size for both summer and winter PM confirming the sensitivity of these indicators for PM effects despite contrasting results in the literature (Mantecca et al. 2009, Dick et al. 2003).

Source-Oriented Particle Composition

Measures of pulmonary inflammation/cytotoxicity, and hematology differed between source-oriented samples compared to corresponding controls as well as between particle size fractions. Source-oriented PM elicited inflammatory responses that were more significant in the lung compared to the blood 24 hours following exposure. Although a number of source-oriented samples produced some degree of biological response in the lungs compared to control, the most biologically responsive samples of the winter season appeared to be CV 10 (a mix of sources present at night) UF and CV 2 (highly processed regional background) SMF and CV3 (EC and OC) SMF, while for the summer season CV 2 and CV5 (vehicles) UF and CV 6 (metals) SMF were most biologically reactive. Hematologic measures were more variable and did not correlate to changes in pulmonary endpoints. However, of interest, were reduced hemoglobin values for CV 8 UF and CV 8 (morning commute) SMF during the winter season and CV 1 (dinnertime cooking) and CV6 UF and CV 1 SMF during the summer season, while elevated blood neutrophils were noted for CV2 UF during the summer season.

While the precise mechanisms for PM-induced cardiovascular effects remain to be established, several studies suggest a role for alterations in systemic inflammation, plasma viscosity and homeostasis of coagulation pathways (Gilmour et al. 2005, Araujo et al. 2008, Bonzini et al. 2010, Calderon-Garciduenas et al. 2008, Hertel et al. 2010). Systemic effects following exposure to source-oriented samples (SOS) include decreased numbers of circulating white blood cells, a finding noted in rats exposed to traffic-related PM (Gerlofs-Nijland et al. 2010). The importance of reduced circulating white blood cell populations is unclear however these types of alterations in systemic cell profile have been previously documented (Gordon et al. 1998). A possible explanation is the importance of timing in the ability to capture the process of leukocyte recruitment from the bone marrow, migration though the cardiovascular system and margination into their final destination within the lungs which may be initiated at an earlier time-point following introduction of PM into the respiratory tract (van Eeden and Hogg 2002, Suwa et al. 2002).

The finding that source-oriented PM with different size profiles and source-oriented compositions elicited differential biological responses in our study is in good agreement with reported studies that highlight the importance of chemical composition such as presence of metals and organic carbons in PM-induced inflammation and oxidative stress (Gerlofs-Nijland et al. 2009, Cho et al. 2009, Happo et al. 2004, Happo et al. 2010, Seagrave et al. 2006, Kodavanti et al. 2005). These differences are supported by reports

linking PM size and chemical composition to source contributions within the San Joaquin Valley (Kleeman, Riddle and Jakober 2008, Ham et al. 2010). These findings improve our understanding of specific chemical components of San Joaquin Valley PM associated with adverse health effects and possible relationships with relevant sources (Ham et al. 2010, Chow 2006, Chow et al. 1992).

Although direct seasonal comparisons are limited, the scale of response to winter source-oriented PM is greater than summer source-oriented PM, as evident in the comparison of CV9 across seasons. CV9 was collected consistently during the summer and winter to represent the mixed atmosphere and was not enriched for any specific source or source combination. UF PM was significantly more potent compared to SMF PM regardless of season; however, no significant differences were observed between summer and winter CV9 samples. Despite similar recruitment of total cells for a given size fraction across seasons, there was a shift in the types of leukocytes recruited to the lung. These differences may be indicative of seasonal and size specific differences in chemical composition and confirm finding from several epidemiological and experimental studies confirming that adverse health outcomes vary with season (Becker et al. 2005, Bell et al. 2007, Bell et al. 2008, Hetland et al. 2005, Moolgavkar 2003, Peng et al. 2005)

As part of our study, we hypothesized that oxidative potential may correlate with measured responses based on previous reports that oxidative potential varies with regional and temporal patterns and particle type and that both primary and secondary emissions containing both metallic and carbonaceous compounds, are highly redox active and can be enhanced by atmospheric processing (Verma et al. 2009, Li et al. 2009, Biswas et al. 2009, Cho et al. 2005). We found that different source-oriented CV samples do possess different oxidative potential. In contrast to previous reports that increased redox activity of UF PM may contribute to increased toxicity compared to other size fractions (Brown et al. 2001), we found a moderately insignificant correlation between these size fractions and oxidative potential. Despite significant differences in oxidative potential for source-oriented particles, there was no consistent correlation between intrinsic toxicity of the PM and measures of cardiopulmonary response. Thus, we can conclude that the chemical composition leading to the observed biological responses is independent of size fraction at aspiration and oxidative potential as measured by the DTT assay. It is important to note that additional oxidative stress assessment such as the macrophage reactive oxygen species (ROS) assay may provide further indication of the role of metals in observed inflammatory and cytotoxic responses (Hu et al. 2008).

Limitations of the Study

The approach used in the present study is limited in that oro-pharyngeal aspiration delivers PM in the form of particle aggregates in contrast to the inhalation of airborne particles. Thus, to some degree the deposition patterns in the lungs differ from that of inhaled PM. However, oro-pharyngeal aspiration possesses distinct advantages over intratracheal introduction, found extensively throughout the literature, because the PM bolus is deposited at the level of the oropharynx rather than instillation of a bolus directly into the trachea. This technique allows the animal to spontaneously inhale the particle suspension directly into the lungs. The technique has been perfected to insure no introduction into the gastrointestinal tract via the esophagus.

Extensive analysis of PM using extremely sensitive methods demonstrated the presence of varying amounts of endotoxin associated with the CV PM samples, but none of the levels of endotoxin correlated with the biological responses induced by the samples. Future studies could be designed to better understand the nature of the endotoxin content associated with PM samples in the field.

Finally, it should be noted that equal mass dosing with each CV sample is not a reflection of actual exposure in the environment. The actual amount and timing for the presence of source-oriented (CV) particles in the atmosphere during the period of collection was highly variable. Therefore, to compare CVs on an equal mass basis for biological response is not the same as actual atmospheric exposure. In a similar fashion, equal dosing of UF PM as SMF PM is not a reflection of the degree of exposure to UF particles under ambient atmospheric conditions. Endpoints were only examined at one time point which may not reflect peak response.

Conclusions

The present study represents a novel approach for toxicity testing that combines sophisticated sampling methods with bioassays that can be readily conducted on biological samples. Toxicity testing of source-oriented PM can lead to improved understanding of physicochemical parameters that correlate with adverse health effects. These findings provide solid scientific evidence to provide a basis for source-specific regulations to support greater protection of human health.

References:

(ICRP), I. C. o. R. P. (1994) Human respiratory tract model for radiological protection. A report of a Task Group of the International Commission on Radiological Protection. Ann ICRP, 24, 1-482.

Alexis, N. E., J. C. Lay, K. Zeman, W. E. Bennett, D. B. Peden, J. M. Soukup, R. B. Devlin & S. Becker (2006) Biological material on inhaled coarse fraction particulate matter activates airway phagocytes in vivo in healthy volunteers. Journal of Allergy and Clinical Immunology, 117, 1396-1403.

Angiolillo, D. J., M. Ueno & S. Goto. 2010. Basic principles of platelet biology and clinical implications. In Circ J, 597-607. Japan.

Anjilvel, S. & B. Asgharian (1995) A Multiple-Path Model of Particle Deposition in the Rat Lung. Fundamental and Applied Toxicology, 28, 41-50.

Araujo, J. A., B. Barajas, M. Kleinman, X. P. Wang, B. J. Bennett, K. W. Gong, M. Navab, J. Harkema, C. Sioutas, A. J. Lusis & A. E. Nel (2008) Ambient particulate pollutants in the ultrafine range promote early atherosclerosis and systemic oxidative stress. Circulation Research, 102, 589-596.

Becker, S., L. A. Dailey, J. M. Soukup, S. C. Grambow, R. B. Devlin & Y. C. Huang (2005) Seasonal variations in air pollution particle-induced inflammatory mediator release and oxidative stress. Environ Health Perspect, 113, 1032-8.

Becker, S. & J. M. Soukup (2003) Coarse (PM2.5-10), fine (PM2.5), and ultrafine air pollution particles induce/increase immune costimulatory receptors on human blood-derived monocytes but not on alveolar macrophages. Journal of Toxicology and Environmental Health Part A, 66, 847-859.

Becker, S., J. M. Soukup, C. Sioutas & F. R. Cassee (2003) Response of human alveolar macrophages to ultrafine, fine, and coarse urban air pollution particles. Exp Lung Res, 29, 29-44.

Bein, K. J., Y. Zhao & A. S. Wexler (2009) Conditional Sampling for Source-Oriented Toxicological Studies using a Single Particle Mass Spectrometer. Environ Sci Technol., 43, Environ Sci Technol.

Bell, M. L., F. Dominici, K. Ebisu, S. L. Zeger & J. M. Samet (2007) Spatial and temporal variation in PM2.5 chemical composition in the United States for health effects studies. Environmental Health Perspectives, 115, 989-995.

Bell, M. L., K. Ebisu, R. D. Peng, J. Walker, J. M. Samet, S. L. Zeger & F. Dominici (2008) Seasonal and Regional Short-term Effects of Fine Particles on Hospital Admissions in 202 US Counties, 1999-2005. American Journal of Epidemiology, 168, 1301-1310.

Bigert, C., M. Alderling, M. Svartengren, N. Plato, U. de Faire & P. Gustavsson (2008) Blood markers of inflammation and coagulation and exposure to airborne particles in employees in the Stockholm underground. Occupational and Environmental Medicine, 65, 655-658.

Biswas, S., V. Verma, J. J. Schauer, F. R. Cassee, A. K. Cho & C. Sioutas (2009) Oxidative Potential of Semi-Volatile and Non Volatile Particulate Matter (PM) from Heavy-Duty Vehicles Retrofitted with Emission Control Technologies. Environmental Science & Technology, 43, 3905-3912.

Bonzini, M., A. Tripodi, A. Artoni, L. Tarantini, B. Marinelli, P. A. Bertazzi, P. Apostoli & A. Baccarelli (2010) Effects of inhalable particulate matter on blood coagulation. Journal of Thrombosis and Haemostasis, 8, 662-668.

Brook, R. D. (2008) Cardiovascular effects of air pollution. Clinical Science (London), 115, 175-187.

Brook, R. D., S. Rajagopalan, C. A. Pope, J. R. Brook, A. Bhatnagar, A. V. Diez-Roux, F. Holguin, Y. L. Hong, R. V. Luepker, M. A. Mittleman, A. Peters, D. Siscovick, S. C. Smith, L. Whitsel, J. D. Kaufman, A. H. A. C. Epidemiol, D. Council Kidney Cardiovasc & M. Council Nutr Phys Activity (2010) Particulate Matter Air Pollution and Cardiovascular Disease An Update to the Scientific Statement From the American Heart Association. Circulation, 121, 2331-2378.

Brown, D. M., M. R. Wilson, W. MacNee, V. Stone & K. Donaldson (2001) Size-dependent proinflammatory effects of ultrafine polystyrene particles: A role for surface area and oxidative stress in the enhanced activity of ultrafines. Toxicology and Applied Pharmacology, 175, 191-199.

Calderon-Garciduenas, L., R. Villarreal-Calderon, G. Valencia-Salazar, C. Henriquez-Roldan, P. Gutierrez-Castrellon, R. Coria-Jimenez, N. Osnaya-Brizuela, L. Romero, R. Torres-Jardon, A. Solt & W. Reed. 2008. Systemic inflammation, endothelial dysfunction, and activation in clinically healthy children exposed to air pollutants. 499-506. Taylor & Francis Inc.

Cassee, F. R., A. J. F. Boere, P. H. B. Fokkens, D. L. A. C. Leseman, C. Sioutas, I. M. Kooter & J. A. M. A. Dormans (2005) Inhalation of concentrated particulate matter produces pulmonary inflammation and systemic biological effects in compromised rats. Journal of Toxicology and Environmental Health Part A, 68, 773-796.

Cho, A. K., C. Sioutas, A. H. Miguel, Y. Kumagai, D. A. Schmitz, M. Singh, A. Eiguren-Fernandez & J. R. Froines (2005) Redox activity of airborne particulate matter at different sites in the Los Angeles Basin. Environmental Research, 99, 40-47.

Cho, S. H., H. Tong, J. K. McGee, R. W. Baldauf, Q. T. Krantz & M. I. Gilmour (2009) Comparative toxicity of size-fractionated airborne particulate matter collected at different distances from an urban highway. Environ Health Perspect, 117, 1682-9.

Chow, J., J. Watson, D. Lowenthal, P. Solomon, K. Maglinano, S. Ziman & L. Richards (1992) PM10 Source Apportionment in California San-Joaquin Valley. Atmospheric Environment Part a-General Topics, 3335-3354.

Chow, J. C. (2006) Health effects of fine particulate air pollution: lines that connect. J Air Waste Manag Assoc, 56, 707-8.

Costa, D. L. & K. L. Dreher (1997) Bioavailable transition metals in particulate matter mediate cardiopulmonary injury in healthy and compromised animal models. Environ Health Perspect, 105 Suppl 5, 1053-60.

Costa, D. L., J. R. Lehmann, D. Winsett, J. Richards, A. D. Ledbetter & K. L. Dreher (2006) Comparative pulmonary toxicological assessment of oil combustion particles following inhalation or instillation exposure. Toxicol Sci, 91, 237-46.

Cozzi, E., C. J. Wingard, W. E. Cascio, R. B. Devlin, J. J. Miles, A. R. Bofferding, R. M. Lust, M. R. Van Scott & R. A. Henriksen (2007) Effect of ambient particulate matter exposure on hemostasis. Translational Research, 149, 324-332.

Daigle, C. C., D. C. Chalupa, F. R. Gibb, P. E. Morrow, G. Oberdorster, M. J. Utell & M. W. Frampton (2003) Ultrafine particle deposition in humans during rest and exercise. Inhal Toxicol, 15, 539-52.

Delfino, R. J., N. Staimer, T. Tjoa, A. Polidori, M. Arhami, D. L. Gillen, M. T. Kleinman, N. D. Vaziri, J. Longhurst, F. Zaldivar & C. Sioutas (2008) Circulating biomarkers of inflammation, antioxidant activity, and platelet activation are associated with primary combustion aerosols in subjects with coronary artery disease. Environmental Health Perspectives, 116, 898-906.

Demokritou, P., T. Gupta, S. Ferguson & P. Koutrakis. 2003. Development of a high-volume concentrated ambient particles system (CAPS) for human and animal inhalation toxicological studies. In Inhal Toxicol, 111-29. United States.

Demokritou, P., I. G. Kavouras, S. T. Ferguson & P. Koutrakis (2002) Development of a High Volume Cascade Impactor for Toxicological and Chemical Characterization Studies. Aerosol Science and Technology, 36, 925-933.

Dick, C. A. J., P. Singh, M. Daniels, P. Evansky, S. Becker & M. I. Gilmour (2003) Murine pulmonary inflammatory responses following instillation of size-fractionated ambient particulate matter. Journal of Toxicology and Environmental Health Part A, 66, 2193-2207.

Dockery, D. W. (2001) Epidemiologic evidence of cardiovascular effects of particulate air pollution. Environmental Health Perspectives, 109, 483-486.

Dockery, D. W., C. A. Pope, 3rd, X. Xu, J. D. Spengler, J. H. Ware, M. E. Fay, B. G. Ferris, Jr. & F. E. Speizer (1993) An association between air pollution and mortality in six U.S. cities. N Engl J Med, 329, 1753-9.

Driscoll, K. E., D. L. Costa, G. Hatch, R. Henderson, G. Oberdorster, H. Salem & R. B. Schlesinger (2000) Intratracheal instillation as an exposure technique for the evaluation of respiratory tract toxicity: Uses and limitations. Toxicological Sciences, 55, 24-35.

Ferin, J., G. Oberdorster & D. P. Penney (1992) Pulmonary Retention of Ultrafine and Fine Particles in Rats. American Journal of Respiratory Cell and Molecular Biology, 6, 535-542.

Gerlofs-Nijland, M. E., M. Rummelhard, A. J. F. Boere, D. L. A. C. Leseman, R. Duffin, R. P. F. Schins, P. J. A. Borm, M. Sillanpaa, R. O. Salonen & F. R. Cassee (2009) Particle Induced Toxicity in Relation to Transition Metal and Polycyclic Aromatic Hydrocarbon Contents. Environmental Science & Technology, 43, 4729-4736.

Gerlofs-Nijland, M. E., A. I. Totlandsdal, E. Kilinc, A. J. F. Boere, P. H. B. Fokkens, D. Leseman, C. Sioutas, P. E. Schwarze, H. M. Spronk, P. W. F. Hadoke, M. R. Miller & F. R. Cassee (2010) Pulmonary and cardiovascular effects of traffic-related particulate matter: 4-week exposure of rats to roadside and diesel engine exhaust particles. Inhalation Toxicology, 22, 1162-1173.

Ghio, A. J., C. Kim & R. B. Devlin (2000) Concentrated ambient air particles induce mild pulmonary inflammation in healthy human volunteers. Am J Respir Crit Care Med, 162, 981-8.

Gilmour, M. I., J. McGee, R. M. Duvall, L. Dailey, M. Daniels, E. Boykin, S. H. Cho, D. Doerfler, T. Gordon & R. B. Devlin (2007) Comparative toxicity of size-fractionated airborne particulate matter obtained from different cities in the United States. Inhal Toxicol, 19 Suppl 1, 7-16.

Gilmour, P. S., E. R. Morrison, M. A. Vickers, I. Ford, C. A. Ludlam, M. Greaves, K. Donaldson & W. MacNee (2005) The procoagulant potential of environmental particles (PM10). Occupational and Environmental Medicine, 62, 164-171.

Gordon, T., C. Nadziejko, R. Schlesinger & L. C. Chen (1998) Pulmonary and cardiovascular effects of acute exposure to concentrated ambient particulate matter in rats. Toxicology Letters (Shannon), 96-97, 285-288.

Ham, W. A., J. D. Herner, P. G. Green & M. J. Kleeman (2010) Size Distribution of Health-Relevant Trace Elements in Airborne Particulate Matter During a Severe Winter Stagnation Event: Implications for Epidemiology and Inhalation Exposure Studies. Aerosol Science and Technology, 44, 753-765.

Happo, M., R. O. Salonen, A. I. Halinen, P. Jalava & M. R. Hirvonen (2004) Inflammation and tissue damage in the mouse lung caused by urban air fine and coarse particulate samples collected during contrasting pollution situations in Europe (pamchar). Toxicology and Applied Pharmacology, 197, 236.

Happo, M. S., R. O. Salonen, A. I. Halinen, P. I. Jalava, A. S. Pennanen, J. Dormans, M. E. Gerlofs-Nijland, F. R. Cassee, V. M. Kosma, M. Sillanpaa, R. Hillamo & M. R. Hirvonen (2010) Inflammation and tissue damage in mouse lung by single and repeated dosing of urban air coarse and fine particles collected from six European cities. Inhalation Toxicology, 22, 402-416.

Harder, S. D., J. M. Soukup, A. J. Ghio, R. B. Devlin & S. Becker (2001) Inhalation of PM2.5 does not modulate host defense or immune parameters in blood or lung of normal human subjects. Environmental Health Perspectives, 109, 599-604.

Hertel, S., A. Viehmann, S. Moebus, K. Mann, M. Broecker-Preuss, S. Moehlenkamp, M. Nonnemacher, R. Erbel, H. Jakobs, M. Memmesheimer, K.-H. Joeckel & B. Hoffmann (2010) Influence of short-term exposure to ultrafine and fine particles on systemic inflammation. European Journal of Epidemiology, 25, 581-592.

Hetland, R. B., F. R. Cassee, M. Lag, M. Refsnes, E. Dybing & P. E. Schwarze (2005) Cytokine release from alveolar macrophages exposed to ambient particulate matter: heterogeneity in relation to size, city and season. Part Fibre Toxicol, 2, 5.

Hu, S., A. Polidori, M. Arhami, M. M. Shafer, J. J. Schauer, A. Cho & C. Sioutas (2008) Redox activity and chemical speciation of size fractioned PM in the communities of the Los Angeles – Long Beach Harbor. Atmospheric Chemistry and Physics Discussions, 3, 11643-11672.

Ito K, Christensen WF, Eatough DJ, Henry RC, Kim E, Laden F, Lall R, Larson TV, Neas L, Hopke PK, Thurston GD (2006) PM source apportionment and health effects: 2. An investigation of inter-method variability in associations between source-apportioned fine particle mass and daily mortality in Washington, DC. J Expo Sci Environ Epidemiol. 2006 Jul;16(4):300-10.

Kleeman, M. J., S. G. Riddle & C. A. Jakober (2008) Size distribution of particle-phase molecular markers during a severe winter pollution episode. Environ Sci Technol, 42**,** 6469-75.

Kodavanti, U. P., M. C. Schladweiler, A. D. Ledbetter, J. K. McGee, L. Walsh, P. S. Gilmour, J. W. Highfill, D. Davies, K. E. Pinkerton, J. H. Richards, K. Crissman, D. Andrews & D. L. Costa (2005) Consistent pulmonary and systemic responses from inhalation of fine concentrated ambient particles: roles of rat strains used and physicochemical properties. Environ Health Perspect, 113**,** 1561-8.

Kreyling, W. G., M. Semmler, F. Erbe, P. Mayer, S. Takenaka, H. Schulz, G. Oberdorster & A. Ziesenis (2002) Translocation of ultrafine insoluble iridium particles from lung epithelium to extrapulmonary organs is size dependent but very low. J Toxicol Environ Health A, 65**,** 1513-30.

Kreyling, W. G., M. Semmler-Behnke, J. Seitz, W. Scymczak, A. Wenk, P. Mayer, S. Takenaka & G. Oberdörster (2009) Size dependence of the translocation of inhaled iridium and carbon nanoparticle aggregates from the lung of rats to the blood and secondary target organs. Inhalation Toxicology, 21**,** 55-60.

Laden, F., L. M. Neas, D. W. Dockery & J. Schwartz (2000) Association of fine particulate matter from different sources with daily mortality in six U.S. cities. Environ Health Perspect, 108**,** 941-7.

Li, N., C. Sioutas, A. Cho, D. Schmitz, C. Misra, J. Sempf, M. Wang, T. Oberley, J. Froines & A. Nel (2003) Ultrafine particulate pollutants induce oxidative stress and mitochondrial damage. Environmental Health Perspectives, 111**,** 455-460.

Li, Q., A. Wyatt & R. M. Kamens (2009) Oxidant generation and toxicity enhancement of aged-diesel exhaust. Atmospheric Environment, 43**,** 1037-1042.

Lotti, M., I. Olivato & L. Bergamo (2009) Inflammation and short-term cardiopulmonary effects of particulate matter. Nanotoxicology, 3**,** 27-32.

Mantecca, P., G. Sancini, E. Moschini, F. Farina, M. Gualtieri, A. Rohr, G. Miserocchi, P. Palestini & M. Camatini (2009) Lung toxicity induced by intratracheal instillation of size-fractionated tire particles. Toxicology Letters, 189**,** 206-214.

McDonald, J. D., I. Eide, J. Seagrave, B. Zielinska, K. Whitney, D. R. Lawson & J. L. Mauderly (2004) Relationship between composition and toxicity of motor vehicle emission samples. Environmental Health Perspectives, 112**,** 1527-1538.

Menache, M. G., F. J. Miller & O. G. Raabe (1995) Particle inhalability curves for humans and small laboratory animals. Annals of Occupational Hygiene, 39**,** 317-328.

Mendez, L. B., G. Gookin & R. F. Phalen (2010) Inhaled aerosol particle dosimetry in mice: A review. Inhalation Toxicology, 22**,** 1032-1037.

Moller, W., K. Felten, K. Sommerer, G. Scheuch, G. Meyer, P. Meyer, K. Haussinger & W. G. Kreyling (2008) Deposition, retention, and translocation of ultrafine particles from the central airways and lung periphery. American Journal of Respiratory and Critical Care Medicine, 177**,** 426-432.

Moolgavkar, S. H. (2003) Air pollution and daily mortality in two U.S. counties: season-specific analyses and exposure-response relationships. Inhal Toxicol, 15**,** 877-907.

Morishita, M., G. J. Keeler, J. D. McDonald, J. G. Wagner, L.-H. Young, S. Utsunomiya, R. C. Ewing & J. R. Harkema (2009) Source-to-receptor pathways of anthropogenic PM2.5 in Detroit, Michigan: Comparison of two inhalation exposure studies. Atmospheric Environment, 43**,** 1805-1813.

Nemmar, A., S. Al-Maskari, B. H. Ali & I. S. Al-Amri (2007) Cardiovascular and lung inflammatory effects induced by systemically administered diesel exhaust particles in rats. American Journal of Physiology - Lung Cellular and Molecular Physiology, 292**,** L664-L670.

Nygaard, U. C., J. S. Hansen, M. Samuelsen, T. Alberg, C. D. Marioara & M. Lovik (2009) Single-Walled and Multi-Walled Carbon Nanotubes Promote Allergic Immune Responses in Mice. Toxicological Sciences, 109**,** 113-123.

Oberdorster, G., J. Ferin, R. Gelein, S. Soderholm, C. Cox, R. Baggs & J. Finkelstein (1991) INHALED ULTRAFINE PARTICLES EVIDENCE OF THEIR INCREASED PULMONARY TOXICITY. American Review of Respiratory Disease, 143**,** A700.

Oberdorster, G., Z. Sharp, V. Atudorei, A. Elder, R. Gelein, W. Kreyling & C. Cox (2004) Translocation of inhaled ultrafine particles to the brain. Inhal Toxicol, 16**,** 437-45.

Ostro, B., R. Broadwin, S. Green, W. Y. Feng & M. Lipsett (2006) Fine particulate air pollution and mortality in nine California counties: results from CALFINE. Environ Health Perspect, 114**,** 29-33.

Ostro, B., W.-Y. Feng, R. Broadwin, S. Green & M. Lipsett (2007) The effects of components of fine particulate air pollution on mortality in California: Results from CALFINE. Environmental Health Perspectives, 115**,** 13-19.

Peel, J. L., K. B. Metzger, M. Klein, W. D. Flanders, J. A. Mulholland & P. E. Tolbert (2007) Ambient air pollution and cardiovascular emergency department visits in potentially sensitive groups. American Journal of Epidemiology, 165**,** 625-633.

Peng, R. D., F. Dominici, R. Pastor-Barriuso, S. L. Zeger & J. M. Samet (2005) Seasonal analyses of air pollution and mortality in 100 US cities. Am J Epidemiol, 161**,** 585-94.

Peters, A., D. W. Dockery, J. E. Muller & M. A. Mittleman (2001) Increased particulate air pollution and the triggering of myocardial infarction. Circulation, 103**,** 2810-2815.

Pinkerton, K. E., F. H. Green, C. Saiki, V. Vallyathan, C. G. Plopper, V. Gopal, D. Hung, E. B. Bahne, S. S. Lin, M. G. Menache & M. B. Schenker (2000) Distribution of particulate matter and tissue remodeling in the human lung. Environ Health Perspect, 108**,** 1063-9.

Pope, C. A., 3rd & D. W. Dockery (2006) Health effects of fine particulate air pollution: lines that connect. J Air Waste Manag Assoc, 56**,** 709-42.

Pope, C. A., 3rd, M. J. Thun, M. M. Namboodiri, D. W. Dockery, J. S. Evans, F. E. Speizer & C. W. Heath, Jr. (1995) Particulate air pollution as a predictor of mortality in a prospective study of U.S. adults. Am J Respir Crit Care Med, 151**,** 669-74.

Quan, C. L., Q. H. Sun, M. Lippmann & L. C. Chen (2010) Comparative effects of inhaled diesel exhaust and ambient fine particles on inflammation, atherosclerosis, and vascular dysfunction. Inhalation Toxicology, 22**,** 738-753.

Rao, G. V. S., S. Tinkle, D. N. Weissman, J. M. Antonini, M. L. Kashon, R. Salmen, L. A. Battelli, P. A. Willard, A. F. Hubbs & M. D. Hoover (2003) Efficacy of a technique for exposing the mouse lung to particles aspirated from the pharynx. Journal of Toxicology and Environmental Health-Part A, 66**,** 1441-1452.

Rohr, A. C., J. G. Wagner, M. Morishita, A. Kamal, G. J. Keeler & J. R. Harkema (2010) Cardiopulmonary responses in spontaneously hypertensive and Wistar-Kyoto rats exposed to concentrated ambient particles from Detroit, Michigan. Inhalation Toxicology, 22**,** 522-533.

Rouse, R. L., G. Murphy, M. J. Boudreaux, D. B. Paulsen & A. L. Penn (2008) Soot nanoparticles promote biotransformation, oxidative stress, and inflammation in

murine lungs. American Journal of Respiratory Cell and Molecular Biology, 39**,** 198-207.

Saldiva, P. H. N., R. W. Clarke, B. A. Coull, R. C. Stearns, J. Lawrence, G. G. K. Murthy, E. Diaz, P. Koutrakis, H. Suh, A. Tsuda & J. J. Godleski (2002) Lung inflammation induced by concentrated ambient air particles is related to particle composition. American Journal of Respiratory and Critical Care Medicine, 165**,** 1610-1617.

Samet, J. M., D. Graff, J. Berntsen, A. J. Ghio, Y.-C. T. Huang & R. B. Devlin (2007) A Comparison of Studies on the Effects of Controlled Exposure to Fine, Coarse and Ultrafine Ambient Particulate Matter from a Single Location. Inhalation Toxicology**,** 29-32.

Samuelsen, M., U. C. Nygaard & M. Lovik (2009) Particles from wood smoke and road traffic differently affect the innate immune system of the lung. Inhalation Toxicology, 21**,** 943-951.

Sayes, C. M., K. L. Reed & D. B. Warheit (2007) Assessing toxicity of fine and nanoparticles: Comparing in vitro measurements to in vivo pulmonary toxicity profiles. Toxicological Sciences, 97**,** 163-180.

Scapellato, M. L. & M. Lotti (2007) Short-term effects of particulate matter: an inflammatory mechanism? Crit Rev Toxicol, 37**,** 461-87.

Seagrave, J., M. J. Campen, J. D. McDonald, J. L. Mauderly & A. C. Rohr (2008) Oxidative stress, inflammation, and pulmonary function assessment in rats exposed to laboratory-generated pollutant mixtures. Journal of Toxicology and Environmental Health Part A, 71**,** 1352-1362.

Seagrave, J., J. D. McDonald, E. Bedrick, E. S. Edgerton, A. P. Gigliotti, J. J. Jansen, L. Ke, L. P. Naeher, S. K. Seilkop, M. Zheng & J. L. Mauderly (2006) Lung toxicity of ambient particulate matter from southeastern U.S. sites with different contributing sources: relationships between composition and effects. Environ Health Perspect, 114**,** 1387-93.

Smith, K. R., J. M. Veranth, U. P. Kodavanti, A. E. Aust & K. E. Pinkerton (2006) Acute pulmonary and systemic effects of inhaled coal fly ash in rats: Comparison to ambient environmental particles. Toxicological Sciences, 93**,** 390-399.

Suwa, T., J. C. Hogg, K. B. Quinlan, A. Ohgami, R. Vincent & S. F. van Eeden (2002) Particulate air pollution induces progression of atherosclerosis. Journal of the American College of Cardiology, 39**,** 935-942.

van Eeden, S. F. & J. C. Hogg (2002) Systemic inflammatory response induced by particulate matter air pollution: The importance of bone-marrow stimulation. Journal of Toxicology and Environmental Health Part A, 65**,** 1597-1613.

Verma, V., Z. Ning, A. K. Cho, J. J. Schauer, M. M. Shafer & C. Sioutas (2009) Redox activity of urban quasi-ultrafine particles from primary and secondary sources. Atmospheric Environment, 43**,** 6360-6368.

Wegesser, T. C., L. M. Franzi, F. M. Mitloehner, A. Eiguren-Fernandez & J. A. Last (2010) Lung antioxidant and cytokine responses to coarse and fine particulate matter from the great California wildfires of 2008. Inhalation Toxicology, 22**,** 561-570.

Wilson, D., H. Aung, M. Lame, L. Plummer, K. Pinkerton, W. Ham, M. Kleeman, J. Norris & F. Tablin (2010) Exposure of mice to concentrated ambient particulate

matter results in platelet and systemic cytokine activation. Inhal Toxicol, 22**,** 267-76.
Zhong, C.-Y., Y.-M. Zhou, K. R. Smith, I. M. Kennedy, C.-Y. Chen, A. E. Aust & K. E. Pinkerton (2010) Oxidative Injury in The Lungs of Neonatal Rats Following Short-Term Exposure to Ultrafine Iron and Soot Particles. Journal of Toxicology and Environmental Health Part A, 73**,** 837-847.

Figure legends

Figure 5.1 Average Particle Size. Average particle size in suspension for summer (A) and winter (B) ultrafine (UF) and sub-micron fine (SMF) was measured using dynamic light scattering on the day of bioassay studies.

Figure 5.2 Particle Oxidative Potential. Oxidative potential was measured in a cell-free dithiothreitol (DTT) assay and is expressed as 1, 4 napthoquinone equivalent. Data is presented as mean ± standard error for summer (A) and winter (B) ultrafine and sub-micron fine PM.

Figure 5.3 Summer 2008 Lung Inflammation. Cellular response measured in the bronchoalveolar lavage fluid of mice (n = 6) exposed to HBSS vehicle alone or 50 μg of summer UF or SMF source-oriented PM suspended in HBSS. Cells/ml (A), neutrophils/ml (B) and eosinophils/ml (C) are expressed as mean ± standard error. * $p < 0.05$ versus HBSS control, # $p < 0.05$ versus SMF for same size fraction.

Figure 5.4 Winter Lung Inflammation. Cellular response measured in the bronchoalveolar lavage fluid of mice (n = 6) exposed to HBSS vehicle alone or 50 μg of winter UF or SMF source-oriented PM suspended in HBSS. Cells/ml (A), neutrophils/ml (B) and eosinophils/ml (C) are expressed as mean ± standard error. * $p < 0.05$ versus HBSS control, # $p < 0.05$ versus SMF for same size fraction. For number designations in the upper right hand corner of a given bar graph, the first number listed is significantly different from all other listed numbers.

Figure 5.5 Summer Cytotoxicity and Cell Damage. Cellular and biochemical response measured in the bronchoalveolar lavage fluid of mice (n = 6) exposed to HBSS vehicle alone or 50 μg of summer UF or SMF source-oriented PM suspended in HBSS. Percent non-viable cells (A), BAL protein (B) and lactate dehydrogenase (LDH) (C) are expressed as mean ± standard error. * $p < 0.05$ versus HBSS control, # $p < 0.05$ versus UF or SMF for same ChemVol. For number designations in the upper right hand corner of a given bar graph, the first number listed is significantly different from all other listed numbers.

Figure 5.6 Winter Cytotoxicity and Cell Damage. Cellular and biochemical response measured in the bronchoalveolar lavage fluid of mice (n = 6) exposed to HBSS vehicle alone or 50 μg of winter UF or SMF source-oriented PM suspended in HBSS. Percent non-viable cells (A), BAL protein (B) and lactate dehydrogenase (LDH) (C) are expressed as mean ± standard error. * $p < 0.05$ versus HBSS control, # $p < 0.05$ versus SMF for same size fraction. For number designations in the upper right hand corner of a given bar graph, the first number listed is significantly different from all other listed numbers.

Figure 5.7 The effect of filter extraction on total cell number recovered by BAL. AIR: No oropharyngeal aspiration of solution. Control : Oropharyngeal aspiration of 50 ml Hank's Balanced Salt Solution. PUF FB: Oropharyngeal aspiration of a suspension

from the Filter/Field blank for polyurethane foam (PUF) filter used to collect submicron fine (SMF) PM. TX40 FB: Oropharyngeal aspiration of a suspension from the Filter/Field blank used to collect ultrafine (UF) PM

Figure 5.8 Summer Systemic Responses. Cellular inflammatory responses in whole blood of mice (n = 6) exposed to HBSS vehicle alone or 50 μg of summer UF or SMF source-oriented PM suspended in HBSS. Platelets (A), monocytes (B), neutrophils (C), eosinophils (D), basophils (E) are expressed as mean ± standard error. * $p < 0.05$ versus HBSS control. Note: Blood samples were not collected for summer CV10 SMF mice.

Figure 5.9 Winter Systemic Responses. Cellular inflammatory responses in whole blood of mice (n = 6) exposed to HBSS vehicle alone or 50 μg of winter UF or SMF source-oriented PM suspended in HBSS. Platelets (A), monocytes (B), neutrophils (C), eosinophils (D), basophils (E) are expressed as mean ± standard error. * $p < 0.05$ versus HBSS control. Note: Blood samples were not collected for winter CV10 SMF mice. For number designations in the upper right hand corner of a given bar graph, the first number listed is significantly different from all other listed numbers.

Figure 5.10 Summer Hematological Responses. Platelet, red blood cell (rbc), hemoglobin and hematocrit levels measured in the blood of mice (n = 6) exposed to HBSS vehicle alone or 50 μg of summer UF or SMF source-oriented PM suspended in HBSS. All values are expressed as mean ± standard error. * $p < 0.05$ versus HBSS control, # $p < 0.05$ versus SMF for same size fraction. For number designations in the upper right hand corner of a given bar graph, the first number listed is significantly different from all other listed numbers.

Figure 5.11 Winter Hematological Responses. Platelet, red blood cell (rbc), hemoglobin and hematocrit levels measured in the blood of mice (n = 6) exposed to HBSS vehicle alone or 50 □g of winter UF or SMF source-oriented PM suspended in HBSS. All values are expressed as mean ± standard error. * $p < 0.05$ versus HBSS control, # $p < 0.05$ versus SMF for same size fraction. For number designations in the upper right hand corner of a given bar graph, the first number listed is significantly different from all other listed numbers.

Figure 5.1. DLS Measured Average Particle Size

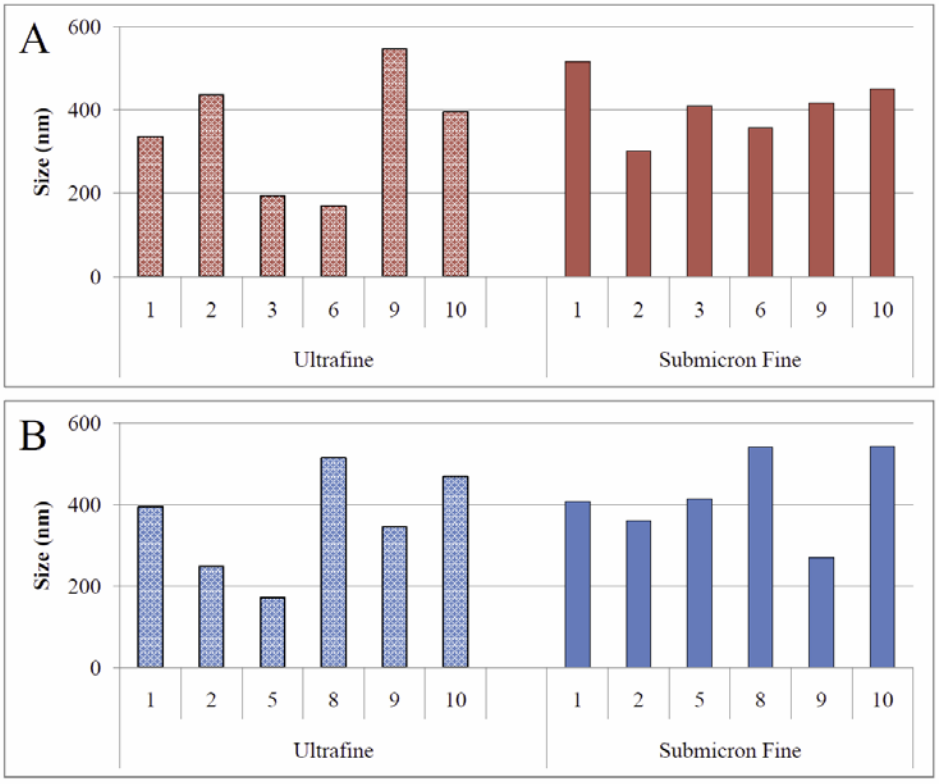

Figure 5.2. Particle Oxidative Potential

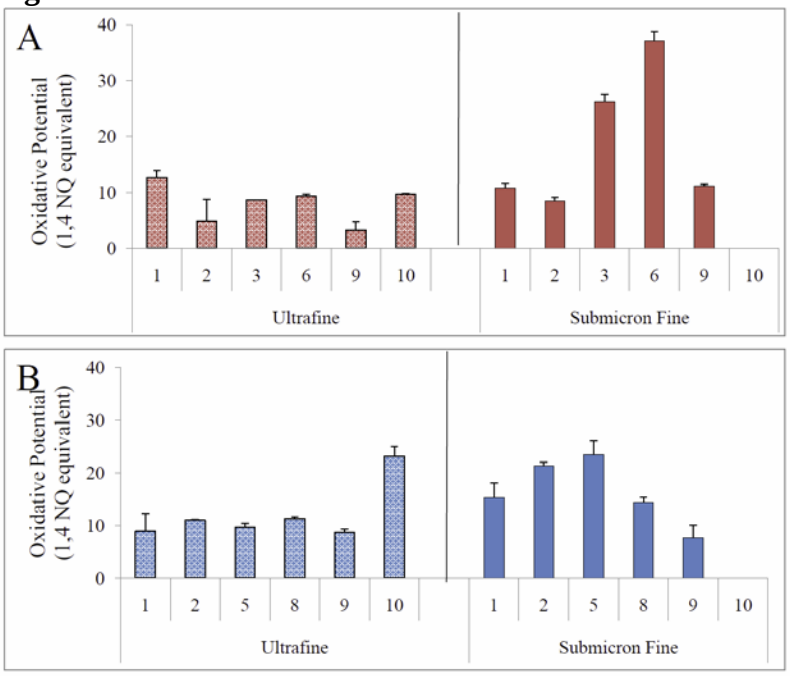

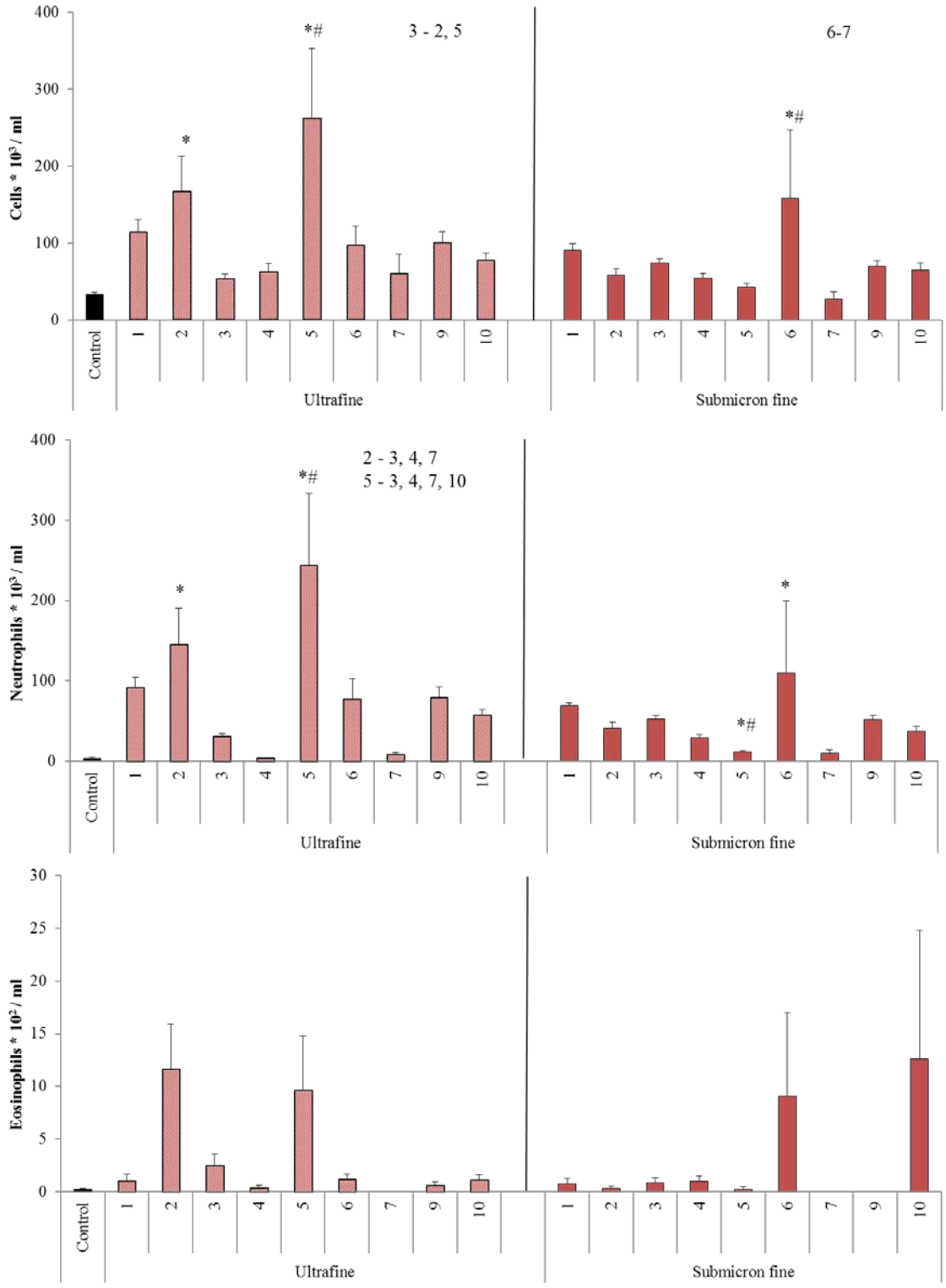

Figure 5.3 Summer Pulmonary Inflammatory Responses

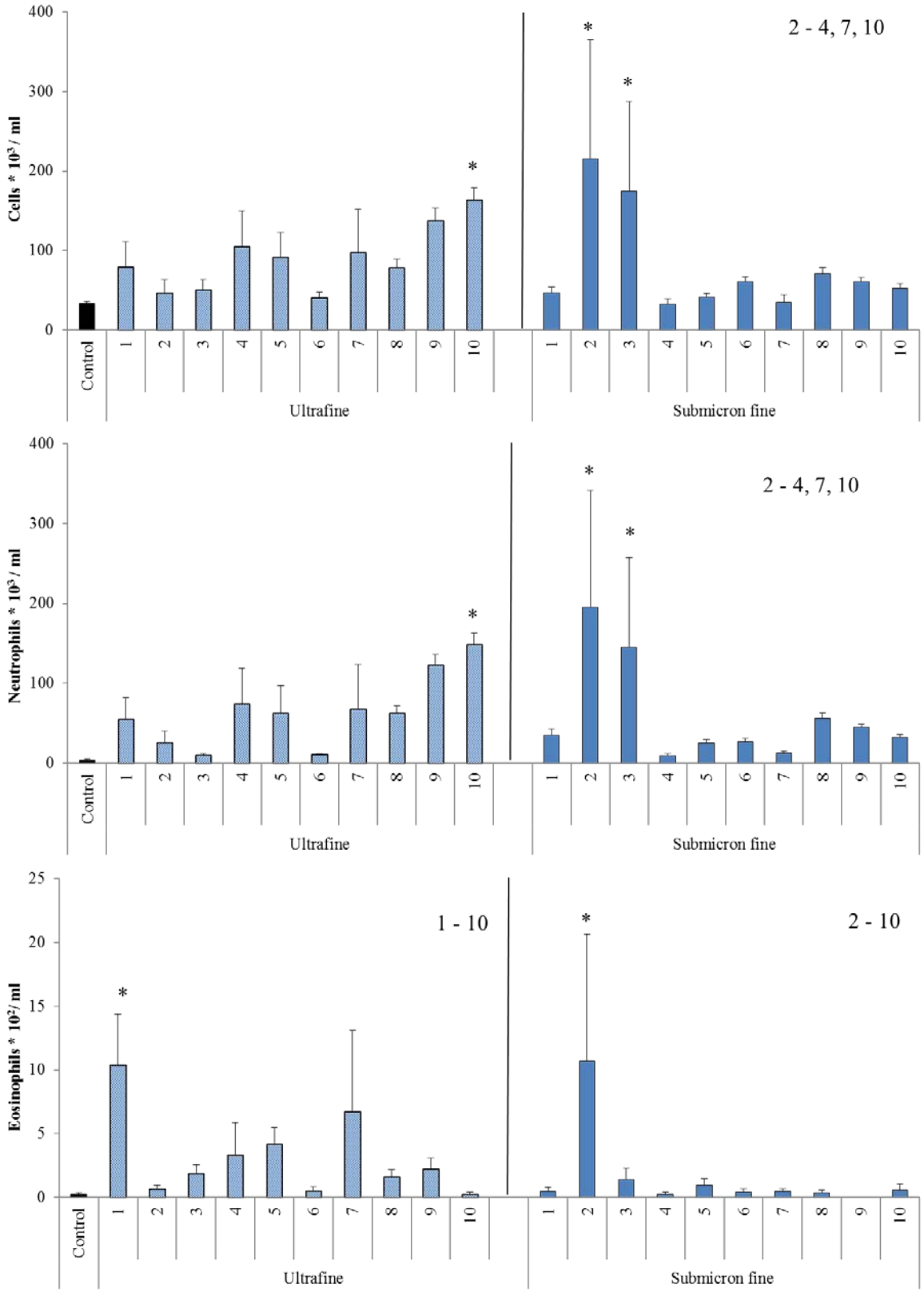

Figure 5.4 Winter Pulmonary Inflammatory Responses

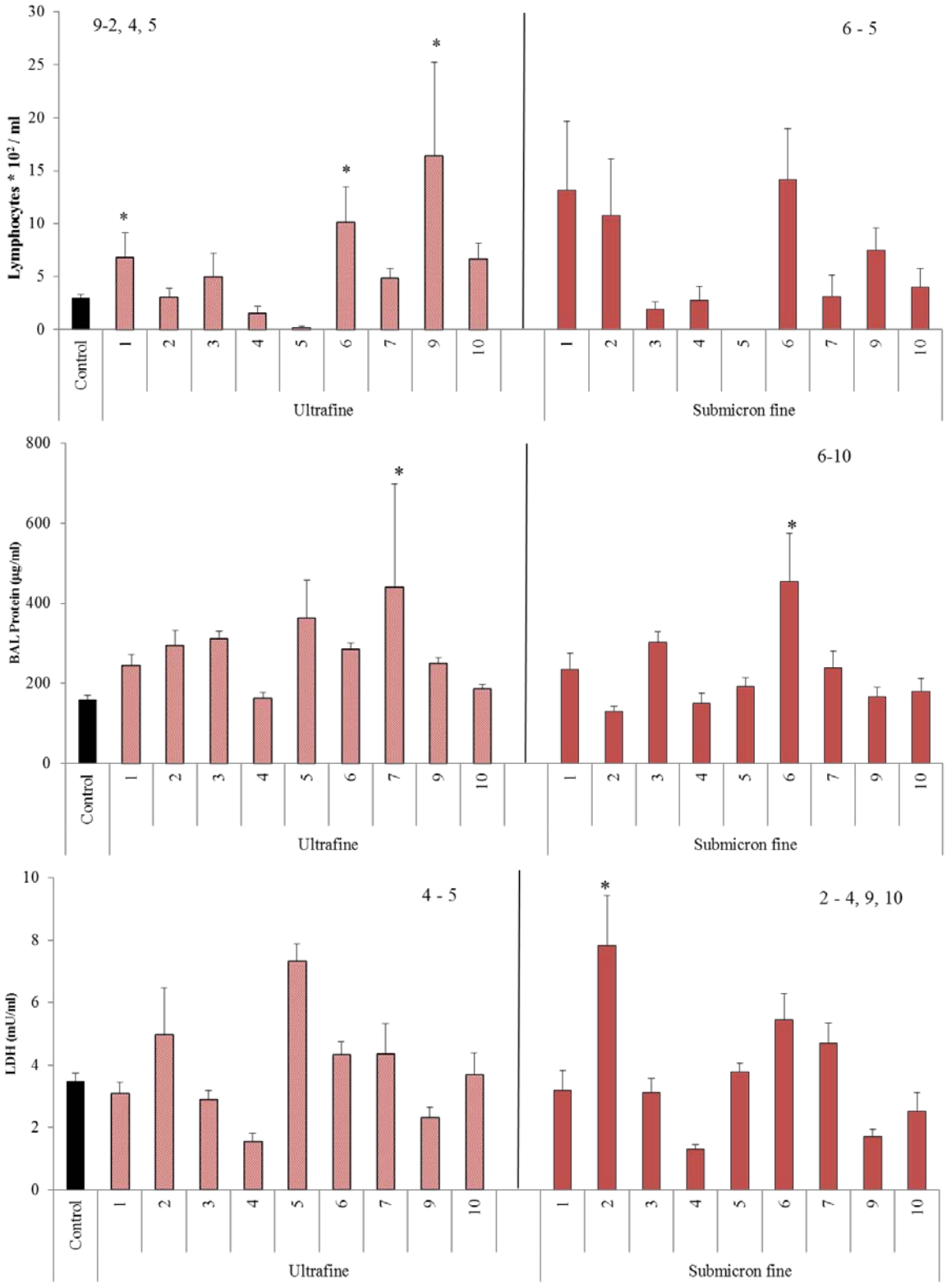

Figure 5.5 Summer Pulmonary Cell Damage and Cytotoxicity

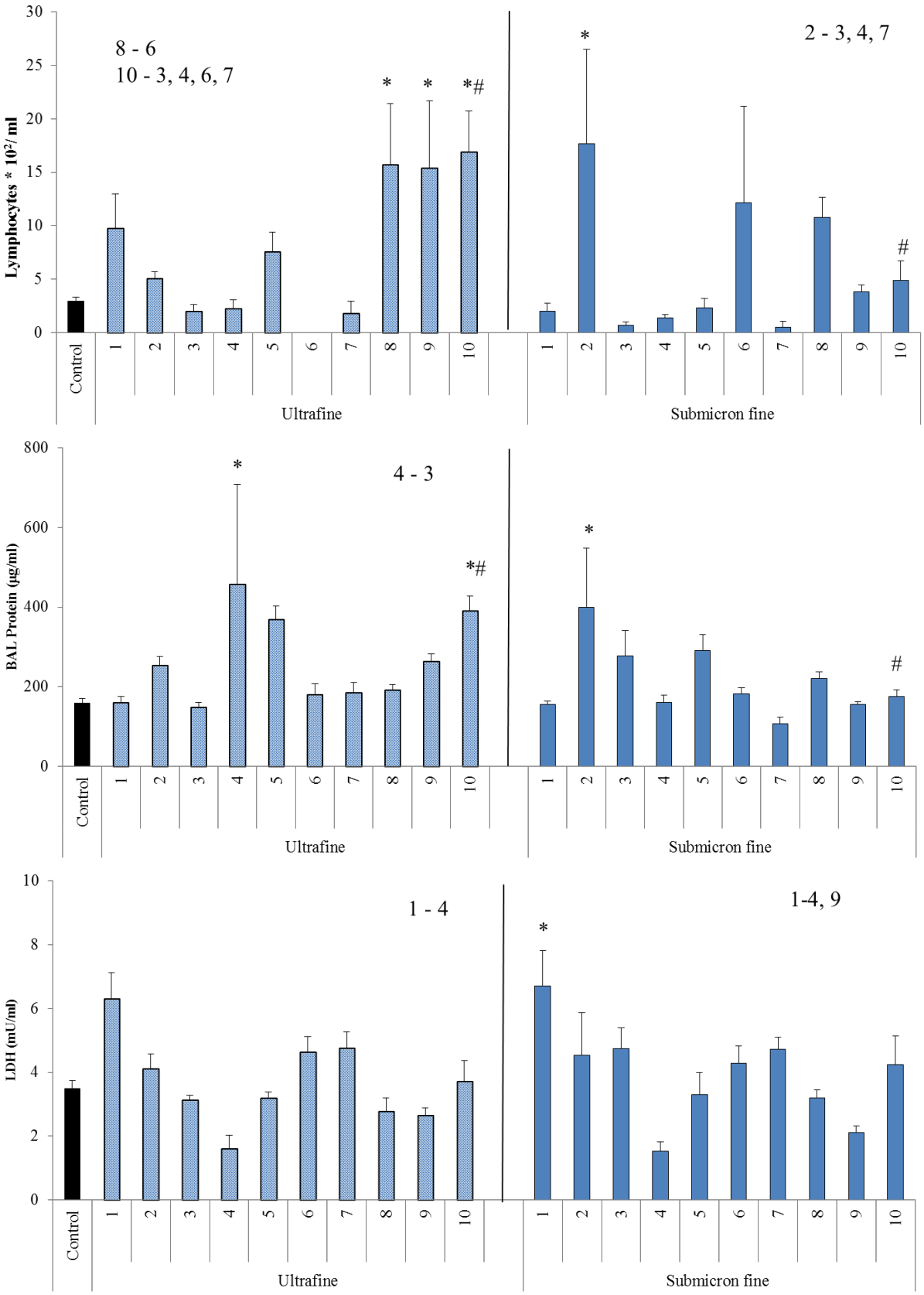

Figure 5.6 Winter Pulmonary Cell Damage and Cytotoxicity

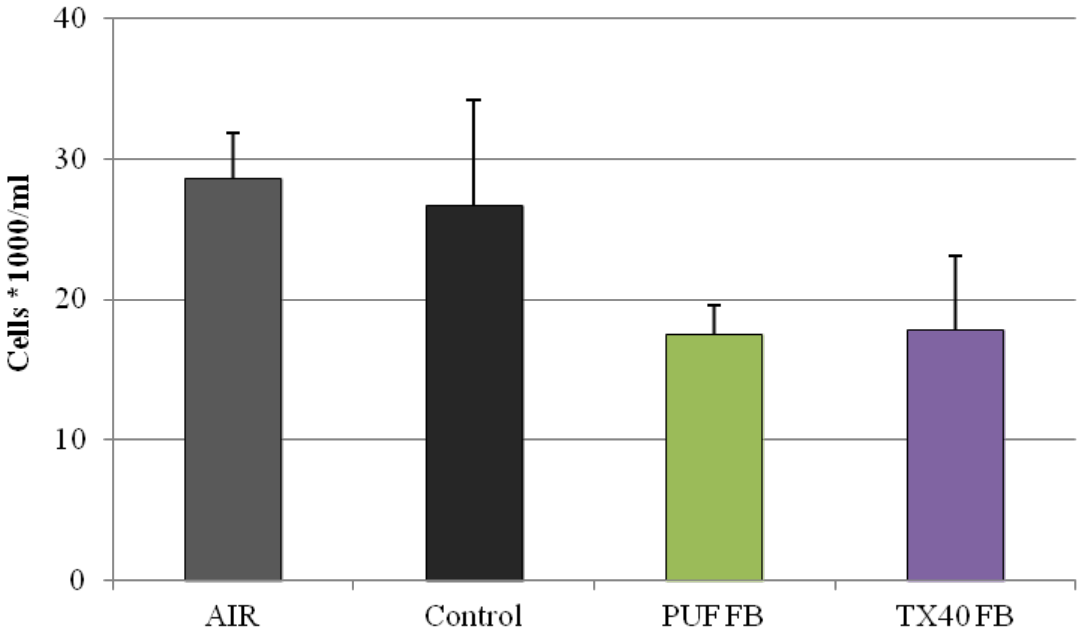

Figure 5.7 The effect of filter extraction on total cell number recovered by BAL. AIR: No oropharyngeal aspiration of solution. Control : Oropharyngeal aspiration of 50 ml Hank's Balanced Salt Solution. PUF FB: Oropharyngeal aspiration of a suspension from the Filter/Field blank for polyurethane foam (PUF) filter used to collect submicron fine (SMF) PM. TX40 FB: Oropharyngeal aspiration of a suspension from the Filter/Field blank used to collect ultrafine (UF) PM

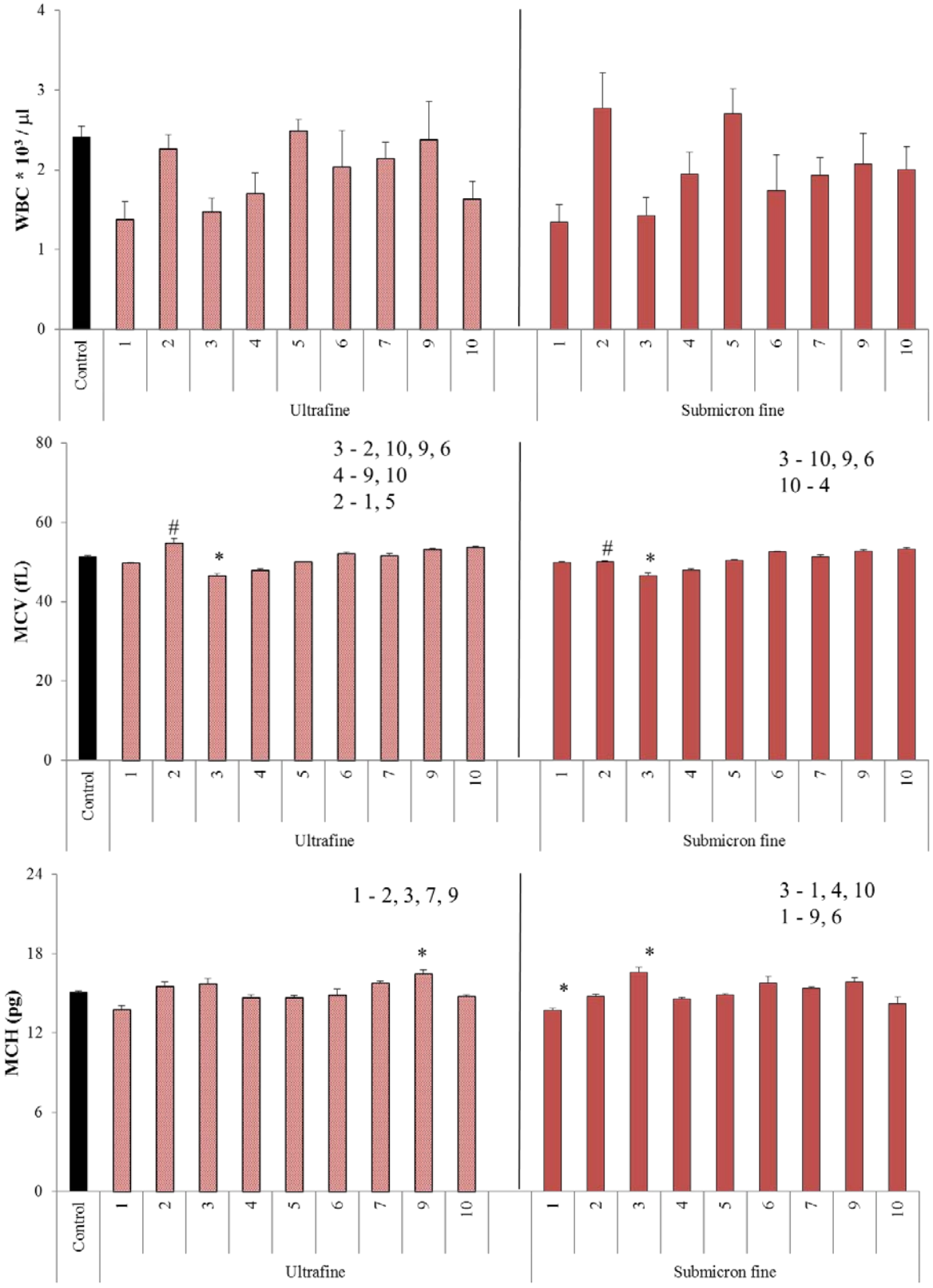
WBC * 10³ / µl
0
1
2
3
4
Control
1
2
3
4
5
6
7
9
10
Ultrafine
Submicron fine
MCV (fL)
0
20
40
60
80
3 - 2, 10, 9, 6
4 - 9, 10
2 - 1, 5
3 - 10, 9, 6
10 - 4
#
*
MCH (pg)
0
6
12
18
24
1 - 2, 3, 7, 9
3 - 1, 4, 10
1 - 9, 6

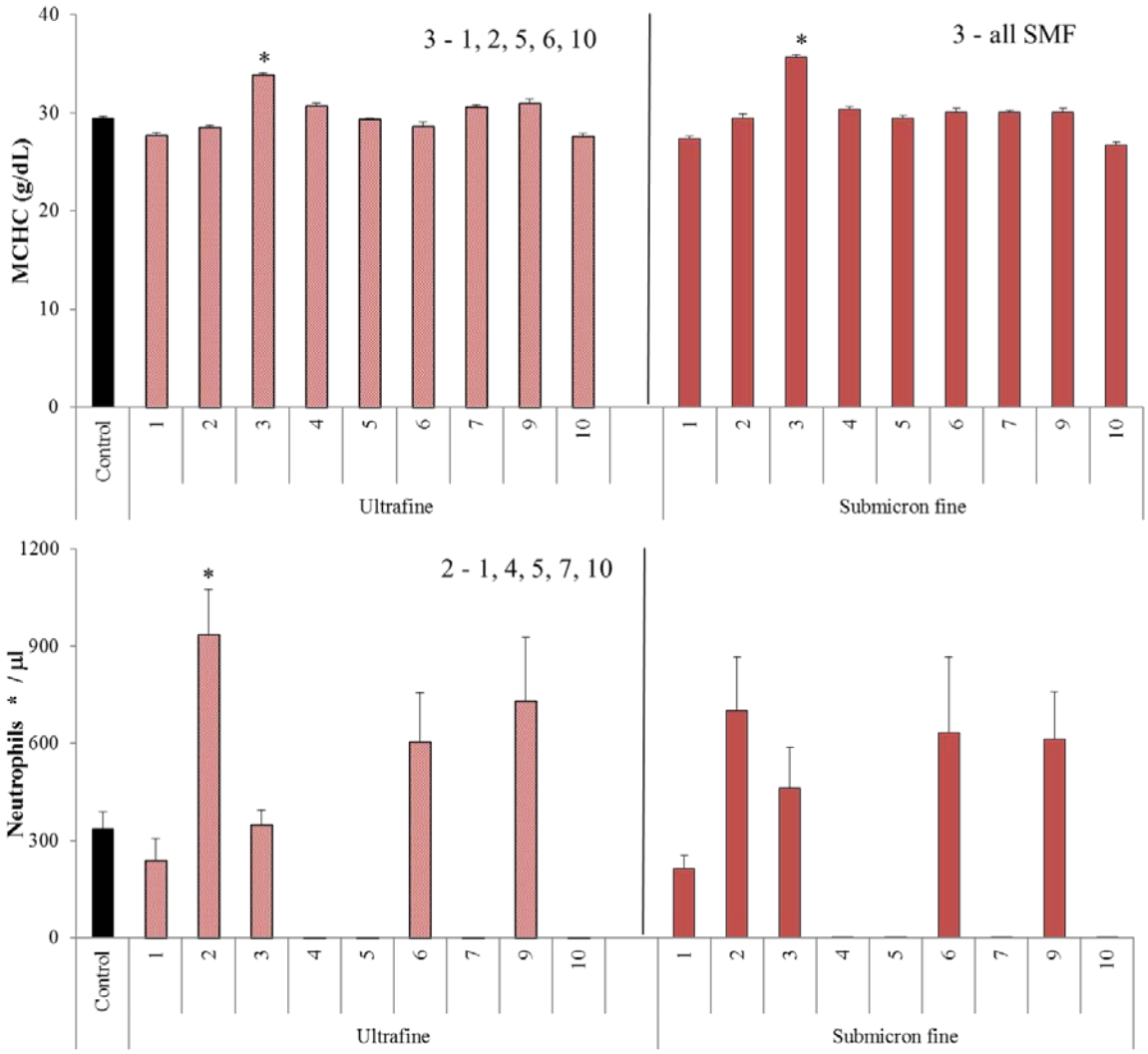

Figure 5.8 Summer Systemic Inflammatory Responses

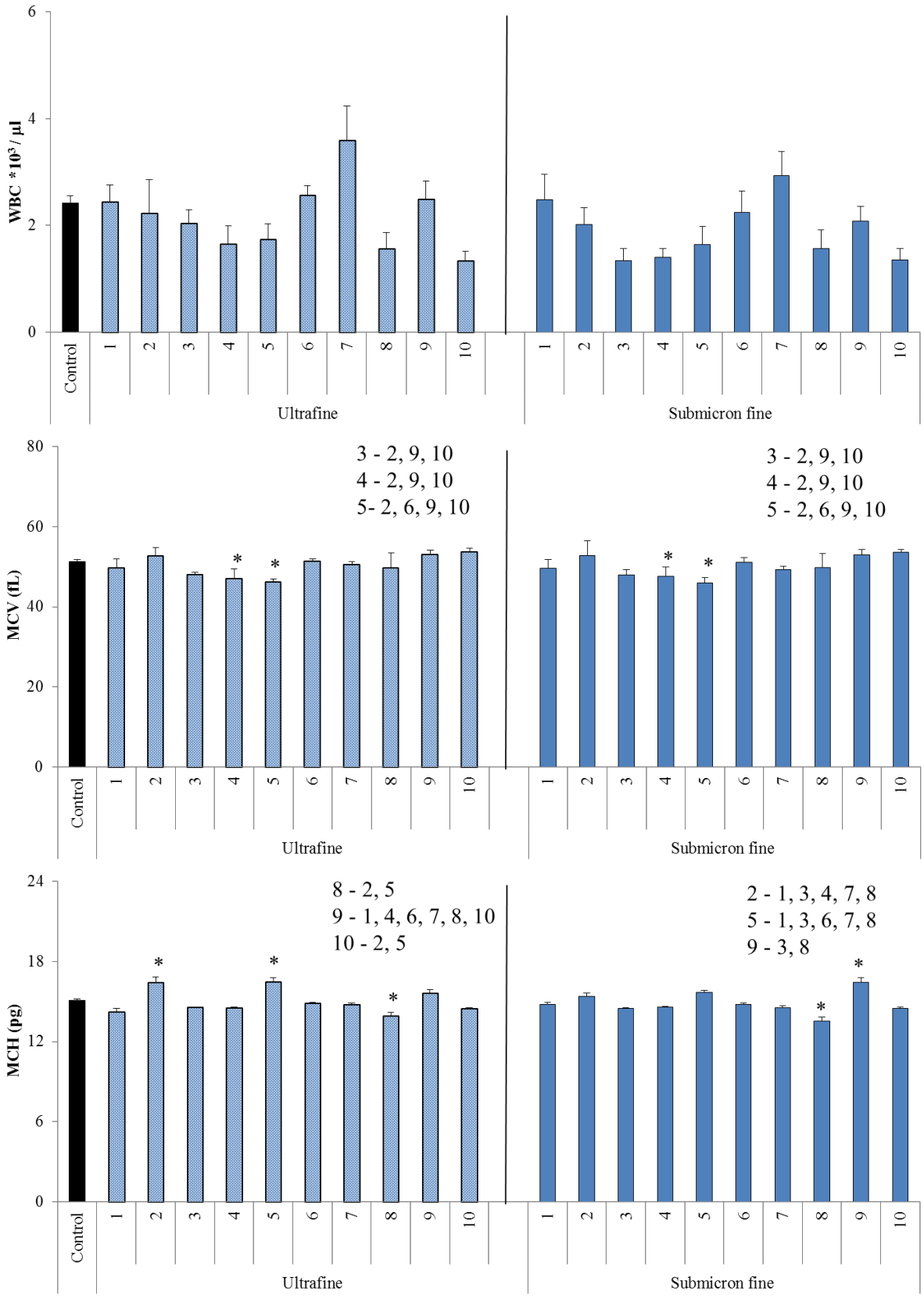
WBC *10³ / µl
6
4
2
0
Control
1
2
3
4
5
6
7
8
9
10
Ultrafine
Submicron fine
MCV (fL)
80
60
40
20
0
3 - 2, 9, 10
4 - 2, 9, 10
5- 2, 6, 9, 10
3 - 2, 9, 10
4 - 2, 9, 10
5 - 2, 6, 9, 10
*
MCH (pg)
24
18
12
6
0
8 - 2, 5
9 - 1, 4, 6, 7, 8, 10
10 - 2, 5
2 - 1, 3, 4, 7, 8
5 - 1, 3, 6, 7, 8
9 - 3, 8

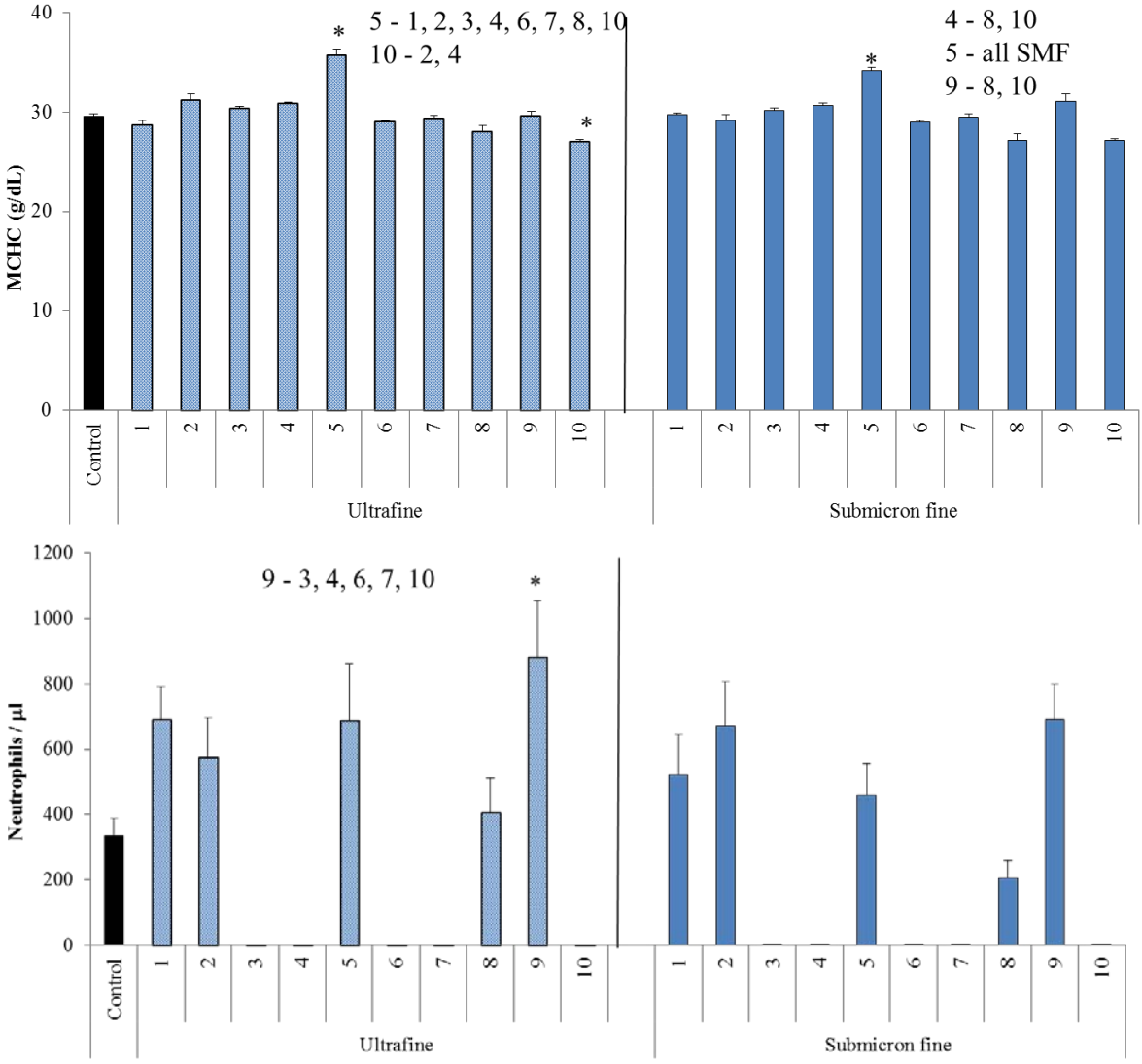

Figure 5.9 Winter Systemic Inflammatory Responses

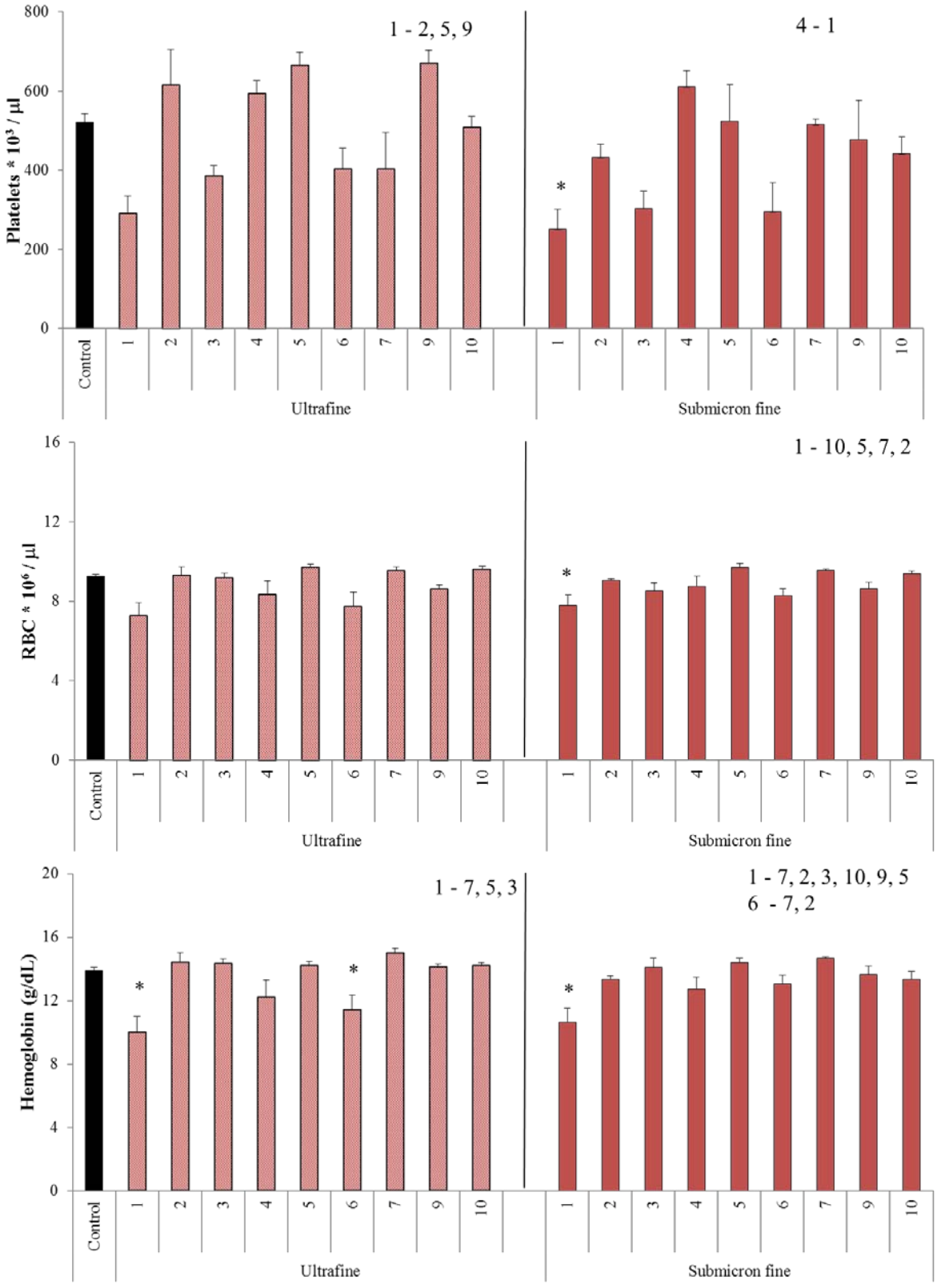
Platelets * 10³ / µl
800
600
400
200
0
1 - 2, 5, 9
4 - 1
*
Control
1
2
3
4
5
6
7
9
10
Ultrafine
Submicron fine
RBC * 10⁶ / µl
16
12
8
4
0
1 - 10, 5, 7, 2
Hemoglobin (g/dL)
20
16
12
8
4
0
1 - 7, 5, 3
1 - 7, 2, 3, 10, 9, 5
6 - 7, 2

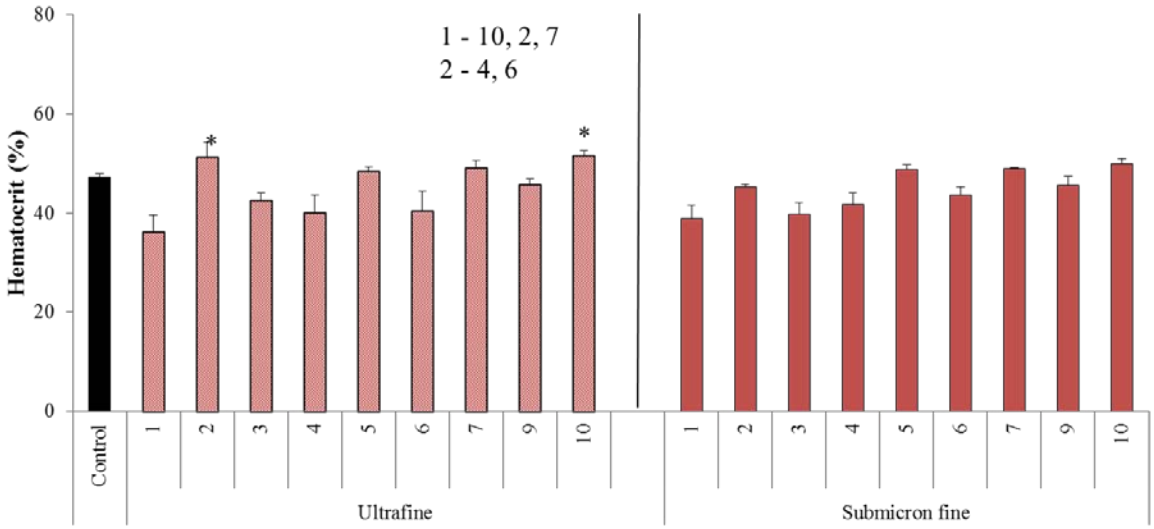

Figure 5.10 Summer Hematological Responses

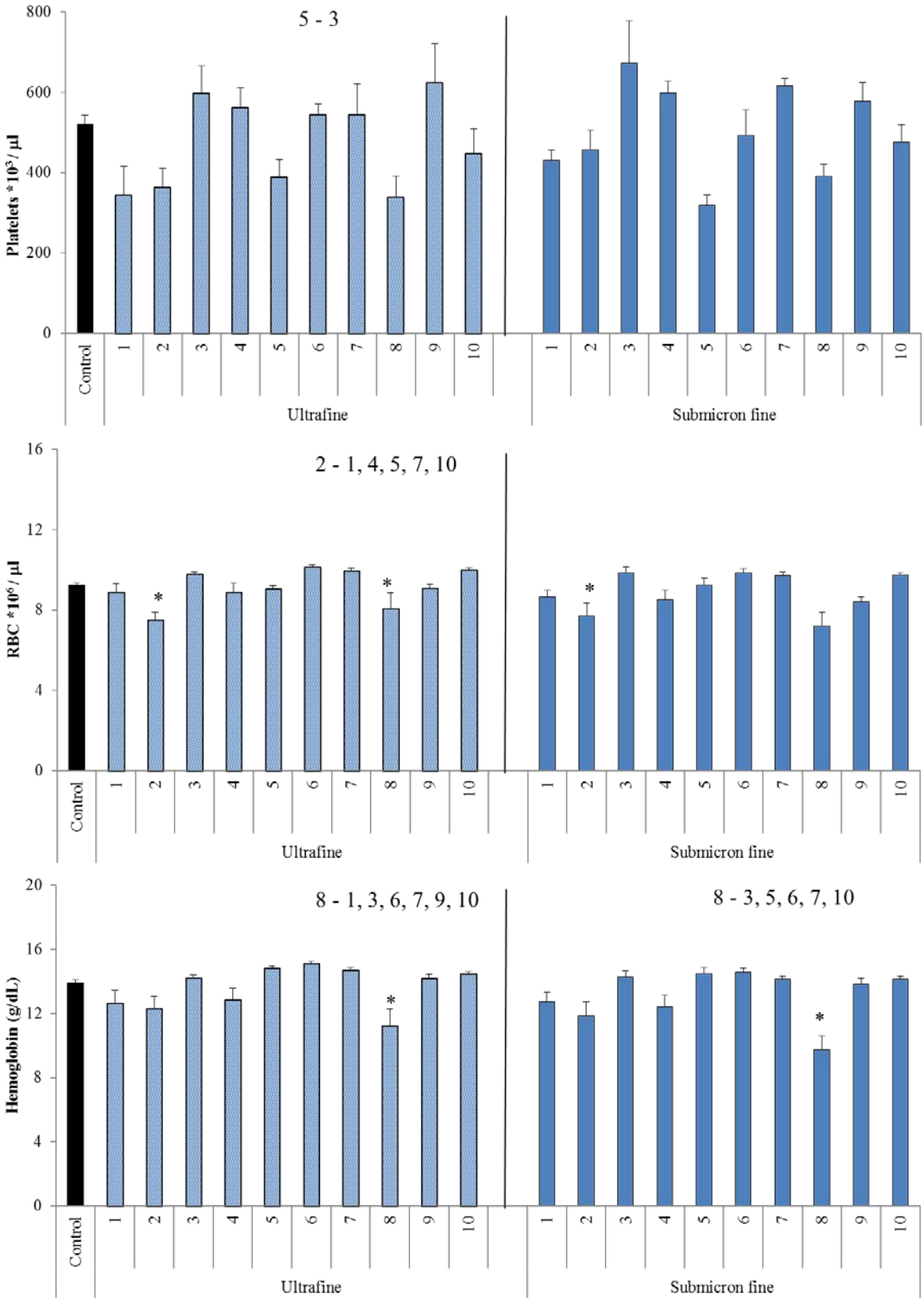
5 - 3
Platelets *10³/µl
800
600
400
200
0
Control
1
2
3
4
5
6
7
8
9
10
Ultrafine
Submicron fine
2 - 1, 4, 5, 7, 10
RBC *10⁶/µl
16
12
8
4
0
*
Ultrafine
Submicron fine
8 - 1, 3, 6, 7, 9, 10
8 - 3, 5, 6, 7, 10
Hemoglobin (g/dL)
20
16
12
8
4
0
*
Ultrafine
Submicron fine

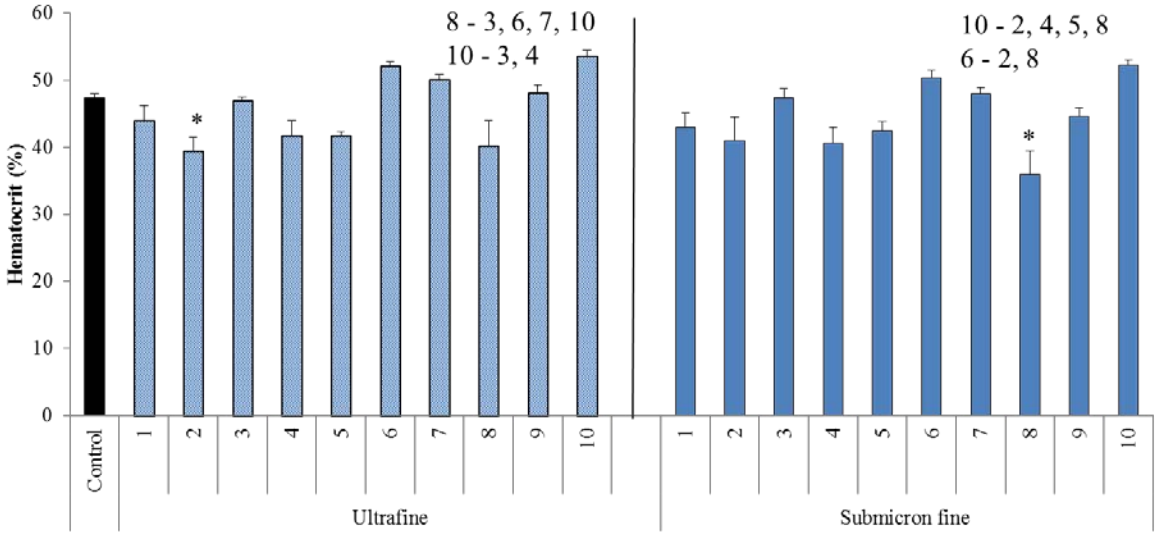

Figure 5.11 Winter Hematological Responses

Chapter 6
Toxicity of Source-Oriented Ambient Submicron Particulate Matter

Summary and Conclusions

Summary and Conclusions

Currently, state and federal air quality standards for particulate matter regulate the mass of particles per unit volume in the atmosphere in the certain size ranges, so called PM10 and PM2.5. These regulations are based on total mass, not on the source or composition of these airborne particles. Logic dictates, and toxicological and epidemiological evidence supports, that certain particles may contain greater or fewer toxic compounds than others. Studies have been performed examining the toxicity of different sources but such toxicological studies have not been performed on source-oriented atmospheric samples because a method for collecting such samples had not been available.

The objectives and accomplishments of this study were

(1) To design and build a source-oriented sampling system capable of sampling size-resolve particles from the atmosphere in such a way that each sample is associated with a source or a combination of a few sources. This system was built and deployed during this project.
(2) Operate this source-oriented sampling system in a polluted city in California for summer and winter seasons and for a sufficient length of time that enough sample is collected for toxicity studies on mice. The system was operated for about 4 weeks in the Summer of 2008 and the Winter of 2009 in Fresno, collecting 10 source-oriented samples in Summer and 9 source-oriented samples in Winter. Each sample was size resolved into a sub-micron fine sample and an ultrafine sample.
(3) Develop extraction protocols that remove the collected particles from their substrates efficiently and with a minimum of composition bias. These protocols were developed and used on the collection substrates to evenly extract both water soluble and water insoluble components on all samples collected.
(4) Test the toxicity of the source-oriented samples on mice examining a battery of pulmonary and systemic endpoints. Oropharyngeal aspiration was used to expose mice to standard aliquots of collected PM, 20 for Summer 2008 (10 submicron fine, 10 ultrafine) and 18 for Winter 2009 (9 submicron fine, 9 ultrafine). At 24 hours post-aspiration, mice were examined for indicators of pulmonary and systemic inflammation and cytotoxicity.
(5) Associate the source-oriented samples with major emitters of particulate matter in and near Fresno. Mass spectra from the source-oriented sampling system and from bulk ICP/MS measurements identified metals and other compounds in the collected particles and these metals were used to associate each source-oriented sample with categories of emitters.

This was a high-risk, high-reward project. Source-oriented sampling from the atmosphere had never been performed before because the hardware, algorithms and software were not available. Although the project was successfully carried out, the extensive development resulted in delays such that some parts of the project are still not complete. We are committed to completing the project and publishing the results.

Objectives 1 and 3 were completely new, so extensive development, testing and quality assessment had to take place for each which inevitably caused delays in the project. For objective 1, the hardware for the source-oriented sampling system was designed, components where purchased or built, and all were assembled and installed in a trailer already in the possession of Dr. Wexler's laboratory. The source-oriented sampling algorithm was designed, coded, debugged and then trained on Fresno summer and winter air pollutants. Developing and testing the source-oriented sampling system took longer than expected delaying other aspects of the project. Chapter 2, which addresses objectives 1 and 2 of this report, has been published in Environmental Science and Technology.

Although there are numerous standard operation procedures available from various sources such as the EPA for extracting PM from impactor substrates and filters, the efficiency of these procedures is known to be low, typically around 50%. Since the source-oriented sampling is expensive and some of the sources had a limited amount of PM on the filters, high efficiency extraction methods needed to be developed. In addition, use of a limited array of solvents in prior procedures may lead to composition biases in the extracted samples. So we endeavored to also develop extraction protocols that minimized composition bias since any such bias may exacerbate interpretation of subsequent source-oriented toxicity results. Extensive development of extraction procedures also delayed work on this project. Although the methods are now complete and documented in Chapter 3, the manuscript describing these methods has not yet been published.

Objectives 1, 2 and 3 had to be completed before Objectives 4 and 5 could even commence. Due to the success of the extraction procedures in Objective 3, sufficient material was extracted from all of the collection substrates to perform the full suite of toxicological studies. We had anticipated that the smallest samples would have insufficient material so this was an unanticipated success. To facilitate project efficiency, toxicological and extraction procedures were performed in tandem.

Objective 4: All source-oriented samples have undergone in vivo toxicological testing.

Objective 5 takes place in two stages. First, we used chemical analysis performed by the single particle mass spectrometer employed in source-oriented sampling to associate the collected samples with sources and source categories in Fresno. That has been described in Chapter 4. Second, we will perform ICPMS and possibly other chemical analyses of the samples to obtain more information that will strengthen the source assignments. We anticipate that Chapters 4 and 5 will be published together as one paper describing the source-oriented toxicity results and the source assignments.

From Chapter 5 (Objective 4) results, it is clear that the different sources exhibit different toxicities with the different measures tested. Interesting is that the different sources appear to be toxic in different ways. Common measures used in

epidemiological studies, such as morbidity and mortality, mask the effects of different pathways that may lead to toxicity – this study begins to elucidate such pathways.

Our original goal when we proposed this work was to identify which sources are toxic over which ones were benign. Certainly, some of the sources identified in Fresno have little toxicity. But a number of the sources that are toxic elicit different types of responses. These responses are based on size and composition. Therefore, the data provided in this work appears to address a more subtle question: Not just which sources are toxic but how are different sources toxic. Tables 6.1 and 6.2 summarize the overall conclusions of this report. Substantial toxicological results were found in different size fractions, in different seasons and with different pulmonary and systemic endpoints. Overall, few systemic responses were observed. In contrast, pulmonary responses in Summer and Winter were primarily from vehicular emissions and cooking while in the Winter secondary compounds are also implicated.

Table 6.1. Summary of source assignments and toxicological results – Summer 2008*

Dominant Source(s)	Pulmonary Response		Systemic Response	
	Submicron Fine	**Ultrafine**	**Submicron Fine**	**Ultrafine**
Local dinnertime cooking emissions		BAL, neutrophils, lymphocytes		reduced platelets
Highly processed regional background PM	LDH			neutrophils
Local vehicular emissions; diesel enhancement		BAL, neutrophils		
Source mixture				
Local vehicular emissions; gasoline + diesel				
Unknown	BAL, neutrophils, BAL protein	lymphocytes		
Local dinnertime cooking emissions		BAL protein		
ChemVol not used during this experiment				
Daytime mixed layer		lymphocytes		
Nightime nocturnal inversion				

* Blank signifies that the results are not significantly different than control

Table 6.2. Summary of source assignments and toxicological results – Winter 2009*

Dominant Source(s)	Pulmonary Response		Systemic Response	
	Submicron Fine	**Ultrafine**	**Submicron Fine**	**Ultrafine**
Local dinnertime cooking emissions	LDH			
Highly processed regional background PM	BAL, neutrophils, eosinophils, lymphocytes, BAL protein			
Local vehicular emissions; diesel enhancement	BAL,neutrophils			
Highly processed biomass combustion PM		BAL protein		
Regional source mixture; vehicular, biomass and ag				
Local dinnertime cooking emissions				
Evening commute and dinnertime cooking				
Morning commute		lymphocytes		
Daytime mixed layer		lymphocytes		neutrophils
Nightime nocturnal inversion		BAL, neutrophils, lymphocytes		

* Blank signifies that the results are not significantly different than control

Recommendations

Although this work was highly successful in that differential toxicity was observed and such toxicity was associated with different primary emissions and secondary processing in Fresno, this first study was performed in what is probably one of the most challenging locations in the country. Air flow patterns in Fresno are indistinct and there are no point sources – the methods developed here will be even more successful when air patterns are clearer and large point sources are present. Locations in the eastern US, such as Pittsburgh or Atlanta, where we have operated RSMS in prior work, will make ideal locations for future studies that explore different mixes of air pollution sources and secondary processing.

List of inventions reported and publications produced

Bein, K.J., Y. Zhao and A.S. Wexler, Conditional Sampling for Source-Oriented Toxicological Studies using a Single Particle Mass Spectrometer. Environ. Sci. Technol. 43:9445-9452, 2009.

Chapters 3, 4 and 5 will be submitted for publication in the summer of 2012. Title and authors have not yet been decided.

No inventions

Glossary Terms

See the beginning of Chapter 5

Appendices

None

Appendix

Response to CARB/EPRI questions – SOTox Final Report (April 7, 2012)

Experimental animals used for toxicity testing with source-oriented PM

In our original contract with CARB/EPRI we had designated the use of rats for all toxicity testing. Sprague Dawley rats and the possible inclusion of Spontaneously Hypertensive rats for these studies were planned. For toxicity testing of source-oriented PM samples, we had also designated timepoints of 18 and 36 hours postinstillation of source-oriented PM to study the biological response in rats. However, in conducting preliminary studies in rats, we made the decision upon consultation with members of CARB and EPRI to switch from rats to mice. The rationale for this change was based on the following findings: 1) intratracheal instillation of source-oriented PM samples in rats required 10 times as much material as for mice and 2) intratracheal instillation, although highly reproducible in rats, was not as effective as oropharyngeal aspiration in mice to provide a more natural and uniform distribution of particles to the lungs for biological testing. Intratracheal instillation is delivered as a bolus of suspended particles to the lungs, while oroparyngeal aspiration allows for the animal to spontaneously inhale the suspended particles into the lungs. Conversion from rats to mice also allowed us to be able to test many more source-oriented PM samples than possible in rats since less material per animal (10 times less material) was required. Many of the source-oriented PM samples, due to the relatively small amounts collected, would have not been able to be tested.

Our decision to switch from rats to mice was also motivated by the fact we had just completed extensive inhalation studies in mice at the Fresno site where CV samples had been collected. Our inhalation studies used balbC mice with concentrated ambient particles (CAP) during the summer and winter seasons. Therefore, the ability to compare biological responses of our source-oriented PM toxicity testing with our studies by inhalation using the identical mouse strain would be desirable. Our decision to use a single timepoint of 24 hours post-aspiration of source-oriented PM samples was based on the finding that this timepoint proved to be optimal for typically measuring the optimal timing of the biological response. The change to mice and the selection of a single timepoint were discussed and approved through consultation with CARB/EPRI.

Assays used for source-oriented PM testing

Although many assays were conducted to measure the biological response of each PM sample during the course of our study, not all assays listed in the original contract were consistently used. Since we were able to complete studies with all ChemVol (CV) samples collected using mice, we found measures of cytokine and glutathione production to be insensitive assays. In pilot studies using a few limited samples we

found a complete lack of sensitivity in the bioplex assay to measure cytokines and chemokines in BAL under the conditions of our experiments. Hematologic assays used for our studies did not include C-reactive protein which has proven to be an insensitive assay for hematologic and cardiac change. Rather we opted to implement what we felt would be more sensitive measures of blood cell counts (cbc), platelet numbers and other measures of cell and blood characteristics. Serum samples were archived, but no assays were performed (such as for cytokines and chemokines) due to a lack of sensitivity, time and costs. However, these samples remain archived for possible future use and analysis.

Based on the complete set of source-oriented PM samples tested, we found histopathology of lung tissues performed 24 hours post-aspiration to be insensitive compared to BAL analysis to compare and contrast the biological response within PM source-oriented samples. Rather, we found total cell numbers, along with measures of neutrophils, eosinophils and lymphocytes to be valuable measures to compare and contrast among the 38 source-oriented PM samples used to complete our study. Measures for tissue cytokines and tissue antioxidant potential proved not feasible due to the sensitivity of the assays performed in pilot studies, along with tissue availability. In a similar fashion, we found preliminary analysis of the heart and vascular tissues to demonstrate no remarkable changes due to oroparyngeal aspiration of CV samples. However, in all instances tissues have been stored with special attention to lung tissues.